Master of Science Thesis

Analysis and Optimization of a Solar ORC driven RO desalination plant

by

IOANNIS KYLINDRIS

Chemical Engineer, 2008

Submitted to the Office of Graduate Studies of

UNIVERSITY OF THESSALY

in partial fulfillment of the requirements for the degree of

MASTER OF SCIENCE

2012

Η έγκριση της μεταπτυχιακής εργασίας από το Τμήμα Μηχανολόγων Μηχανικών της Πολυτεχνικής Σχολής του Πανεπιστημίου Θεσσαλίας δεν υποδηλώνει αποδοχή των απόψεων του συγγραφέα (Ν. 5343/32 αρ. 202 παρ. 2).

Approved by:

Chair of Committee:	Dr. Anastasios Stamatis Mechanical engineer, Assistant Professor in the Department of Mechanical and Industrial Engineering, University of Thessaly, Volos, Greece
Committee Members	Dr. Tassos Stamatellos Mechanical engineer, Professor in the Department of Mechanical and Industrial Engineering, University of Thessaly, Volos, Greece
	Dr. Nikolaos Andritsos Chemical engineer, Associate Professor in the Department of Mechanical and Industrial Engineering, University of Thessaly, Volos, Greece

Analysis and Optimization of a Solar ORC driven RO desalination plant

Ioannis Kylindris
Chemical Engineer, 2008

Chair of Advisory Committee: Dr. Anastasios Stamatis

ABSTRACT

Water scarcity can be defined as a mismatch between water sources and water demands. The raise agriculture and chemical industry have led to pollution of groundwater aquifers and surface water. Furthermore, higher living standards result in higher water consumption. Thus, alternative ways of water production must be developed.

Desalination of saline (seawater and brackish) water is one of the most promising and modern techniques to produce fresh water. There are several desalination methods, such as multi stage flash (MSF), vapor compression (VC) and multi-effect distillation (MED), with reverse osmosis (RO) rapidly gaining market share.

In this present work, a RO seawater desalination plant was designed. The required amount of energy was provided by an organic Rankine cycle (ORC) suited to solar power generation for various working fluids. The system was coupled with two different energy recovery systems: a hydraulic turbine and a pressure exchanger. The most economical system is a RO desalination plant coupled with pressure exchanger using toluene as ORC working fluid.

It was also taken into consideration RO membrane fouling. With the pass of years, more energy is required and thus greater solar collector area must be used. Optimization was made for constant solar collector area for various ORC working fluids and energy recovery systems. All configurations proved that toluene is the best choice for ORC working fluid. The most economical plant is a RO desalination plant coupled with a pressure exchanger unit providing less irreversibility than the other configurations.

ACKNOWLEDGEMENTS

I would like to express my appreciation to the many who have given of their time and consideration in helping me carrying out this research. Foremost, I would like to thank Dr. Anastasios Stamatis, my Advisor, for his helpful ideas, encouragement and patience in guiding me through the research process.

I would like to thank Dr. Nikolaos Andritsos and Dr. Tassos Stamatellos for serving on my committee and for providing their valuable time.

Finally, I would like to thank my parents, Asterios and Maria Kylindris, and my sister, Paraskevi for their loving support and patience. This work is dedicated to my family.

Ioannis Kylindris

NONMENCLATURE

Symbol	Name, unit	Symbol	Name, unit
Symbols			
$1/k_c$	Membrane area per unit volume of fiber bundle	TCF	Temperature correction factor
A	Membrane area, m^2	TDS	Total dissolved solids, ppm
ACC	Annualized Capital Cost, $/yr	U	heat transfer coefficient, kW/m^2 K
A_f	Amortization factor, yr^{-1}	u	Velocity, m/sec
b	Coefficient	V	Volumetric flux flow rate, m^3/m^2 sec
C	Concentration, kg/m^3	W	Work, kW
C_{ORC}	Total cost for ORC unit, $/h	WD	Width, m
C_{RO}	Total cost for RO unit, $/h	X	Salt concentration, ppm
C_t	Specific annual cost, $/m^3	z	z-direction
d	Diameter, m	Z	Total investment and operating and maintenance cost, $/h
D	Diffusivity of the salt in the water, m^2/sec		
DCC	Direct Capital Cost, $	*Subscripts*	
E	Energy, J	A	specific surface
f	Fanning friction factor	amb	ambient
G_b	Normal beam solar Radiation, W/m^2	av	Average
h	Enthalpy, kJ/kg	B	Bulk
I	Exergy destruction rate, kW	b	Brine
i	Interest, %	CHM	Chemicals
ICC	Investment Capital Cost, $	co	Operating
IR	Intrinsic Rejection	col	solar collector
J	Flux, kg/m^2 sec	cond	condenser
k	Permeability constant, kg/m^2 Pa sec	cool	cool side
K	Mass transfer coefficient, m/sec	d	Distillate
L	Fiber length, m	e	Element
M	Mass flow rate, m^3/h	eqp	equipment costs
M'	Molality	f	Feed
m_{orc}	Cycle flow rate, kg/sec	hot	hot side
N	number	hpp	High pressure pump costs
OC	Operating Cost, $	hydro	Hydraulic turbine
P	Pressure, bar	i	Inner
P_p	Membrane Permeator price, $	INS	Insurance
R	Fiber bundle radius, m	LB	Labour
r	Fiber radius, m	M	Membrane surface
Re	Reynolds number ($2r_o u_s/v$)	o	Outer
RR	Recovery ratio	p	Pump
RS	Resistance	PWR	Power
Sc	Schmidt number (v/D)	ro	Reverse osmosis
Sh	Sherwood number ($2Kr_o/D$)	s	salt
SP	Salt Passage	sf	Superficial
SPC	Specific Power Consumption, kWh/m^3	site	site costs
SR	Salt Rejection	swip	seawater and intake pretreatment
T	Temperarure, ^{0}C	t	Turbine
TCC	Total Capital Cost, $	v	Vessel

Symbol	Name, unit	Symbol	Name, unit
w	Water	*Abbreviations*	
π	osmotic	CPC	Compound parabolic collector
		ED	Electrodialysis
Greek letters		EES	Engineering Equation Solver
α	Efficiency parameter, W/m^2	FF	Fouling factor
Γ	Polarization Factor	FPC	Flat plate collector
Δ	Difference	HP	High pressure pump
δ	Boundary layer width, m	MED	Multi effect distillation
ε	Porosity of the fiber bundle	MSF	Multi stage flash
η	Efficiency	NF	Nanofiltration
μ	Dynamic viscosity of salt solution, Pa.sec	ORC	Organic Rankine Cycle
Π	Osmotic pressure, bar	PTC	Parabolic trough collector
ρ	Density, kg/m^3	RO	Reverse Osmosis
φ	Concentration polarization factor	UF	Ultrafiltration
		VC	Vapor compression

Table of Contents

1. INTRODUCTION

1.1 Desalination

Water is precious to our lives. Every day, numerous activities that involve water are performed, very often in large quantities. Water is important for industrial, agricultural and domestic use.

In the last decades, however, more and more countries face fresh water shortage problems. It is very likely that the water issue will become one of the determining factors of world stability. In many areas fresh water resources do not exist in the form of surface water, such as lakes or rivers, but limited underground brackish water resources. [69]

Table 1: Water classification based on salinity [4]

Type	Total Dissolved Solids, ppm
Potable water	Up to 1500
Brackish water	1500-10000
Salt water	More than 10000
Seawater	10000-45000

Desalination has proven to be a reliable method of potable water production since the second half of the 20th century. Many processes exist, with advantages and disadvantages making them more suitable for each region. [4] Desalination refers to a process which removes amount of salt and minerals from water. It can be applied in seawater, brackish and salt water. Sometimes the process produces salt as by-product. [1]

Table 2: Seawater composition [4]

Chemical Ion	Concentration, ppm	Percentage of TDS, %
Chloride, Cl^-	19,345	55.0
Sodium, Na^+	10,752	30.6
Sulfate, SO_4^{2-}	2,701	7.6
Magnesium, Mg^{2+}	1,295	3.7
Calcium, Ca^{2+}	416	1.2
Potassium, K^+	390	1.1
Bicarbonate, HCO^{3-}	145	0.4
Bromide, Br^-	66	0.2
Borate, BO_3^{3-}	27	0.08
Strontium, Sr^{2+}	13	0.04
Fluoride, F^-	1	0.003

Ancient Greeks were the first to apply seawater desalination at the 4th century BC. Aristotle reports that Greek sailors boiled and distillated seawater to produce drinking water. [39]

Figure 1: Sailors producing potable water [39]

In the 18th century AD with the growth of steam navigation, desalinated water was used to steam engines, in order to avoid corrosion. The British manufactured the first desalination plant in 1870 for the needs of their fleet at Aden. The first industrial desalination plant was manufactured by the Dutch at Aruba in 1930.
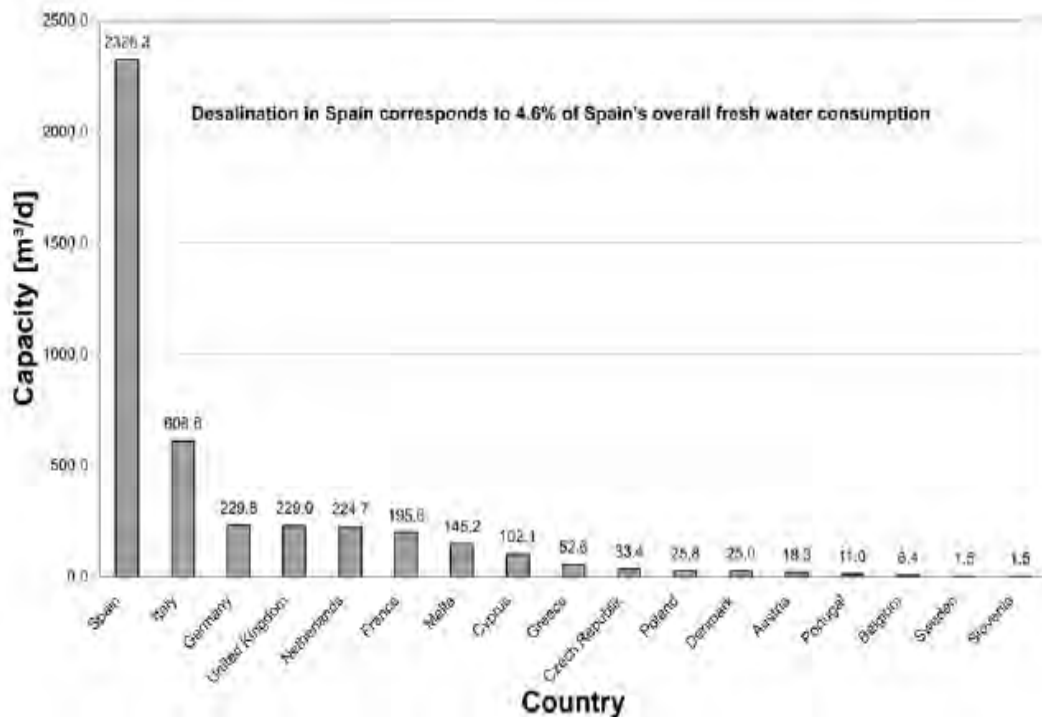

Figure 2: Desalination capacities of European countries [31]

In the early '70ies, large desalination plants were installed to produce potable water in several countries such as USA, Russia, Mexico, Saudi Arabia, Egypt and Israel. [73], [79]

Ioannis Kylindris

Figure 3: RO desalination plant in Barcelona, Spain [67]

The largest desalination plant of the world is at Jebel Ali, United Arab Emirates, producing 300 million m^3/year water. The largest desalination plant in USA is at Tampa Bay, Florida, producing 34.7 m^3/year water and the largest plant in Europe is at Carboneras, Spain. [60]

Figure 4: RO desalination plant in Japan [68]

There are various desalination plants located in Greece particularly in the Cyclades and Dodecanese island complexes. Only large islands such as Andros, Naxos and Rhodes have sufficient water resources [37], while small islands such as Oia, Ios, Ithaki, Syros and Mykonos have their desalination plants. [21]

Ioannis Kylindris

Table 3: Installed desalination units in some islands of Cyclades [42]

Island	Site	Water capacity, m³/d	Year of installation
Ios	Mylopotas	1000	2001
Paros	Naousa	1200	2002
Sifnos	Kamares	500	2001
Tinos	Tinos	500	2001
Santorini	Oia	380	2001

1.2 Energy and applications to desalination processes

1.2.1 Diesel generation

The majority of desalination plants use diesel generators. [24] The produced electricity feeds the electrically-driven parts of the plant, such as the pumps, the control system and the pretreatment process. Even though, diesel generators are well known due to their excessive use for decades, the use of energy recovery systems is essential with the rapid increase of petroleum price.

Avlonitis proposed the Pelton wheel turbine as energy recovery system in Oia RO desalination plant. The high pressure brackish water is lead into a Pelton wheel type hydraulic turbine, which produces a rotating power output to assist the main electric motor in driving the high-pressure pump.[20], [21]
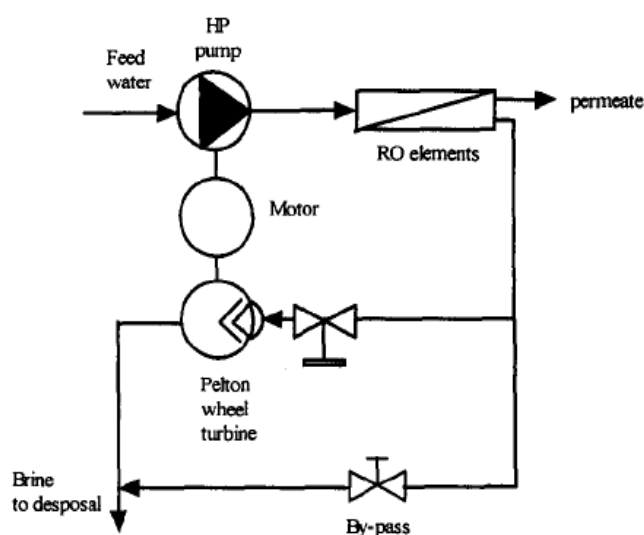

Figure 5: Pelton wheel turbine [20]

He has also proposed a turbo changer energy recovery system and pressure exchangers. The turbo changer is a centrifugal system and the energy saving is achieved due to lower pressure which the high-pressure pump works. [21]
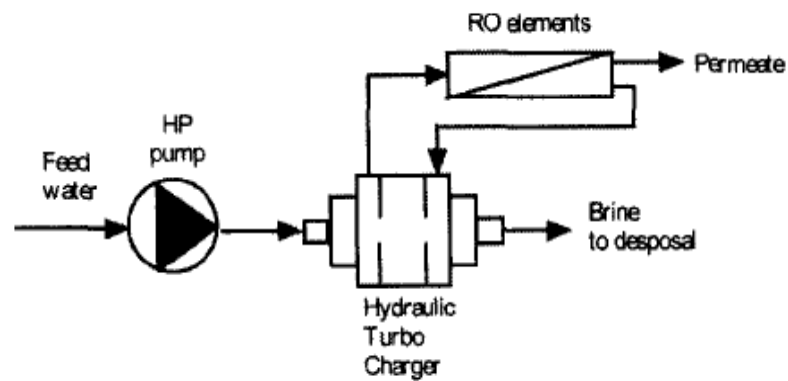
Ioannis Kylindris

Figure 6: Turbo changer energy recovery systems [21]

Pressure exchangers transfer the energy in the brackish water stream to the new seawater stream. Decreasing the volumetric output of the high-pressure pump helps saving energy. [20]
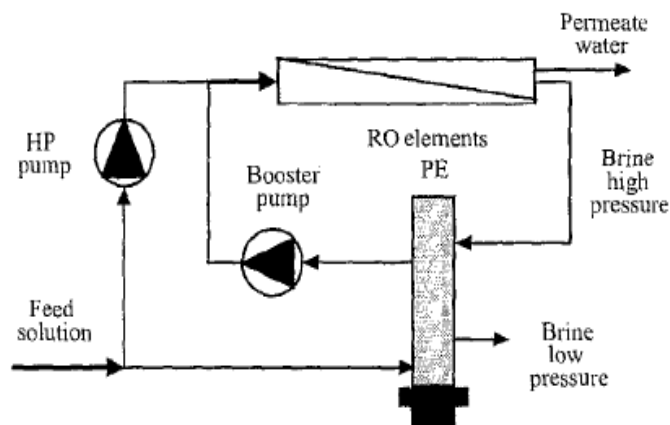

Figure 7: Pressure exchanger system [20]

1.2.2 Renewable energy driven plants

With prices for petroleum escalating rapidly in recent years and scarcity of new oil resources, scientific community has elaborated alternative solutions for energy. Delyannis and Belesiotis, in 1995, were the first to propose solar energy driven desalination plants for the Aegean islands. Photovoltaic systems were installed and produced electrical power to drive the distillation plant. There were two main disadvantages in this project: (1) the plant operated in unsteady-state conditions, as PV systems depend on ambient meteorological conditions of the region and (2) large installation areas were needed. [28]
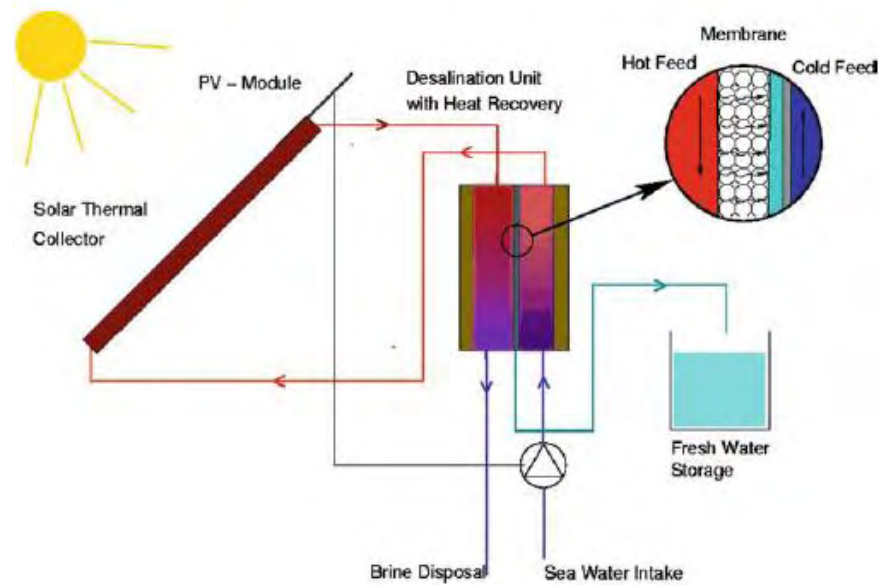
Figure 8: Solar-driven desalination process [4]

In 2004, Kaldellis et al. designed a desalination plant based on a combination of wind converter and PV plant, while additional energy was bought from either the existing electrical network or an existing back-up diesel generator. The wind turbine and the PV station were used to feed the desalination plant and the excess of energy was sold to the local grid. [38]
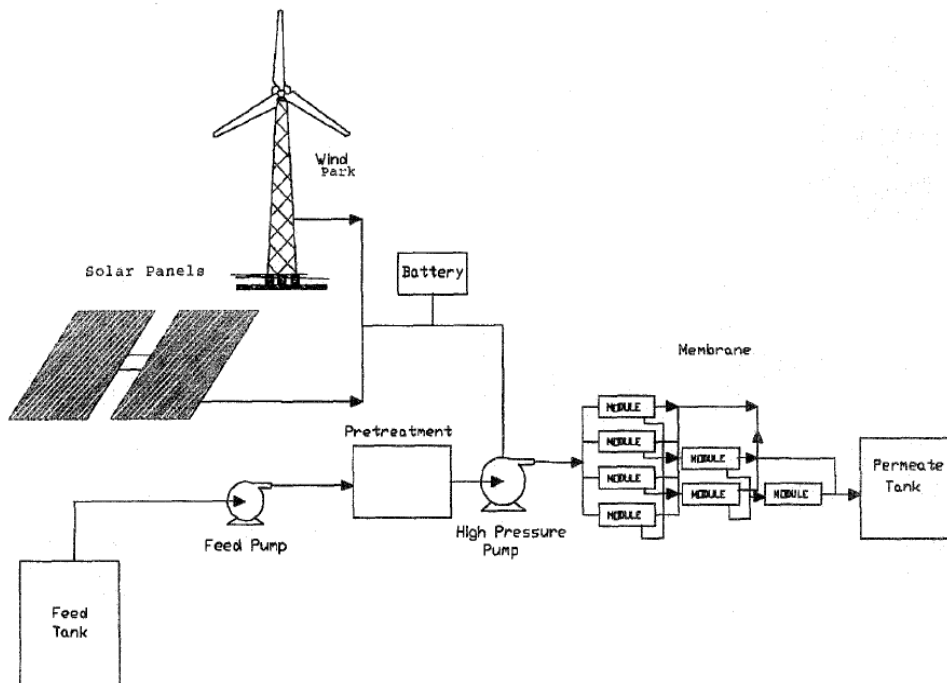

Figure 9: Schematic presentation of RO desalination plant using wind power and solar collectors [38]

Fig. 10 demonstrates the distribution of the combinations between methods of desalination and renewable energy sources.
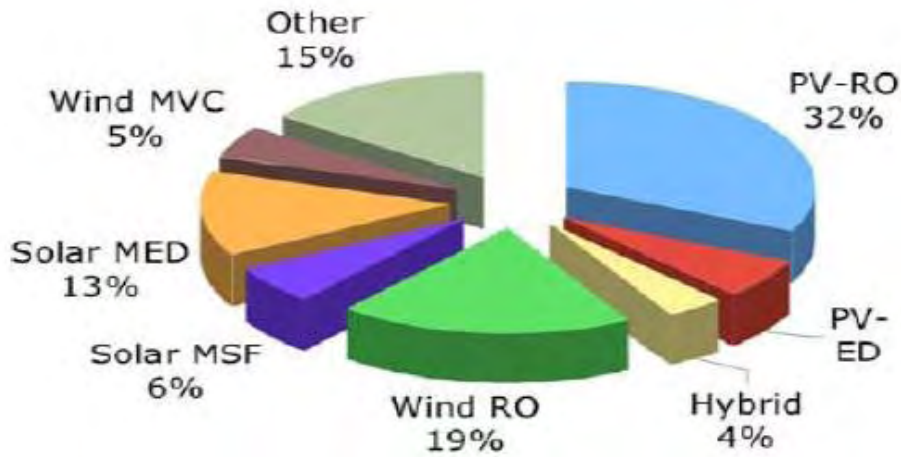
Figure 10: Combinations between desalination and renewable energy sources [63]

1.2.3 Solar Organic Rankine Cycle Plants

In the last ten years, several attempts have been made to combine Rankine cycle with PV systems. Manolakos, Kyritsis, Karagiannis and Soldatos presented an autonomous low-temperature solar Rankine cycle driven desalination plant in the International Conference on Environment, Ecosystems and Development in 2005 on Venice, Italy. [62]
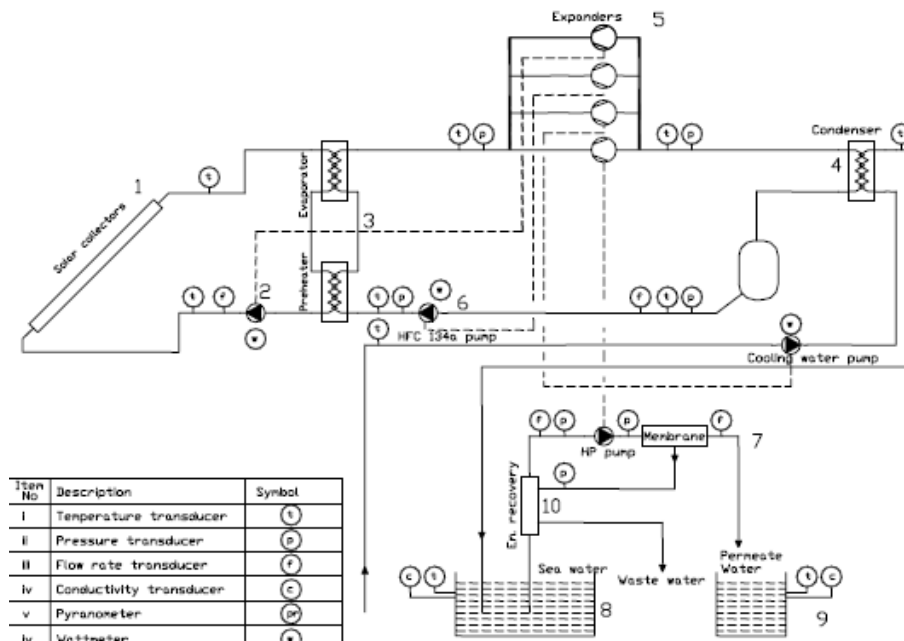
Figure 11: Schematic representation of low-temperature solar Rankine cycle system for RO desalination

Fig.11 represents the designed desalination plant. The thermal energy produced by the solar collector (1) preheats and evaporates the working fluid (HFC-134a) in the evaporator surface (3). HFC-134a enters at temperature 70^0C and it is driven to the expanders (5) at temperature 77^0C. The generated mechanical work is used to feed the RO high pressure pump, the cooling water pump, the HFC-134a pump (6) and the

circulating pump (2). The saturated vapor is led to the condenser (4) from the expanders. On the condenser surface seawater is preheated and is driven to seawater reservoir (8) and then to the RO desalination unit. [62]

Bruno et al., in 2008, designed a desalination plant with various working fluids in the ORC. The flow diagram is represented in Fig.12. The system is consisted by: the ORC, the RO unit and the solar field. The working fluid is heated to boiling and the expanded vapor is used to drive a turbine. The energy required to drive the high-pressure RO pump is provided by the expander. It also provides the energy to drive the high-pressure ORC pump and solar plant circulation plants. [25]

$$W_{turbine} + W_{rec} = W_{RO} + W_{ORCp} + W_{solarp}$$

where W_{rec} is the mechanical work recovered in RO pump.
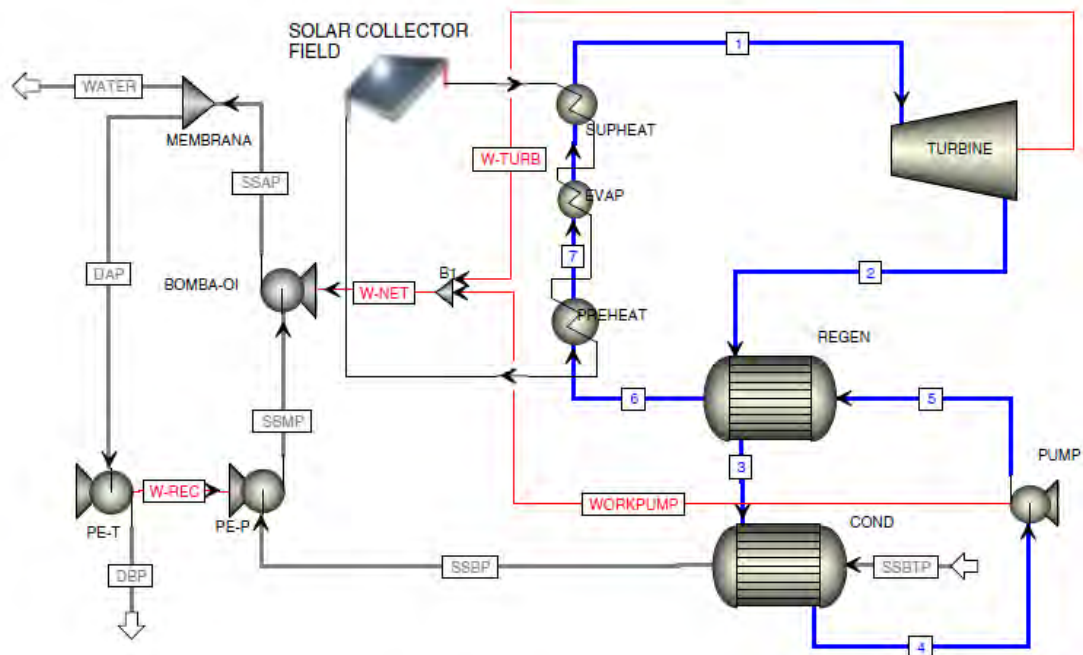
Figure 12: Integrated ORC-RO plant [25]

The working fluid, after its expansion, turns back to liquid using seawater feed as a coolant. The preheated water is driven to the RO unit and the condensed working fluid is recycled back to produce work again. [25]

In Nafey's work a combined solar organic Rankine cycle desalination process with different energy recovery units is presented. The ORC working fluid is toluene which is heated in the solar field. The superheated toluene is directed to a turbine, which produces mechanical power to drive the RO unit. The condenser unit turns back toluene to fluid and preheats the seawater that is driven to the desalination unit. Toluene is recycled back with the help of a pump to produce energy again. [53]

Figure 13: Block diagram of the ORC [52]

The solar collector efficiency, η_{col}, can be determined from its characteristic curve using as data the solar irr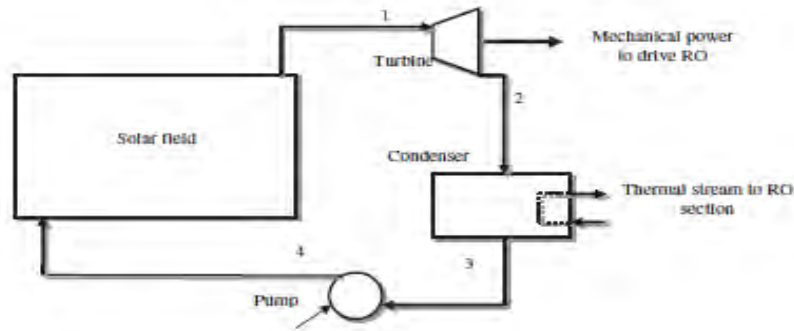adiance, mean collector temperature, T_{co}, and ambient temperature, T_{amb}. For Flat Plate Solar collector (*FPC*) and Compound Parabolic Concentrator (*CPC*), the curve is expressed by the equation: [52]

$$\eta_{col} = \eta_0 - \alpha_1 \left(\frac{T_{co} - T_{amb}}{G_b}\right) - \alpha_2 \left(\frac{T_{co} - T_{amb}}{G_b}\right)^2 G_b$$

The efficiency equation for Parabolic Trough Collectors (*PTC*) is:

$$\eta_{col} = \eta_0 - \alpha_{11}(T_1 - T_{amb}) - \alpha_{21} \left(\frac{T_1 - T_{amb}}{G_b}\right) - \alpha_{31} \left(\frac{T_1 - T_{amb}}{G_b}\right)^2$$

The collector total area, A_{col}, can be estimated as:

$$A_{col} = \frac{Q_u}{\eta_{col} G_b}$$

Where Q_u is the collector useful thermal power and G_b is the normal beam solar radiation. The collector useful thermal power can be calculated from the following relation:

$$Q_u = m_{ORC}(h_1 - h_4)$$

Table 4: Efficiency parameters for different collector types [52]

Solar collector	α_1, W/m^2	α_2, W/m^2	α_{11}, W/m^2	α_{21}, W/m^2	α_{31}, W/m^2	η_0	Operating Temperature, ^{0}C
FPC	2.9	0.0108	-	-	-	0.768	80-100
CPC	0.59	0.0019	-	-	-	0.665	120-170
PTC	-	-	4.5×10^{-6}	0.039	3×10^{-4}	0.75	170-300

The outlet enthalpy of the turbine:

$$h_2 = h_1 - \eta_t(h_1 - h_{2s})$$

and the turbine efficiency η_t is expressed by the following equation:

$$m_{ORC} = \frac{W_{turbine}}{\eta_t \eta_g (h_1 - h_{2s})}$$

The condenser heat rejection:

$$Q_{cond} = m_{ORC}(h_2 - h_3)$$

Pump work is estimated from the relation:

$$W_P = \frac{m_{ORC} \Delta P}{\rho \eta_P}$$

where ΔP is the pressure difference between condenser low pressure and turbine high pressure, ρ the density of the working fluid and η_p pump efficiency.

The pump outlet enthalpy can be estimated:

$$h_4 = \frac{W_p}{m_{ORC}} + h_3$$

1.3 Desalination processes

1.3.1 Thermal processes

Thermal processes require an amount of energy in order to form low temperature steam or hot water at temperature range of 70-120 ^{0}C. [42] The thermal distillation processes are Multi-Stage Flash (MSF) distillation, Multi-Effect Distillation (MED) and Vapor Compression (VC). [29]

The MSF distillation plant is consisted by: the seawater or brine heater, the heat recovery section and the heat rejection section. [19] When seawater enters an evacuated chamber, it turns to vapor due to a sudden pressure reduction. The process is repeated for many stages at successively decreasing temperature. [39] The MSF distillation process requires an amount of thermal energy at a low temperature, below 100 ^{0}C. [40]
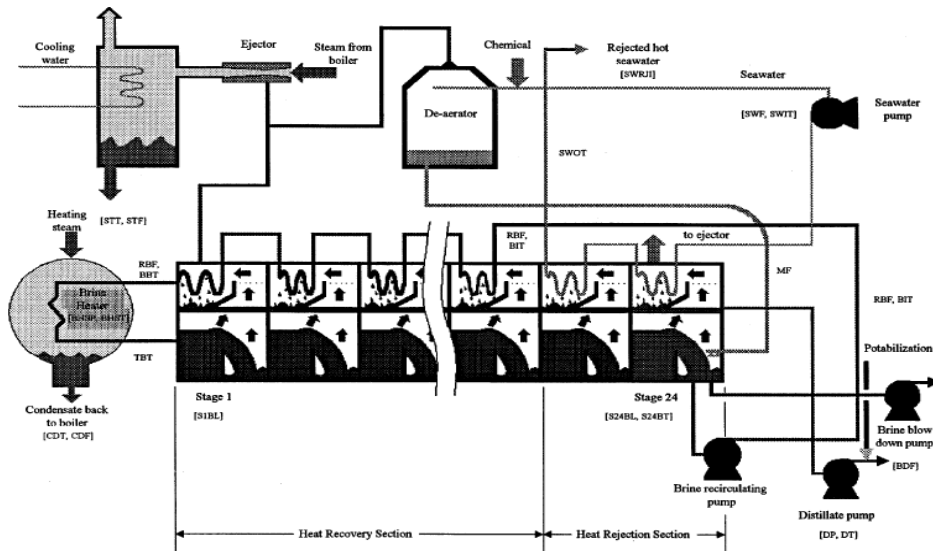
Figure 14: MSF distillation plant

The main disadvantage of this method is salt scaling. Thus, the maximum temperature is limited due to the salt concentration and this maximum limits the plant performance. [39]

The main components of MED process are the steam ejector, horizontal film evaporators (effects) and a condenser. [55] Seawater absorbs energy and vapors are generated. The steam generated at one effect heats the salt solution in the next effect due to the fact that the next effect has lower pressure and temperature. [39]
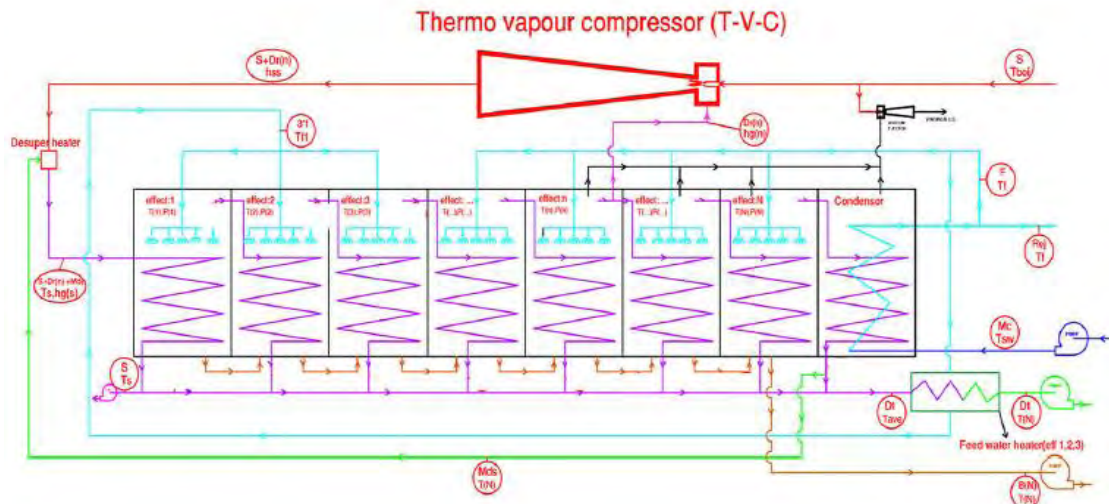
Figure 15: MED plant

On VC, part of seawater feed is compressed (Mechanical VC) or heated (Thermal VC). [32] That initial stream is used to produce more vapors from seawater. [39] The produced vapor is directed to a condenser where seawater is heated. [58]
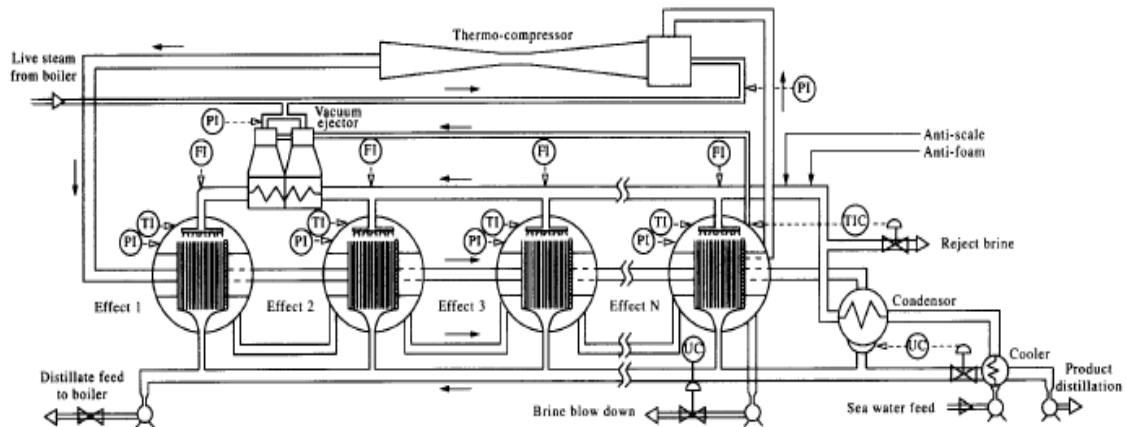
Figure 16: Thermal VC desalination plant

Finally, there are membrane distillation processes (Fig.17). Hot seawater stream passes through a semi-permeable membrane and is lead to a condensation channel. Potable water is produced by the condensation of permeate water.
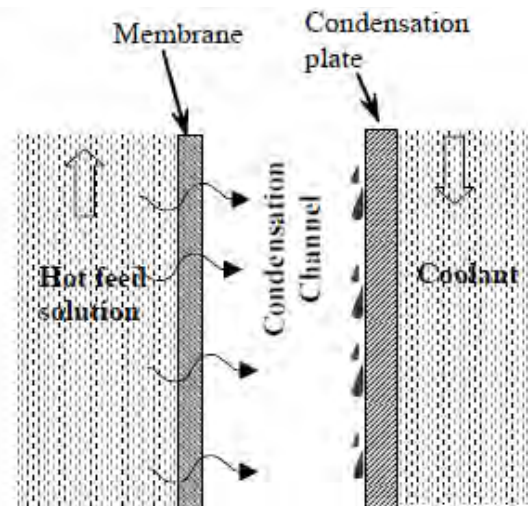
Figure 17: Principle of membrane distillation processes [51]

1.3.2 Membrane processes

The second category of industrial desalination systems is the membrane separation systems. These systems do not involve phase change, but mass transfer through a semi-permeable membrane. The most important desalination techniques are Reverse Osmosis (RO), Microfiltration (MF), Ultrafiltration (UF) and Electrodialysis (ED).[17], [39]

The main difference between RO, UF and MF processes are based on the pore size of the membranes, which is presented in Fig.18. [1]
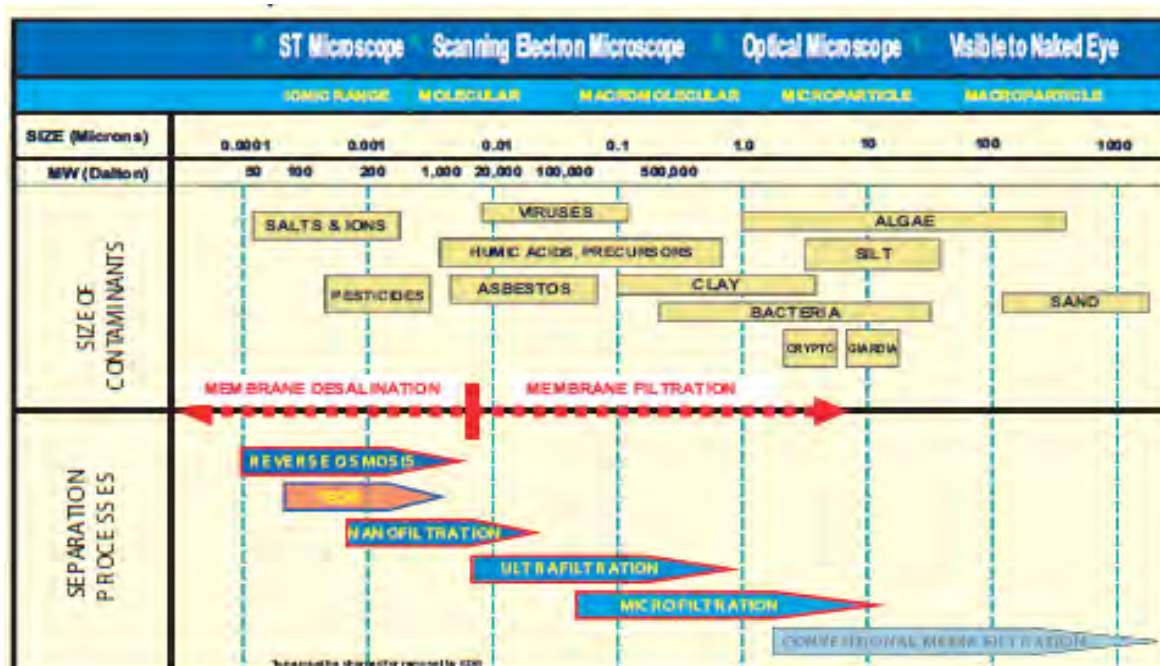
Figure 18: Membrane separation processes relative to contaminant size [66]

RO, UF and MF depend on three phenomena, which are central in order to understand these processes: osmotic pressure, solute diffusion across a membrane at constant pressure and temperature and solvent transport using a pressure difference to force pure water across a membrane. [5] Specific amount of energy is applied to a pump that increases the pressure of seawater to that required. That applied pressure is related to the concentration of the saline solution. [39]

MF method is applied to pharmaceutical industry to produce ultrapure water and to food industry in cold sterilization of beer, wine and other beverages. [2], [17] UF membranes are common in food industry to remove lactose and salts from milk [1] and as desalination pretreatment to remove colloids and macromolecules from seawater [60].

In ED, electrically charged membranes are used to separate ions from aqueous solutions under the driving force of an electrical potential difference. The ED stack is consisted by alternate cationic and anion membranes between two electrodes. The solution flows through the cells between one pair of membranes. When it is applied between the two electrodes positively charged cations move towards the cathode. They easily pass the negatively charged membrane, but not the positively charged one. Similarly, negatively charged anions pass through positively charged membrane and are retained by the negatively charged one. Due to this arrangement, ions are removed from the aqueous feed solution and are concentrated into two separate streams: concentrated effluent stream and demineralized product stream. [1], [17]
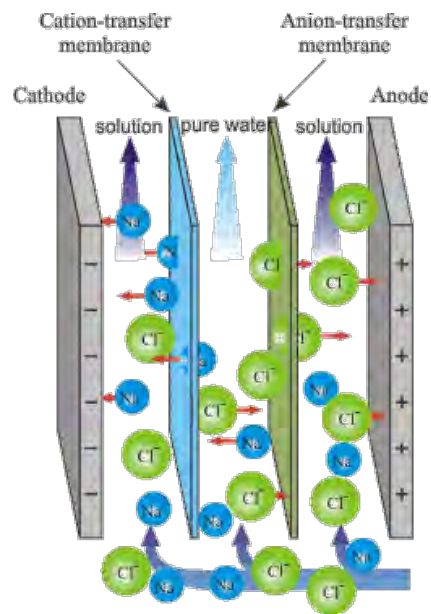
Figure 19: Electrodialysis

This method is mainly used for brackish water desalination, production of ultrapure water and the production of table salt by seawater. [1]

2. REVERSE OSMOSIS

2.1 Osmosis

In 1748 Jean-Antoine Nollet did an experiment to answer if digested food could pass through a membrane. Red wine was placed in a bladder, which was placed in a cylinder filled with water, and he waited for the red dyes to come through. Instead, the bladder swelled (and sometimes burst) and there was no red dye in the outside concentration. Today, this is explained by *The 2nd Law of Thermodynamics*: systems tend towards the maximum disorder. Another way to state this with solution is that high concentration goes to low concentration until the concentration is equal on each side of the membrane or until it is stopped by osmotic pressure. [9]
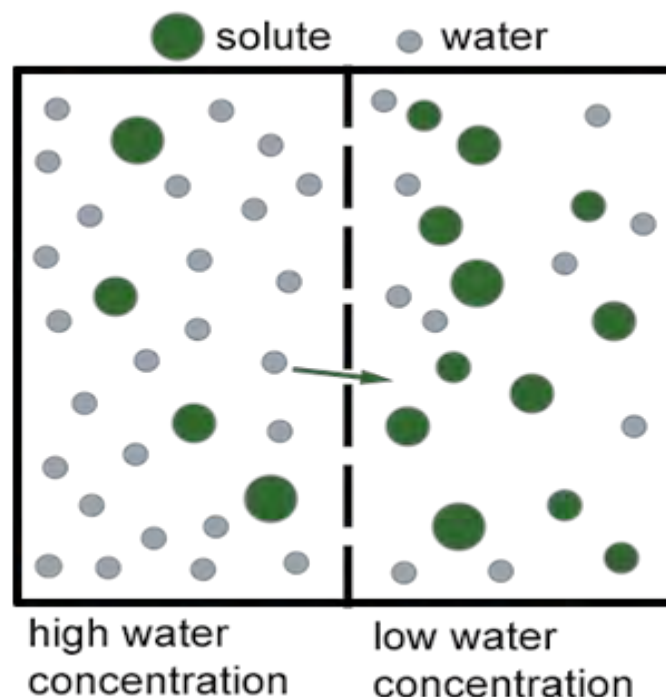
Figure 20: Osmosis [74]

Osmosis is the movement of solvent molecules through a semi-permeable membrane down a water potential gradient. [13] Figure 20 illustrates the process of osmosis. The process takes place due to a difference in thermodynamics potential. The Gibbs free energy of the solution is lower than that of the pure solvent. Because of the tendency of any system to reach equilibrium (free energy of both the solvent and the solution are equal), the driving force of osmosis is considered to be the initial difference in the free energy of the system. [9]

The required pressure difference to produce zero solvent flow is defined as osmotic pressure *Π*. [14] When the system reaches equilibrium, if the pure solvent reaches pressure P_2 and the solution pressure P_1, the osmotic pressure *Π* will be given by the equation: [17]

$$\Pi = P_1 - P_2$$

or it can be described by:

$$\Pi = -\frac{RT}{V_w} ln a_w$$

where T the operating temperature, a_w the activity of solvent in solution, V_m the partial molar volume of the solvent and R the global gas constant. [13]

Osmotic pressure can also be calculated by the following empirical equation: [3]

$$\Pi = 1.12(T + 273) \sum M'_\iota$$

With $\sum M'_\iota$ the sum of molalities of ions and nonionic compounds.

Table 5: Typical Osmotic Pressures at 25 ^{0}C [2]

Compound	Concentration, mg/L	Osmotic pressure, psi
NaCl	35000	398
Seawater	32000	340
NaCl	2000	22.8
Brackish water	2000	15

2.2 Reverse Osmosis

Reverse Osmosis (RO), also known as hyperfiltration [12], is a process where the solvent is forced through a semi-permeable membrane by an applied pressure and the undesired co-products pass through the membrane by diffusion. [10]
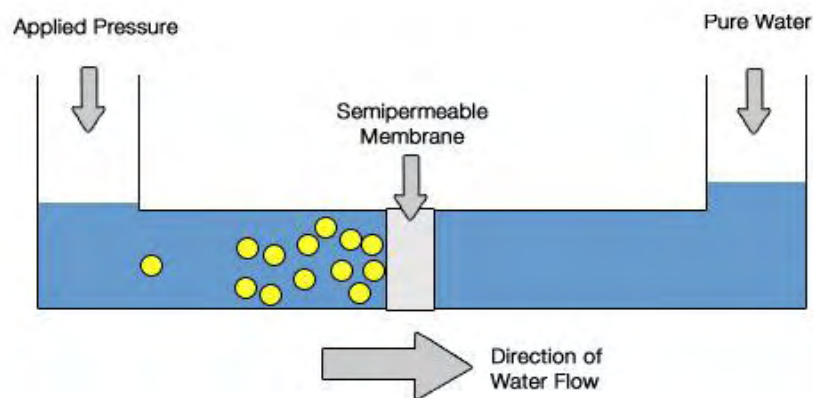
Figure 21: Reverse Osmosis [76]

Two parameters affect the RO membrane performance. The first is the flux of water through the membrane J, which is described by the equation:

$$J = k_w(\Delta P - \Delta \Pi)$$

Ioannis Kylindris

where k_w is the water permeability constant, ΔP is the pressure difference across the membrane and $\Delta \Pi$ is the osmotic pressure difference across the membrane, and

$$J_s = k_s(\Delta C)$$

where J_s is the salt flux through RO membranes, k_s is the salt permeability constant and ΔC is the salt concentration difference across the membrane. This means that the membrane performance improves as the applied pressure increases. Thus RO membranes are usually operated at high pressures. [1]

The second parameter affecting the membrane performance is the salt rejection, *SR*, defined by the equation:

$$SR = \left(1 - \frac{C_d}{C_f}\right) \times 100\%$$

where C_d is the concentration of the product water and C_f is the concentration of the feed water. [1]

Fig.22 shows the effect of pressure, temperature and water recovery on the membrane flux and the product quality of RO membranes.
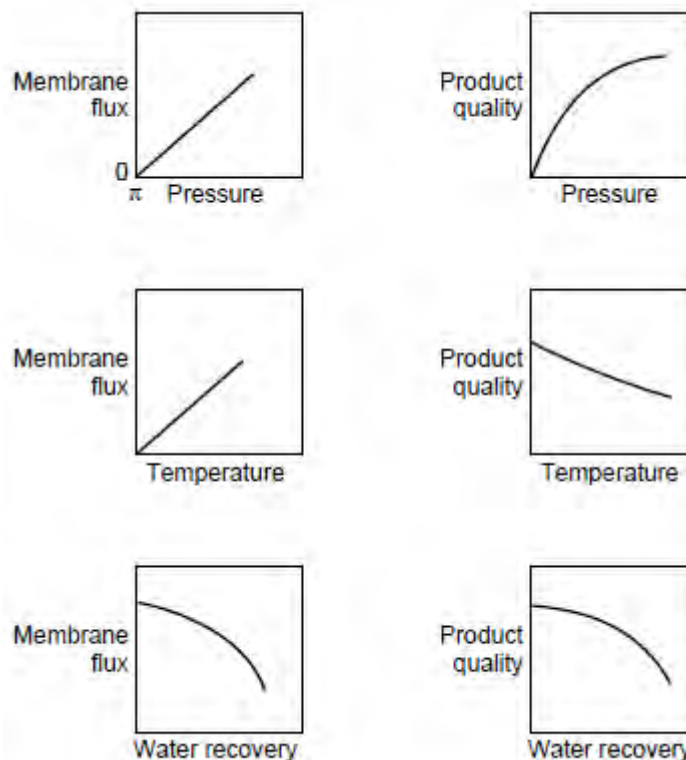
Figure 22: Schematic curves showing the effect of pressure, temperature and water recovery on membrane flux and product quality [2], [10]

Ioannis Kylindris   Page 27

2.3 Membranes

2.3.1 Membrane classification

Membranes are usually classified according to their morphology (Fig.23): dense homogeneous polymer membranes, porous membranes and thin film composite membranes. [4]
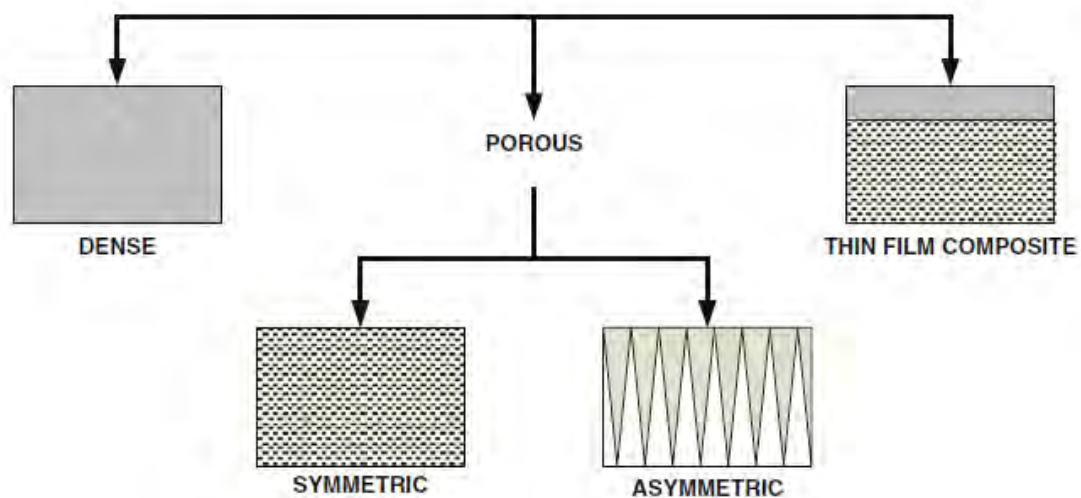
Figure 23: Membrane classification [4]

Porous membranes can be either symmetric or asymmetric. Symmetric membranes are uniformly isotropic throughout. Thus, the permeability of the membrane does not change from point to point within the membrane. [17] It must be mentioned that they can be dense or porous. [2]
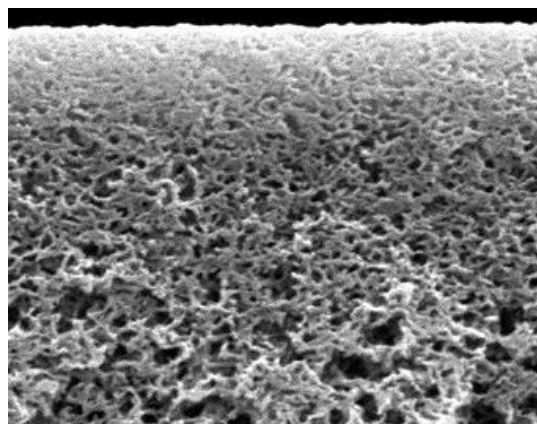
Figure 24: Porous membrane

Asymmetric membranes have a thin dense skin layer often supported on an open microporous substrate. The separation is generally performed on the surface layer, which is the main barrier to flow through the membrane. [2]
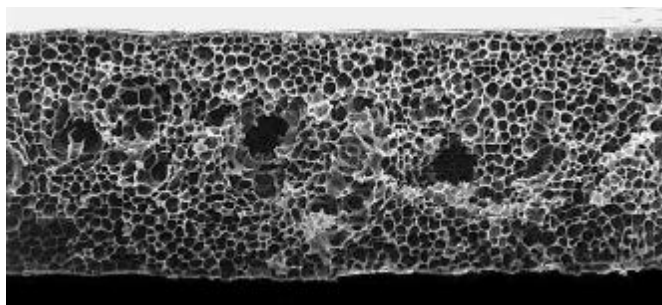
Figure 25: Porous bulk structure of an asymmetric membrane [11]

There are also ceramic and metal membranes. They can be either symmetric or asymmetric. These membranes are grouped separately from the above due to the fact that their preparation methods differ from polymeric. [2]

Finally, there are liquid membranes. These membranes' permselective barrier is a liquid phase, often with dissolved carriers. These selectively react with particular permeants to improve their transport rates through the membrane. [2]

Asymmetric and thin film composite membranes are usually applied in RO desalination. [4] Porous symmetrical membranes are used in MF and UF, while liquid membranes are used in liquid membrane processes. [2]
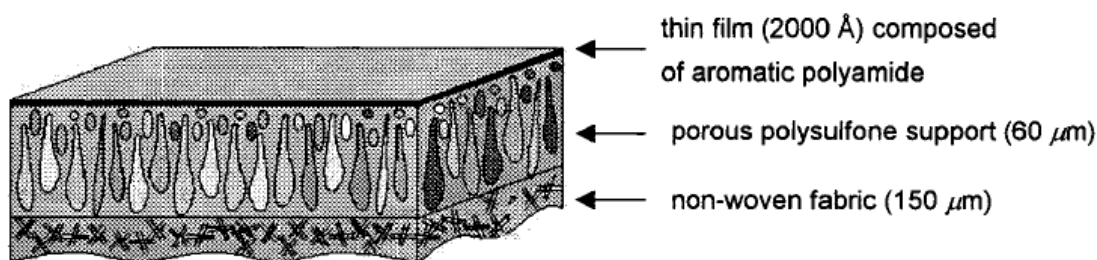
Figure 26: Schematic representation of a thin film composite RO membrane [44]

2.3.2 Membrane preparation

There are numerous techniques to produce membranes according to their classification. These processes can be either physical or chemical. [17]

Table 6: Some polymers used on membrane preparation [11]

Membrane Material	
Cellulose regenerated	UF, MF
Cellulose nitrate	MF
Cellulose acetate	RO, UF, MF
Polyamide	RO, NF, UF, MF
Polysulfone	UF, MF
Poly(ether sulfone)	UF, MF

Large numbers of RO membranes are prepared using the phase inversion method. [4] Phase inversion or solution precipitation or polymer precipitation is the most important asymmetric membrane technique, which was perfected by Loeb and Sourirajan. [13] In this method, a clear polymer solution is precipitated in two phases: the first is a solid, rich in polymer phase that forms the membrane matrix and the second is a liquid, poor in polymer phase forming the pores. [2]
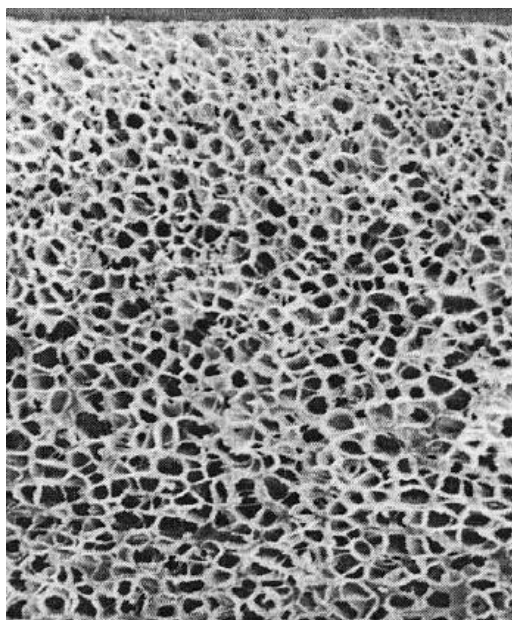
Figure 27: Loeb-Sourirajan asymmetric membrane

A hot one-phase cast solution is used to cast a film. As the cast film cools (often in 5 days [17]), it reaches the point at which polymer precipitation happens. Polymer precipitation continues with further solution cooling. The precipitation is plunged on water (Loeb-Sourirajan process) or alcohol. The membrane is prepared by partial evaporation of the solvent. [17]

Another way to produce RO membrane is by UF membrane recycling. In this chemical method, a coating is applied on a loose asymmetric membrane. It is polymerized in situ to become a salt rejecting membrane. [10]

Most common polymers that have been used to manufacture membranes are cellulose acetate (CA) and aromatic polyamide (PA). [4]

2.3.3 Mass transport through the membrane

Mass transport through a membrane demands a suitable driving force. That driving force can be for example pressure difference, concentration difference or even electric potential difference. [17] There are various theories about membrane semi-permeability and mass transport through the membrane. [14]

There are many theories attempted to explain osmosis based on the difference between the surface tensions of the solvent and the solution. Solvent permeated

Ioannis Kylindris

the membrane through the capillaries and moved from the side where the surface tension was lower to the side where the surface tension was higher. The disadvantage of this theory is that some solutions have lower surface tensions than the pure solvent, whereas with RO membranes, it always occurs from the solvent to the solution. [14]

In recent years, the main argument has been whether osmosis occurs by a diffusion mechanism or a solution-diffusion mechanism. In diffusion mechanism, permeants are separated through the pores by a pressure driven flow. Large particles are excluded from the pores, while smaller permeants pass through the membrane. [2]
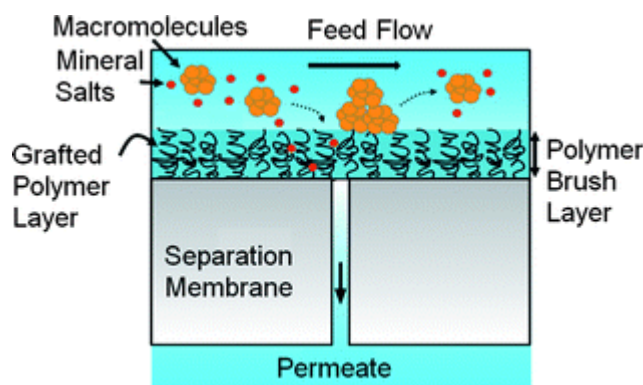
Figure 28: Diffusion transport mechanism

In solution diffusion mechanism, membranes are dense and have no fixed pores. Permeants dissolve in membrane material as in a liquid and pass through the membrane by diffusion. Separation of different permeants is achieved due their solubility difference in the membrane material and the different diffusion rate of the permeants through the membrane. [2], [14]

2.3.4 Membrane fouling
Membrane fouling is a very important which determines the operating cost and the RO unit lifetime. Properly operated membrane means longer plant lifetime and lower maintenance and operating costs. [2]

Figure 29: Membrane surface after pure water phase [46]

The most common type of fouling is because of suspended particles. RO membranes can remove dissolved solids, but they are not designed for suspended particles.

Thus, it is of major importance to remove suspended solids before they enter the RO unit. If they are not removed, they are deposited as a cake on the membrane surface. [2]
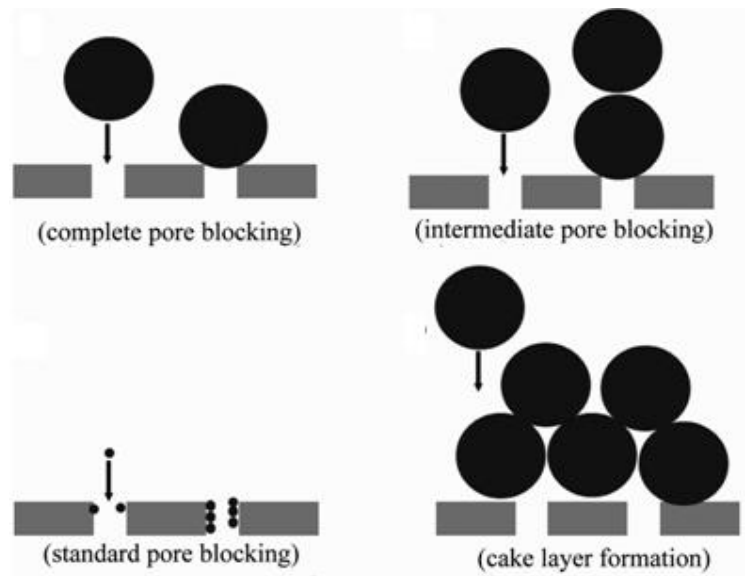
Figure 30: Fouling due to suspended particles [35]

Membrane fouling can be attributed to several independent but coexisting phenomena. Generally, the time-dependent permeate flux is: [36]

$$J_d(t) = \frac{J_{d,0}}{(1+bt)^n}$$

Where $J_{v,0}$ the initial permeate flux and *b*, *n* constants. For intermediate and complete pore blocking *n*=1 and:

$$b = k_A J_{d,0} \equiv b_1$$

Where k_A the membrane surface area blocked per unit of total permeate volume. For internal constriction with loss of open pore volume (standard pore blocking) *n*=2:

$$b = k_b J_{d,0} \equiv b_2$$

Where k_b is the decrease in the pore cross section area per unit of total permeate volume. Finally, when a cake layer is formed, *n*=0.5:

$$b = (2RS)k_c J_{d,0} \equiv b_3$$

With *RS* the cake specific resistance and $1/k_c$ the total filtrate volume per unit of membrane area.

Ioannis Kylindris

Figure 31: Biofouled spiral-wound membrane [23]

Microorganisms are present in all water systems. They tend to adhere to the membrane surface and form biofilms. As a result of this, membrane flux declines, consumed energy increases and water quality deteriorates. The accumulated effects of biofouling are increased maintenance and operational costs, deterioration of product quality and shorter membrane lifetime. [30]

Figure 32: Membrane biofouling

Concentration polarization is a factor that cannot be ignored. In this case, flux increases the mass rate of stranded particles at the membrane and cross-flow velocity decreases, leading rejected materials concentrate near the membrane to an unacceptable level (scaling). As a result of that, osmotic pressure increases with product flow decreasing. [10]
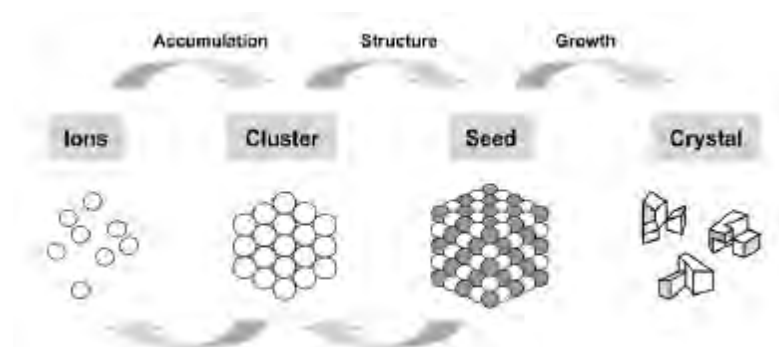
Figure 33: Scaling stages [31]

Ioannis Kylindris

In the majority of concentration polarization analyses, bulk solution is considered to be well mixed in laminar or turbulent flow. A Nerst-type film is assumed to exist (Fig.34): [54]
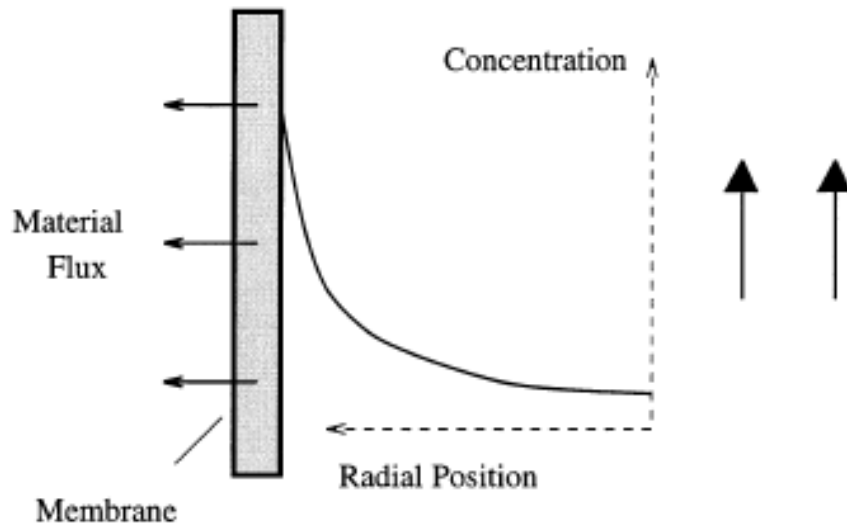
Figure 34: Radial concentration profile [50]

Mass balance:

$$VC_d + VC + D\frac{dC}{dy} = 0$$

Where *V* is the volumetric flow flux rate of water through membrane. Boundary conditions are:

At membrane surface, $C=C_w$ and $y=\delta$ (edge of bulk layer), $C=C_B$

Concentration polarization is often described as:

$$\varphi = \frac{C_w}{C_B} = \frac{\exp{(V\delta/D)}}{IR + (1-IR)\exp{(V\delta/D)}}$$

Where φ is concentration polarization factor and *IR* is intrinsic rejection. In order to eliminate the boundary layer width δ, it is assumed that δ is the same in any case of mass transfer to an impermeable wall, which allows to defining a mass transfer coefficient:

$$K = \frac{D}{\delta}$$

And:

$$\varphi = \exp\left(\frac{V}{K}\right)$$

Ioannis Kylindris   Page 34

Sherwood et al. expressed the above relation as:

$$\varphi = \exp\left(\frac{VSc^{0.66}}{j_D u_B}\right)$$

Where j_D is the Chilton-Colburn factor and u_B is the bulk velocity. For turbulent flow in round tubes $j_D=0.5f$, where f the fanning friction factor:

$$\varphi = \exp\left(\frac{2VSc^{0.66}}{f u_B}\right)$$

Finally, it must be referred that concentration polarization is often described by polarization factor Γ defined as: [8]

$$\Gamma = \frac{C_w - C_f}{C_f} = 1 - \varphi$$

And it can be estimated from correlations as the above.

2.3.5 Membrane modules

There are two main membrane modules that are widely used in the modern membrane era. The first is hollow-fiber membrane module which is a loop of fiber or a closed bundle contained in a pressure vessel. The feed fluid is pressurized from the shell side and the product passes through the fiber wall and exists via the open fiber ends. [2] Even though their design allows very large membrane areas and they are considered to be economical [2], hollow-fiber membrane modules cannot be operated in high pressures and thus are not used in RO process. [17]
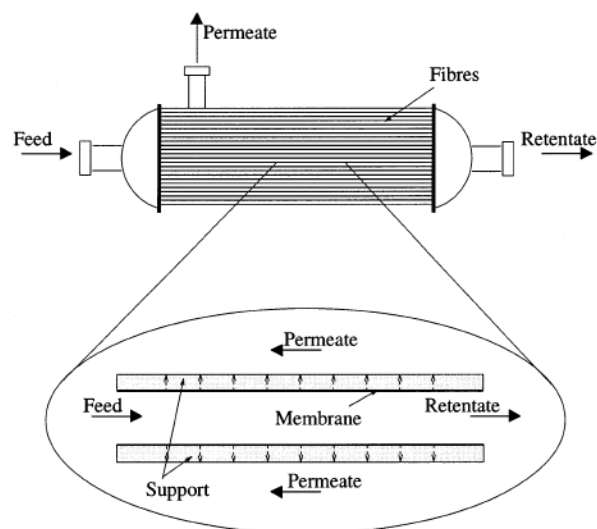
Figure 35: Flow patern in a hollow-fiber membrane module [50]

Al-Bastaki and Abbas [18] proposed the following mathematical model for hollow-fiber membrane modules:

Applying a material balance on the solution and the solute in the shell side, the following equations can be obtained:

$$\frac{dQ_b}{dR} = -2\pi R L \epsilon u_w \frac{1}{k_c}$$

$$\frac{dQ_b C_b}{dR} = -2\pi R L \epsilon u_w \frac{1}{k_c} C_d$$

Where Q_b the brine volumetric flow rate, R the fiber bundle radius, L the fiber length, $1/k_c$ the membrane area per unit volume of the fiber bundle, ε the fiber-bundle porosity and u_w the permeation velocity.

The pure water and salt water fluxes, J_w and J_s, are:

$$J_w = k_w[(P_B - P_d) - (\Pi_B - \Pi_d)]$$

$$J_s = k_s(C_M - C_d)$$

Where P is the pressure, Π is the osmotic pressure and C is the salt concentration. The subscripts B, d and M indicate the bulk solution on the high-pressure side, the distillate and the membrane surface on the high-pressure side, respectively.

Due to concentration polarization, the solute concentration at the membrane wall will be much higher than that in the bulk of the high-pressure side solution. This effect can be calculated as:

$$\varphi = \frac{C_M - C_d}{C_B - C_d} = \exp\left(\frac{u_w}{K}\right)$$

Where K is the mass transfer coefficient and it can be calculated via the *Sherwood number*:

$$Sh = \frac{1.09}{\epsilon}(Re \times Sc)^{\frac{1}{3}}$$

The permeation velocity u_w is given by the following relation:

$$u_w = \frac{J_w + J_s}{\rho_d}$$

And the distillate concentration C_d is:

$$C_d = \frac{J_s}{u_w}$$

Ioannis Kylindris

The pressure drop in the fiber bore can be calculated as:

$$\frac{dP_d}{dz} = \frac{8\mu Q_d}{\pi r_i^4}$$

The distillate flow rate Q_d can be described as follows:

$$\frac{dQ_d}{dz} = 2\pi r_o u_w$$

And it can be easily obtained:

$$\frac{d^2 P_d}{dz^2} = \frac{16\mu}{r_i^4} r_o u_w$$

Where r_i and r_o the inner and the outer fiber radius, respectively. On the shell side, the pressure drop in the radial direction can be estimated from the Ergun's equation:

$$\frac{dP_B}{dR} = 150 \frac{(1-\epsilon)^2}{\epsilon^3} \mu \frac{u_{sf}}{d_A^2} + 1.75 \frac{(1-\epsilon)}{\epsilon^3} \rho \frac{u_{sf}}{d_A}$$

Where d_A is the specific surface diameter and u_{sf} is the superficial velocity in the radial direction. The superficial velocity at the inner and at the outer diameter of the fiber bundle can be estimated as:

$$u_{sfi} = \frac{Q_f}{2\pi R_i L}$$

$$u_{sfo} = \frac{Q_f - u_w A_M}{2\pi R_o L}$$

Where Q_f the feed flow rate, A_M the membrane area, R_i the inner radius of the fiber bundle and R_o the outer radius of the fiber bundle.

The superficial velocity is estimated as:

$$u_{sf} = \frac{u_{sfi} - u_{sfo}}{\ln (u_{sfi}/u_{sfo})}$$

Finally, assuming a constant average flux, the pressure drop in the fiber bore is:

$$\Delta P_d = \frac{16\mu}{r_i^4} r_o u_w L^2$$

Ioannis Kylindris

Figure 36: Hollow-fiber membrane [75]

In this category can be classified capillary membrane modules. The main difference from hollow-fiber membrane modules is the diameter of the fiber used. Capillary membrane modules have much smaller fiber diameter than hollow-fiber modules. [17]

Spiral-wound membrane modules are mainly used in RO desalination systems. Fig.37 presents the most common and simple design, consisting of a membrane envelope wound around a permeate conducting channel. [12] The module is placed inside a pressure vessel and the feed fluid is axially circulated down the module across the membrane envelope. A part of the feed permeates into the membrane envelope, spirals towards the center of the module and exits through the collection tube. [2]
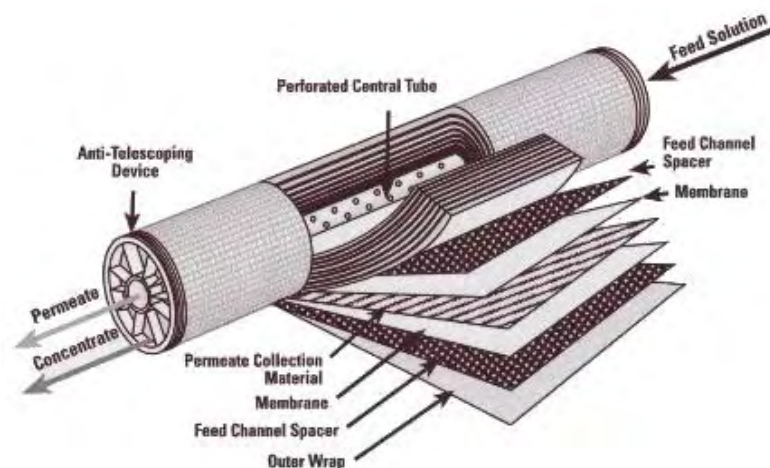
Figure 37: Spiral-wound module [78]

In the *12th International Water Technology Conference* in Alexandria, Egypt, Djebedjian, Gad, Khaled and Abou Rayan [61] presented a mathematical model of spiral-wound membrane modules based on the solution-diffusion model:

The pure water and salt water fluxes, *J_w* and *J_s*, are:

$$J_w = k_w[(P_B - P_d) - (\Pi_B - \Pi_d)]$$

$$J_s = k_s(C_M - C_d)$$

Due to concentration polarization, the steady-state water flow rate, J_w, can also be calculated as:

$$J_w = K_s ln \frac{C_M - C_d}{C_B - C_d}$$

Where K_s is the salt mass transfer coefficient. Combining the upper equations:

$$J_w = k_w\{\Delta P - b_\pi[C_B - \frac{k_s C_B \exp{(J_w/K_s)}}{J_w + k_s \exp{(J_w/K_s)}}]\exp{(J_w/K_s)}\}$$

And

$$C_d = C_B - \frac{k_s C_B}{k_s + J_w \exp{(-J_w/K_s)}}$$

Where b_π the osmotic coefficient, which can be estimated as follows:

$$b_\pi = \frac{\Pi}{C_f}$$

Where C_f the salt concentration in the feed solution and Π the osmotic pressure obtained by the equation proposed by Sourirajan: [13]

$$\Pi = 0.7949 C_f - 0.0021 C_f^2 + 7.0 \times 10^{-5} C_f^3 - 6.0 \times 10^{-7} C_f^4$$

The mass transfer coefficient K_s can be calculated by an empirical *Sherwood number* equation for spiral-wound modules:

$$Sh = 0.08 Re^{0.875} Sc^{0.25}$$

For seawater, D, μ and ρ can be expressed as:

$$D = 6.725 \times 10^{-6} \exp\left(0.1546 \times 10^{-3} C_f - \frac{2513}{273.15 + T}\right)$$

$$\mu = 1.234 \times 10^{-6} \exp\left(0.00212 C_f + \frac{1965}{273.15 + T}\right)$$

And

$$\rho = 498.4b + \sqrt{248400 b^2 + 752.4 b C_f}$$

With:

$$b = 1.0069 - 2.757 \times 10^{-4}T$$

Finally, the velocity u can be defined:

$$u = \frac{Q_f}{WDd\epsilon}$$

Where Q_f the feed flow rate, *WD* the membrane width, *d* module diameter and *ε* the membrane porosity.

Figure 38: Spiral-wound membrane module [77]

2.4 Reverse Osmosis Desalination Plants

Fig.39 presents a typical RO desalination plant. It is consisted of two parts: the first is the pretreatment unit and the second the RO unit.
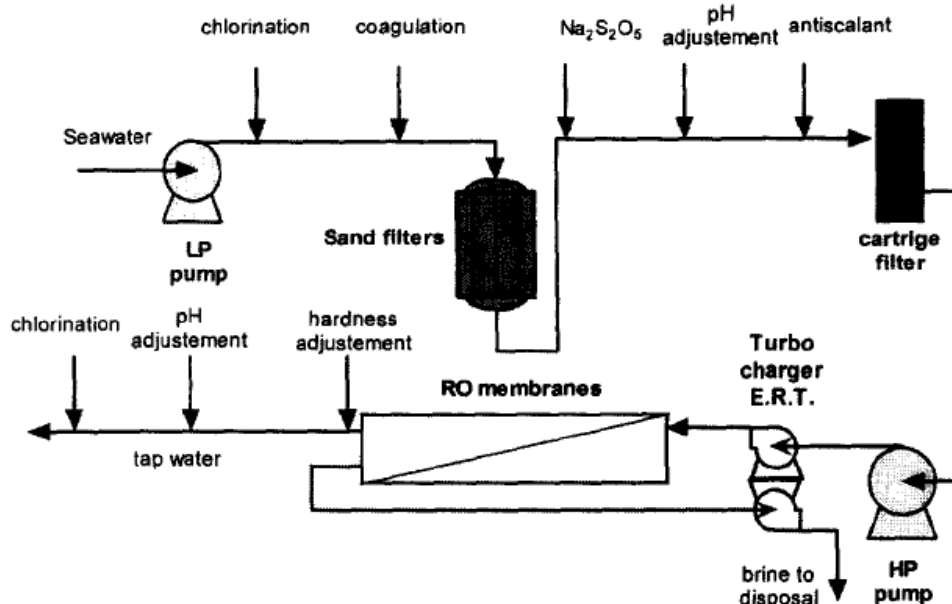
Figure 39: Typical RO desalination plant [22]

In order to remove suspended particles, seawater is chlorinated and then is driven to a Coagulation/Flocculation tank. [60] In order to achieve coagulation and flocculation, $Al_2(SO_4)_3$ and $FeCl_3$ are added, creating precipitates which can be easily removed. The water is then led to sand filters containing successive layers of thin

gravel (4-7 mm), thick sand and thin sand. [15] Ph-adjustment and addition of antiscalants may also be needed in order to prevent membrane fouling. Cartridge is the final step of the pretreatment, where particles larger than five microns are removed. [60]

In recent years, there are many studies in RO pretreatment. Wolf et al. suggested UF membrane pretreatment, where particles and pathogens are removed in one step. Another advantage of this method is that chemical dosing is reduced or eliminated. UF membrane can be cleaned with filtered water by reversing the flow from outside in to in outside. [60]
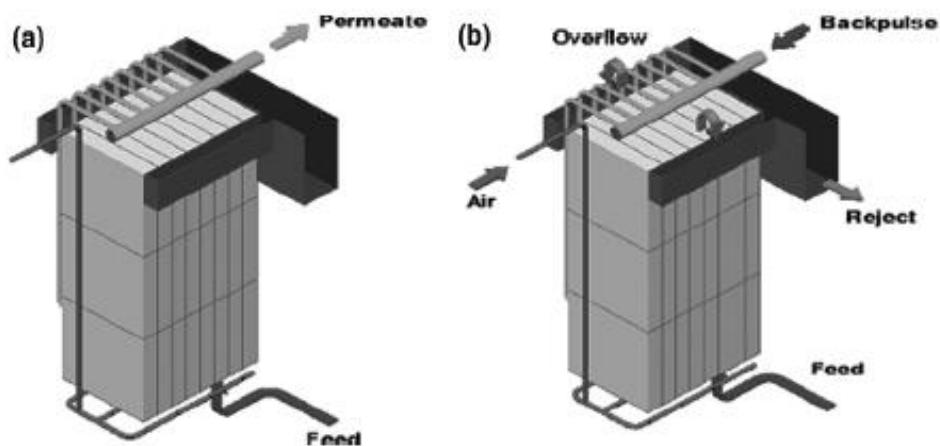
Figure 40: a; UF membrane in filtration mode. b; UF membrane in cleaning mode [60]

In the RO unit, the filtered water is lead to the membrane by a high pressure pump. There are three main plant designs for straight through operation as they are presented in Fig.41. Selection of the proper design occurs with taking into consideration the desired plant capacity and product water quality. [27]
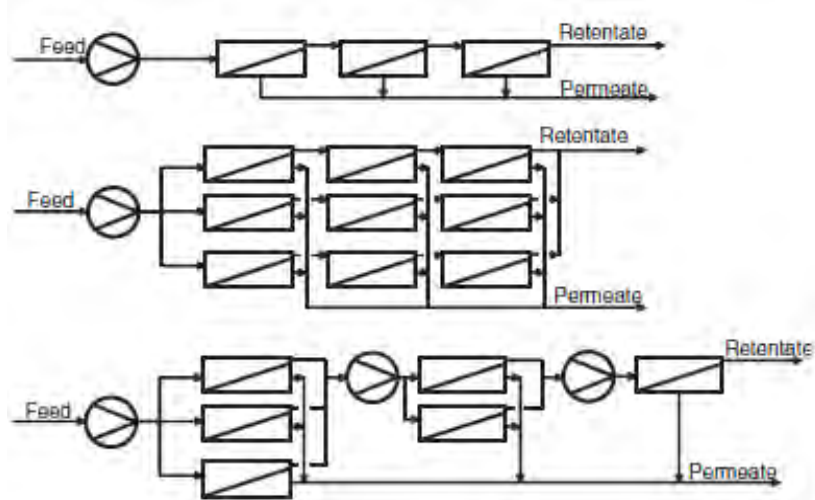
Figure 41: RO plant configurations. Top: series array. Middle: parallel array. Bottom: tapered array [27]

The basic equations for a typical RO system are: [3]

Flow balance:

$$Q_f = Q_b + Q_d$$

Plant Recovery:

$$RR = \frac{Q_d}{Q_f}$$

Material balance:

$$Q_f C_f = Q_b C_b + Q_d C_d$$

Salt Rejection:

$$SR = \frac{C_b}{C_f} \times 100 \times 100$$

Salt passage:

$$SP = 9 \frac{C_d}{C_f} \times 100 = 1 - SR$$

Voivontas et al. [58], in 2001, simulated a RO desalination process as follows:

The overall mass balance for a RO plant is:

$$Q_f = Q_b + Q_d$$

And the salt balance:

$$Q_f C_f = Q_b C_b + Q_d C_d$$

Assuming that the salt concentration is very low in the distillate stream compared to that in brine and in feed, the brine concentration is given by the following relation:

$$C_b = \frac{C_f}{1 - RR}$$

Where *RR* the plant recovery ratio described by the equation:

$$RR = \frac{Q_d}{Q_f}$$

The feed flow rate is defined as:

$$Q_f = \frac{b_M A_M (dP - d\Pi)}{RR}$$

The osmotic pressure differential $d\Pi$ can be obtained from the relation:

$$d\Pi = b\varphi C_b$$

Where b is a constant and φ is the polarization factor described as:

$$\varphi = \frac{C_{fb} + C_b}{C_b}$$

The feed-brine C_{fb} salt concentration can be calculated by:

$$C_{fb} = \frac{Q_f C_f + Q_b C_b}{Q_f + Q_b} = \frac{2}{2 - RR} C_f$$

Finally, the required work W_{ro} is calculated by the following relation:

$$W_{ro} = \frac{Q_f dP}{RR \varrho_f}$$

In 2010, Nafey et al. [52] presented the following mathematical model:

The feed mass flow rate M_f based on distillate mass flow rate M_d and recovery ratio RR is:

$$M_f = \frac{M_d}{RR}$$

And the rejected brine mass flow rate is:

$$M_b = M_f - M_d$$

The brine concentration is estimated by the equation:

$$X_b = \frac{M_f X_f - M_d X_d}{M_b}$$

And the average salt concentration:

$$X_{av} = \frac{M_f X_f - M_b X_b}{M_b}$$

The temperature correction factor *TCF* is:

$$TCF = \exp\left[2700\left(\frac{1}{273 + T} - \frac{1}{298}\right)\right]$$

Ioannis Kylindris

The membrane water permeability k_w and the salt permeability k_s are:

$$k_w = 6.87 * 10^{-8} \frac{18.6865 - 0.177X_b}{T + 273}$$

$$k_s = FF * TCF * 4.72 * 10^{-7} * \{0.06201 - [5.31 * 10^{-5}(T + 273)]\}$$

Where *FF* the membrane fouling factor. Osmotic pressures on the feed side Π_f, the brine side Π_b and the product side Π_d are calculated as follows:

$$\Pi_f = 75.84X_f$$

$$\Pi_d = 75.84X_d$$

$$\Pi_b = 75.84X_b$$

The average osmotic pressure on the feed side Π_{av} and the net osmotic pressure across the membrane ΔΠ are:

$$\Pi_{av} = 0.5(\Pi_f - \Pi_d)$$

$$\Delta\Pi = \Pi_{av} - \Pi_d$$

The pressure difference across the membrane Δ*P* is:

$$\Delta P = \frac{M_d}{3600 * TCF * FF * A_e * \eta_e * \eta_v * k_w} + \Delta\Pi$$

Where A_e the element area, n_e the number of membrane elements and n_v the number of pressure vessels. The required power for the high-pressure pump W_{ro} is:

$$W_{ro} = \frac{1000 \times M_f \times \Delta P}{3600 \times \rho_f \times \eta_p}$$

Where ρ_f is the feed flow rate density and η_p is the high-pressure pump efficiency.

3. DESALINATION PLANT

3.1 Plant description

The flow sheet diagram is presented in Fig.42. The plant is consisted of two parts: the Organic Rankine Cycle engine (ORC) which produces energy to move the second part, the Reverse Osmosis unit (RO).
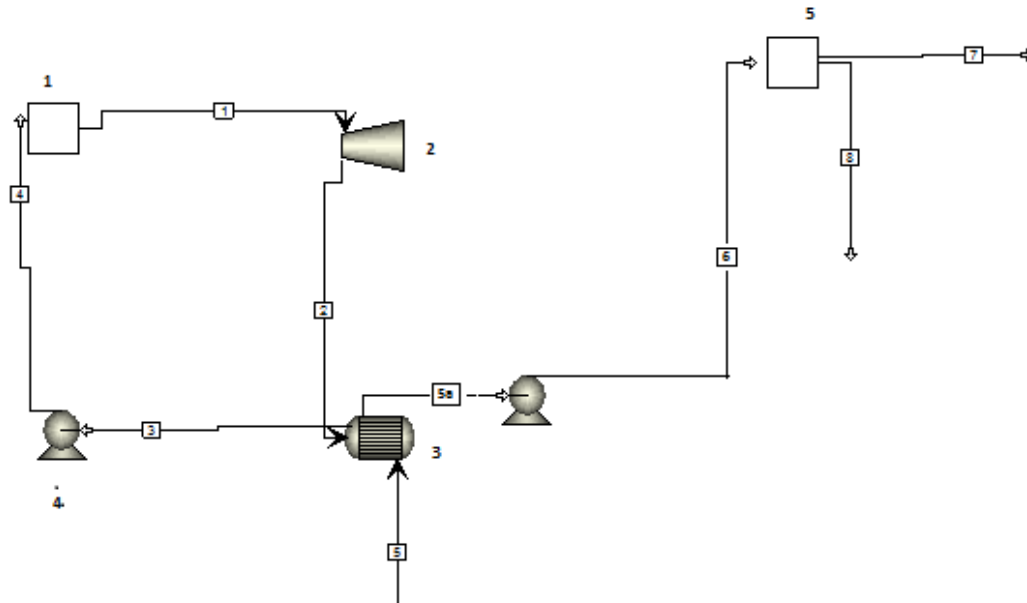
Figure 42: RO desalination plant flow diagram

The ORC is consisted of a solar collector (1), a turbine (2), a condenser (3) and a pump (4). The working fluid after being superheated in the solar collector is driven to the turbine which produces energy to drive the high pressure pump in the RO unit. The condenser turns the working fluid from superheated steam back to fluid using the incoming seawater as a coolant. Finally, a pump recycles it to produce energy again.

Figure 43: ORC engine [48]

The RO-unit is consisted of a high pressure pump and a membrane unit. After being pretreated, seawater is drawn up by a pump and is preheated in the condenser. The high pressure pump leads it to the membrane where potable and brine water are produced.

Figure 44: RO vessels [27]

3.2 Mathematical modeling

3.2.1 Organic Rankine Cycle [52]

The solar collector efficiency, η_{col}, can be determined from its characteristic curve using as data the solar irradiance, mean collector temperature, T_{co}, and ambient temperature, T_{amb}. The efficiency equation for Parabolic Trough Collectors (*PTC*) is:

$$\eta_{col} = \eta_0 - \alpha_{11} \times (T_1 - T_{amb}) - \alpha_{21} \times \left(\frac{T_1 - T_{amb}}{G_b}\right) - \alpha_{31} \times \left(\frac{T_1 - T_{amb}}{G_b}\right)^2$$

Figure 45: Parabolic trough collector [64]

The collector total area, A_{col}, can be estimated as:

$$A_{col} = \frac{W_1}{\eta_{col} \times G_b}$$

Where W_1 is the collector useful thermal power and G_b is the normal beam solar radiation. The collector useful thermal power can be calculated from the following relation:

$$W_1 = m_{ORC} \times (h_1 - h_4)$$

Table 7: *PTC* specified design parameters [52]

Working fluid	α_{11}, W/m^2	α_{21}, W/m^2	α_{31}, W/m^2	η_0	T_1, ^{0}C	T_{amb}, ^{0}C	G_b, W/m^2
Toluene	4.5×10^{-6}	0.039	3×10^{-4}	0.75	300	25.4	850

The outlet enthalpy of the turbine:

$$h_2 = h_1 - \eta_t \times (h_1 - h_{2s})$$

where subscript *s* tends to isentropic state. The turbine efficiency η_t is expressed by the following equation:

$$m_{ORC} = \frac{W_2}{\eta_t \times \eta_g \times (h_1 - h_{2s})}$$

The condenser heat rejection:

$$W_3 = m_{ORC} \times (h_2 - h_3)$$

Pump work is estimated from the relation:

$$W_4 = \frac{m_{ORC} \times \Delta P_{ORC}}{\rho \times \eta_P}$$

where *ΔP* is the pressure difference between condenser low pressure and turbine high pressure, *ρ* the density of the working fluid and η_p pump efficiency.

The pump outlet enthalpy can be estimated:

$$h_4 = \frac{W_4}{m_{ORC}} + h_3$$

Table 8: ORC specified design parameters

T_3, ^{0}C	η_g	η_t	η_p
35	0.95	0.75	0.75

Finally, the ORC efficiency is given by the relation: [41]

$$\eta_{orc} = \frac{h_1 - h_2 + h_3 - h_4}{h_1 - h_4}$$

3.2.3 RO unit [52]

A typical RO model can be described by the following equations: [3]

Flow balance:

$$Q_f = Q_b + Q_d$$

Plant Recovery:

$$RR = \frac{Q_d}{Q_f}$$

Salt balance:

$$Q_f \times X_f = Q_b \times X_b + Q_d \times X_d$$

The average salt concentration:

$$X_{av} = \frac{Q_f \times X_f - Q_b \times X_b}{Q_b}$$

The temperature correction factor *TCF* is:

$$TCF = \exp\left[2700\left(\frac{1}{273 + T} - \frac{1}{298}\right)\right]$$

The membrane water permeability k_w is:

$$k_w = 6.87 * 10^{-8}\frac{18.6865 - 0.177X_b}{T + 273}$$
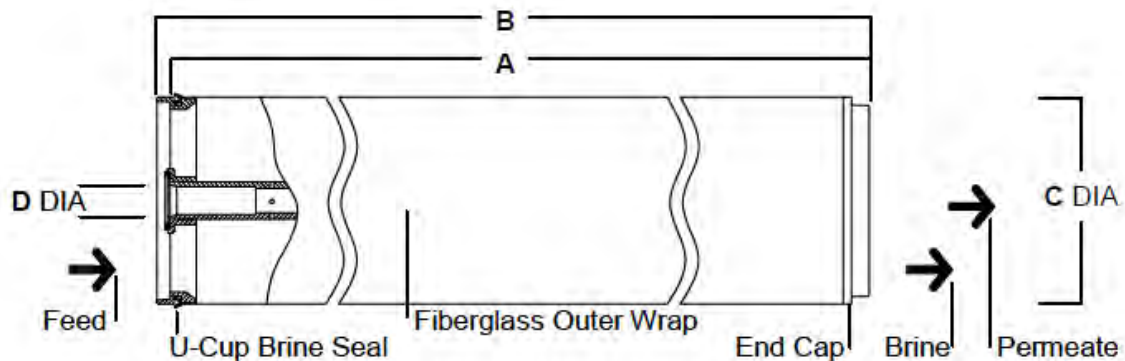
Figure 46: Dow-Filmtec spiral wound membrane [72]

Ioannis Kylindris

Osmotic pressures on the feed side Π_f, the brine side Π_b and the product side Π_d are calculated as follows:

$$\Pi_f = 75.84 X_f$$

$$\Pi_d = 75.84 X_d$$

$$\Pi_b = 75.84 X_b$$

Table 9: Membranes used classified according to their operating pressure and element area [72]

Product	Maximum operating pressure, bar	Maximum operating temperature, °C	Element area, m²	A, mm	B, mm	C, mm	D, mm
TW30-1812-24	21	45	0.08	254	298	44.5	10.5
XLE-2521	41	45	1.2	533	593	19	61
SW30-2514	55	45	0.6	356	416.2	19	61
SW30HR-380	69	45	35.4	1016	1016	201	29
SW30HRLE-370/34*i*	83	45	34.4	1016	1029	201	29
SW30XLE-440*i*	83	45	41	1016	1029	201	29

The average osmotic pressure on the feed side Π_{av} and the net osmotic pressure across the membrane $\Delta\Pi$ are:

$$\Pi_{av} = 0.5 \times \left(\Pi_f - \Pi_d \right)$$

$$\Delta\Pi = \Pi_{av} - \Pi_d$$

The pressure difference across the membrane ΔP is:

$$\Delta P = \frac{Q_d}{3600 \times TCF \times FF \times A_e \times \eta_e \times \eta_v \times k_w} + \Delta\Pi$$

Where *FF* the fouling factor, A_e the element area, n_e the number of membrane elements and n_v the number of pressure vessels. The required power for the high-pressure pump W_5 is:

$$W_5 = \frac{1000 \times Q_f \times \Delta P}{3600 \times \eta_p}$$

The potable water pressure is: [57]

$$P_7 = P_6 - \Delta P$$

Ioannis Kylindris

The specific power consumption can be calculated as:

$$SPC = \frac{W_5}{Q_d}$$

Finally, the ORC gross work is consumed by the RO unit and the ORC pump: [41]

$$W_2 = W_4 + W_5$$

Table 10: Specified design parameters of RO plant

Sea Temperature T_5, ^{o}C	Feed Sea Pressure P_5, bar	Salt Rejection, *SR*	Feed Salinity X_f, ppm
20	2	0.994	45000
Element Type	**# of pressure vessels**	**# of elements**	**Element Area A_e, m^2**
FTSW30HR-380	42	7	35.4
Feed flow rate Q_f, m^3/h	**Product flow rate Q_d, m^3/h**	**RO operation pressure P_6, bar**	**Fouling factor *FF***
468	145.8	69	0.85

3.2.4 Membrane fouling

Complete pore blocking fouling model is given by ref. [35]:

The total membrane area with open pores A_t is:

$$A_t = A_e - A_p$$

Where A_p the projected area of the suspended particles on the membrane:

$$A_p = \sigma \times m_p$$

With σ the particle projected area on the membrane surface normalized to a unit of particles and m_p the mass of particles attached to the membrane surface and cause fouling:

$$\sigma = \frac{1.5}{\rho_p \times d_p \times \psi}$$

Where ρ_p the particle density, d_p the particle diameter and ψ the particle shape factor. The mass of particles attached to the membrane m_p is given by the following relation: [26]

$$m_p = X_f \times \int_0^t u \times dt$$

Where u is the bulk velocity. And the pressure difference across the membrane ΔP becomes:

$$\Delta P = \frac{Q_d}{3600 \times TCF \times FF \times A_t \times \eta_e \times \eta_v \times k_w} + \Delta\Pi$$

The concentration polarization factor is defined as: [17], [54]

$$\varphi = \frac{X_w}{X_f}$$

With X_w the concentration of solute on the membrane surface. Hoek and coworkers estimated φ from the following relation: [34]

$$\varphi = \left[1 - SR + SR \times \exp\left(-\frac{u_p}{k_s} \right) \right]$$

With u_p the characteristic particle velocity through the membrane expressed as: [61]

$$u_p = \frac{Q_d}{3600 \times A \times d_{sp} \times \epsilon}$$

Where d_{sp} the spacer thickness, ε the membrane porosity and A the membrane element length. Concentration polarization factor affects the osmotic pressure differential, which becomes: [58]

$$\Delta\Pi = (\Pi_{av} - \Pi_d) \times \varphi$$

Table 11: Membrane fouling specified parameters [6], [61], [65]

Particle diameter d_p, m	Particle density ρ_p, kg/m^3	Shape factor ψ	Bulk porosity ε
5×10^{-9}	2147	0.8	0.9

3.2.5 Energy recovery systems

The outlet brine water is highly pressurized by the high pressure pump. [43] Thus an energy recovery system has to be used. In this study, two different energy recovery systems where investigated: a hydraulic turbine and a pressure exchanger system.

A hydraulic turbine has the same equations with a water pump and the same cost estimation as a turbine [7], [16]. So, the hydraulic turbine work is given as:

$$W_6 = \frac{Q_b \times \Delta P_{hydro}}{\eta_g \times \eta_P}$$

Where:

$$\Delta P_{hydro} = P_8 - P_9$$

With the outer brine pressure P_9 set to 1 bar for hydraulic turbine case. The outer brine enthalpy h_9 is given by the following relation:

$$h_9 = \frac{W_6}{\rho_w \times Q_b} + h_8$$

The energy mass balance becomes:

$$W_2 + W_6 = W_4 + W_5$$

In pressure exchanger case, things are much simpler. The 67% of feed seawater exchange pressure with the brine stream. [56] So, only the 33% of the original seawater is pumped, saving energy by this way: [45]

$$W_5 = \frac{0.33 \times 1000 \times Q_f \times \Delta P}{3600 \times \eta_p}$$

The outer pressure P_8 in this case is set equal to 1.8 bar.

3.3 Exergy analysis

According to *The 1st Law of Thermodynamics*, energy is conserved in any process. Unlike energy, exergy is destroyed due to irreversibilities taking place creating or increasing entropy. The exergy balance can be given by the following relation in a control volume:

$$\frac{dE}{dt} = \sum_j (1 - \frac{T_0}{T_j})Q_j - \left(W_{cv} - P_0 \frac{dV_{cv}}{dt}\right) + \sum_i m_i e_i - \sum_e m_e e_e - I$$

The first term describes the availability rate and is equal to zero in steady state condition. The second term is the availability transfer due to heat transfer between the control volume and its surroundings and the third one is equal to the value of the work produced by the control volume. The forth and the fifth term describe the inlet and the outlet availability, respectively, and *I* expresses the exergy destruction rate.

Based on the above equation, exergy analysis can be performed for every part of the flow sheet diagram. Total exergy destruction can be calculated by summing all the unit irreversibilities: [52]

$$I_{total} = I_1 + I_2 + I_3 + I_4 + I_5$$

where:

$$I_1 = A_{col} G_b \left(1 - \frac{T_{amb}}{T_{sun}}\right) + m_{orc}[h_4 - h_1 - T_{amb}(s_4 - s_1)]$$

with T_{sun}=6000 K

$$I_2 = m_{orc}[h_1 - h_2 - T_{amb}(s_1 - s_2)] - W_2$$

$$I_3 = m_{orc}[h_2 - h_3 - T_{amb}(s_2 - s_3)] + \rho Q_f[h_6 - h_5 - T_{amb}(s_6 - s_5)]$$

$$I_4 = m_{orc}[h_3 - h_4 - T_{amb}(s_3 - s_4)] + W_4$$

$$I_5 = W_5 - \rho Q_b(h_6 - h_8) + \rho Q_d(h_6 - h_7)$$

3.4 Cost analysis

Cost analysis is performed based on two parts: the solar organic Rankine cycle and the reverse osmosis unit. The amortization factor A_f is given by the following relation:

$$A_f = \frac{i(1 + i)^{LT_p}}{(1 + i)^{LT_p} - 1}$$

where i the interest rate and LT_p the plant lifetime. Table 12 shows the investment capital cost (*ICC*) and operation and maintenance costs (*O&M*) of solar Rankine cycle: [52]

Table 12: ICC and O&M costs for ORC components [52]

Unit	ICC, $	O&M, $	TCC, $/yr	$Z^{ICC\&OM}$, $/h
Solar Collector	$639,5 \times A_{col}^{0.95}$	$0.15 \times ICC_{col}$	$A_f \times (ICC + O\&M)_{col}$	$TCC_{col}/8760$
Turbine	$4750 \times W_2^{0.75}$	$0.25 \times ICC_{turbine}$	$A_f \times (ICC + O\&M)_{turbine}$	$TCC_{turbine}/8760$
Condenser	$150 \times A_{cond}^{0.8}$	$0.25 \times ICC_{cond}$	$A_f \times (ICC + O\&M)_{cond}$	$TCC_{cond}/8760$
ORC-Pump	$3500 \times W_4^{0.47}$	$0.25 * ICC_{pump}$	$A_f \times (ICC + O\&M)_{pump}$	$TCC_{pump}/8760$

For the RO unit, Malek et.al. provide a simple mathematical model including seawater intake and pretreatment cost (CC_{swip}). It is presented in Table 13: [47]

Table 13: ICC and O&M costs for RO unit [47]

DCC, $	ICC, $	TCC, $	ACC, $/yr	O&M, $/yr	$Z^{IC\&OM}$, $/hr
$CC_{swip}=996 \times Q_f^{0.8}$	$0.27 \times DCC$	$ICC+DCC$	$TCC \times A_f$	$OC_{PWR}=LF \times 0.06 \times SPC \times Q_d$	$(ACC+OC_{RO})/8760$
$CC_{hpp}=393000+10710 \times \Delta P$				$OC_{LB}=LF \times 0.1 \times Q_d$	
$CC_e=Fe \times P_p \times N_p + Fe \times PV_p \times n_v$				$OC_{CHM}=LF \times 0.04 \times Q_d$	
$CC_{eqp}= CC_{swip}+ CC_{hpp}+ CC_e$				$OC_{INS}=0.005 \times TCC \times A_f$	
$CC_{site}=0.1 \times CC_{eqp}$				$OC_{MMB}=P_P \times N_P/LT_m$	
$DCC= CC_{eqp}+ CC_{site}$				$OC_{RO}= OC_{PWR}+ OC_{LB}+ OC_{CHM}+ OC_{INS}+ OC_{MMB}+OC_e$	

Finally, the specific total cost for the ORC-RO desalination plant can be calculated by the equation:

$$C_t = \frac{C_{ORC} + C_{RO}}{M_d}$$

Table 14: Specified economic parameters

Interest rate, i	Plant lifetime, LT_p	Membrane lifetime, LT_m
0.05	20	5
Corrective factor, Fe	**Load factor, LF**	**Number of permeators, N_p**
1	0.9	6

3.5 Assumptions

> 5% pressure drop is considered in the solar field, the condenser and the RO unit:

$$P_3=0.95 \times P_2$$
$$P_6=0.95 \times P_5$$
$$P_8=0.95 \times P_6$$

> Condenser area A_{cond} is set to 66 m^2. [53]
> Mediterranean Sea temperature is 15 ^{0}C in the winter months and 25 ^{0}C in the summer months. [70] So T_5 is set to 20 ^{0}C.
> Feed salinity, brine and distillate water enthalpies were calculated with the help of ref. [52] presented in Appendix B.

- ➢ Inlet pump temperature is set equal to outer temperature:
$$T_3 = T_4$$
- ➢ Inlet RO temperature is considered equal to outer temperatures:
$$T_6 = T_7$$
$$T_6 = T_8$$
- ➢ Permeator price is calculated as: [49]
$$P_p = 10000 \times A_e$$
- ➢ Pressure vessel price is estimated by the following relation: [33]
$$PV_p = 3 \times W_5$$
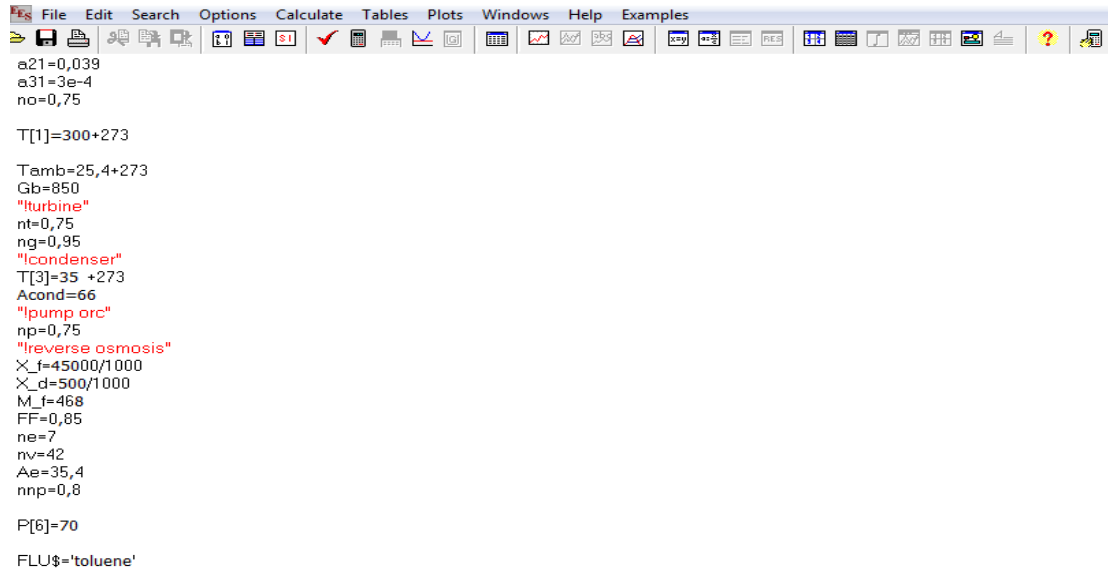
4. RESULTS
4.1 EES [71]

The problem was solved with Engineering Equation Solver (*EES*) version 7.2 and *EES Demo 2009*.

Figure 47: *EES* equation window

EES is a general equation-solving program that can numerically solve thousands of coupled non-linear algebraic and differential equations. The program can also be used to solve differential and integral equations, do optimization, perform linear and non-linear regression, convert units, check unit consistency, and generate publication-quality plots. A major feature of *EES* is the high accuracy thermodynamic and transport property database that is provided for hundreds of substances in a manner that allows it to be used with the equation solving capability.
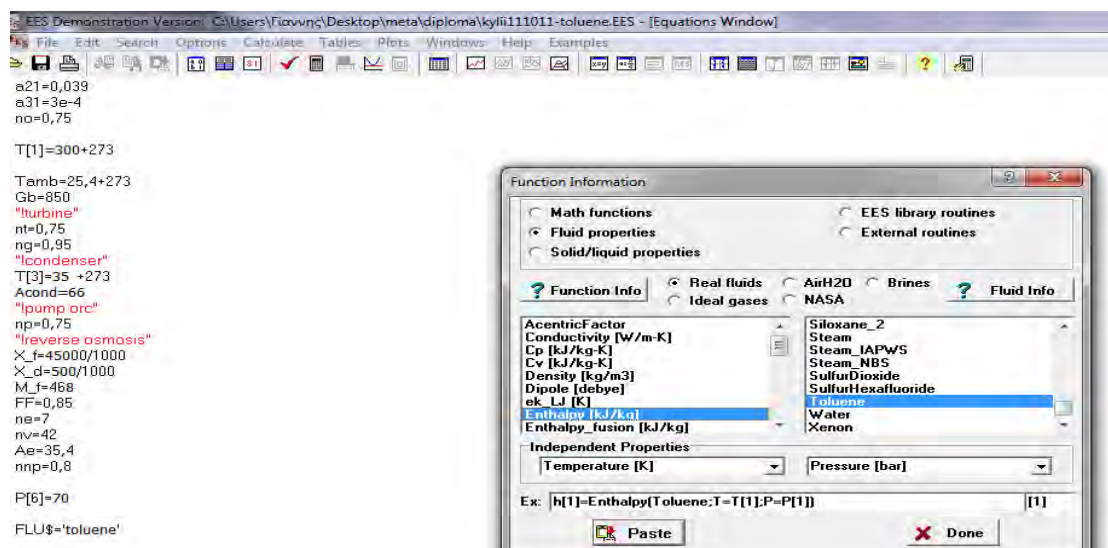
Figure 48: Fluid properties window

EES is particularly useful for design problems in which the effects of one or more parameters need to be determined. The program provides this capability with its *Parametric Table*, which is similar to a spreadsheet. First, the user identifies the design variables by entering their values in the table cells. *EES* then calculates the values of the dependent variables in the table.

4.2 Program development

The first step was to develop the *EES* code for ref. [52]. Toluene T-s relation for the ORC-unit is the following diagram:
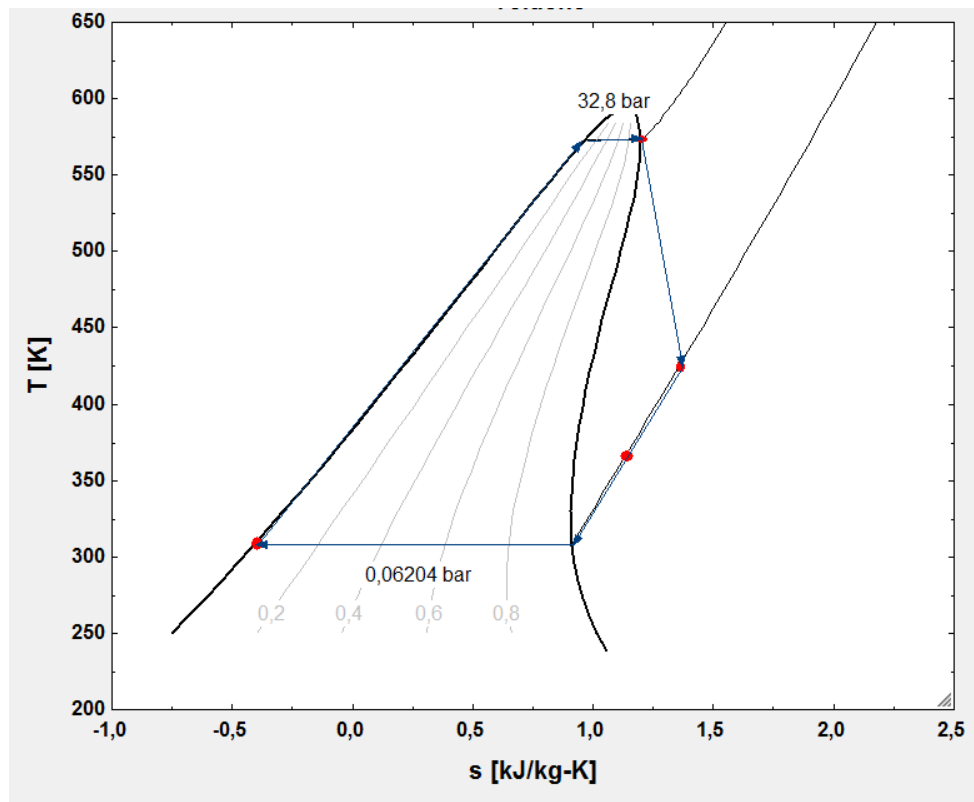
Diagram 1: ORC T-s diagram for toluene as working fluid

The second step was to determine recovery ratio *RR* and brine/potable water pressure as specified design parameters. Also, it is determined that the gross work is consumed by both the RO unit and ORC pump work. The results are presented in the following tables:

Table 15: Present results

Cycle flow rate, m_{orc}, kg/s	Collector area A_{col}, m²	ORC-pump required energy W_4, kW	High pressure pump required energy W_5, kW
5.932	6971	31.96	1133
Specific Power Consumption *SPC*, kWh/m³	Total Exergy Destroyed I_{total}, MW	Specific Total Cost C_t, $/m³	
8.073	5.007	0.9413	

Table 16: Arrays table

	Pressure, bar	Temperature, ^{0}C	Enthalpy, kJ/kg	Entropy, kJ/kg K
1	32.8	300	599.4	1.195
2	0.06531	148.8	423.6	1.341
3	0.06204	35	-141.3	-0.4088
4	34.52	35	135.9	-0.4131
5	2	20	81.56	0.294
6	69	25.65	107.4	0.3721
7	-0.751	25.65	114.3	
8	65.55	25.65	104.5	

The next step was to determine product flow rate equal to 140 m^3/h and *RR* equal to 0.3. Results are presented in the following tables:

Table 17: Present results with product flow rate determined

Cycle flow rate, m_{orc}, kg/s	Collector area A_{col}, m^2	ORC-pump required energy W_4, kW	Feed flow rate Q_f, m^3/h
5.908	6943	31.83	466.7
High pressure pump required energy W_5, kW	**Specific Power Consumption *SPC*, kWh/m^3**	**Total Exergy Destroyed I_{total}, MW**	**Specific Total Cost C_t, $/m^3**
1129	8.063	4.986	0.9429

Table 18: Arrays table with product flow rate determined

	Pressure, bar	Temperature, ^{0}C	Enthalpy, kJ/kg	Entropy, kJ/kg K
1	32.8	300	599.4	1.195
2	0.06531	148.8	423.6	1.341
3	0.06204	35	-141.3	-0.4088
4	34.52	35	135.9	-0.4131
5	2	20	81.56	0.294
6	69	25.64	107.4	0.372
7	-0.6682	25.64	114.2	
8	65.55	25.67	104.4	

The fourth step was to add the membrane fouling model which is consisted of two parts: complete pore blocking and concentration polarization. This model develops with time, thus at the beginning of each year different results were obtained. As expected, due to fouling more energy is needed and thus greater collector area should be used.
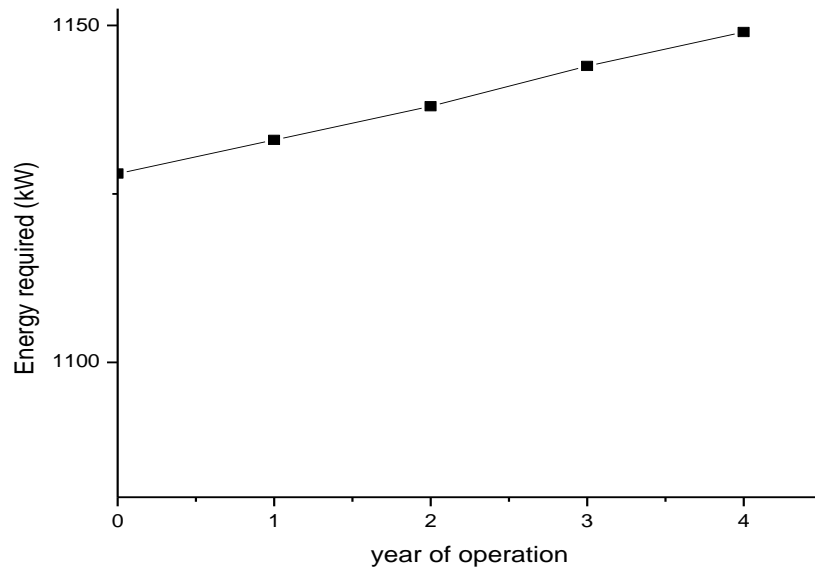
Diagram 2: Slight raise of high pressure pump required energy with the development of time

Finally, the two energy recovery systems were studied. The desalination plant flow diagram using a hydraulic turbine as energy recovery system is presented on Figure :
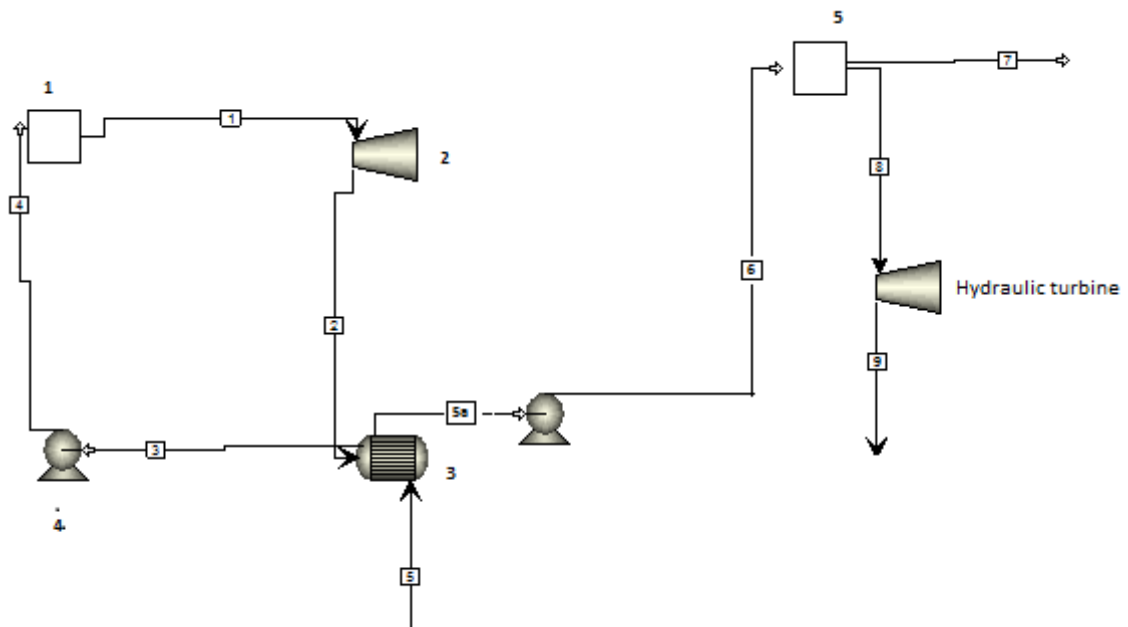
Figure 49: RO desalination plant flow diagram using a hydraulic turbine as energy recovery system

The results for the *EES* code with hydraulic turbine as energy recovery system are the following:

Table 19: Present results using a hydraulic turbine as energy recovery system

Cycle flow rate, m_{orc}, kg/s	Collector area A_{col}, m^2	ORC-pump required energy W_4, kW	Feed flow rate Q_f, m^3/h
1.549	1821	8.346	466.7
High pressure pump required energy W_5, kW	**Specific Power Consumption SPC, kWh/m^3**	**Total Exergy Destroyed I_{total}, MW**	**Specific Total Cost C_t, \$/m^3**
1072	7.66	2.908	0.8041

Table 20: Arrays table using a hydraulic turbine as energy recovery system

	Pressure, bar	Temperature, ^{0}C	Enthalpy, kJ/kg	Entropy, kJ/kg K
1	32.8	300	599.4	1.195
2	0.06531	148.8	423.6	1.341
3	0.062	35	-141.3	-0.4088
4	34.52	35	135.9	-0.4131
5	2	20	81.56	0.294
6	69	21.52	88.33	0.3141
7	2.814	21.52	94.21	0.3156
8	65.55	21.58	85.8	0.315
9	1	23.61	94.88	0.3452

The flow diagram with a pressure exchanger becomes:
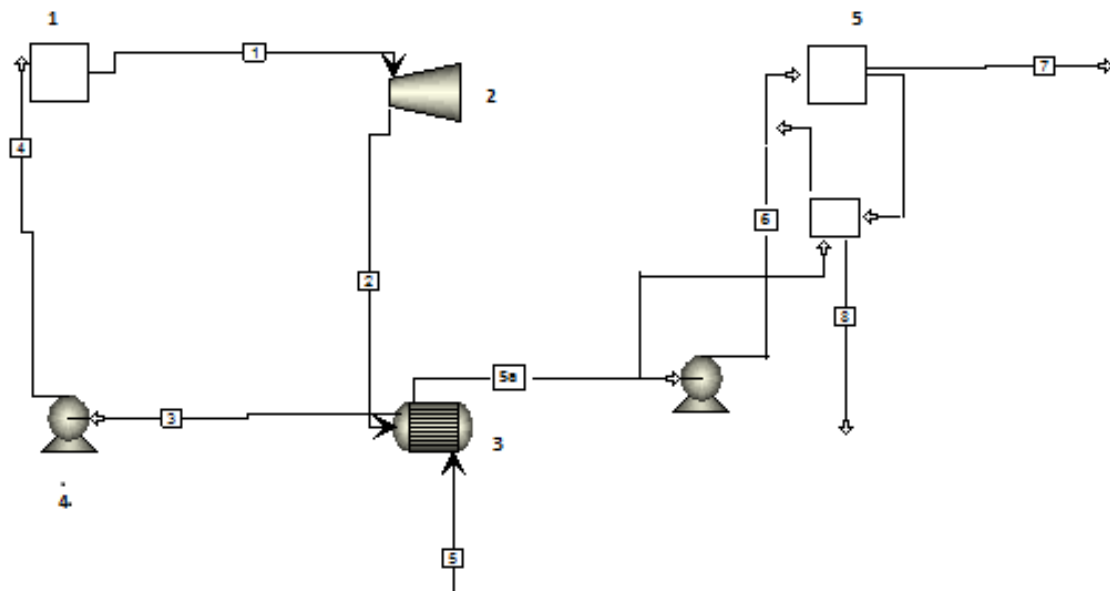
Figure 50: Desalination plant flow diagram using a pressure exchanger as energy recovery unit

And the results are:

Table 21: Present results using a pressure exchanger as energy recovery system

Cycle flow rate, m_{orc}, kg/s	Collector area A_{col}, m^2	ORC-pump required energy W_4, kW	Feed flow rate Q_f, m^3/h
1.859	2184	10.01	466.7
High pressure pump required energy W_5, kW	**Specific Power Consumption SPC, kWh/m^3**	**Total Exergy Destroyed I_{total}, MW**	**Specific Total Cost C_t, \$/m^3**
355.2	2.537	1.265	0.7595

Table 22: Arrays table using a pressure exchanger as energy recovery system

	Pressure, bar	Temperature, ^{0}C	Enthalpy, kJ/kg	Entropy, kJ/kg K
1	32.8	300	599.4	1.195
2	0.06531	148.8	423.6	1.341
3	0.062	35	-141.3	-0.4088
4	34.52	35	135.9	-0.4131
5	2	20	81.56	0.294
6	69	21.82	89.68	0.3183
7	2.575	21.82	95.64	0.3199
8	1.8	21.87	88.61	0.3207

4.3 Parameter analysis

Parameter analysis was made using the program without energy recovery system or membrane fouling. With this way, problems can be solved simpler and optimization parameters can be detected easier. All diagrams were constructed with *OriginPro 8.5*.

4.3.1 Recovery ratio

Recovery ratio *RR* affects many thermo-economic variables as long as the plant size depends on it. From bibliography, *RR* varies between 0.1 and 0.5. [6]
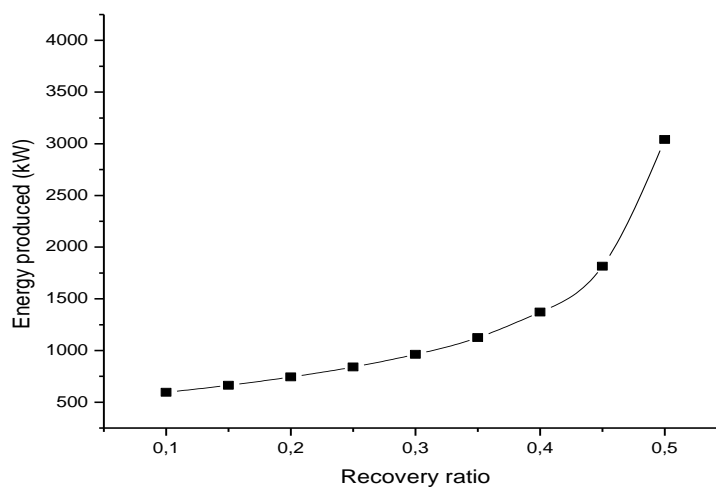
Diagram 3: Effect of recovery ratio on turbine work

Diagram 3 illustrates the relationship between RR and turbine work produced W_2: with the growth of RR (and so the Q_d) more power is needed to be generated by the ORC-cycle.

The effect of RR on the high pressure pump required energy, W_5, is presented on Diagram 4:
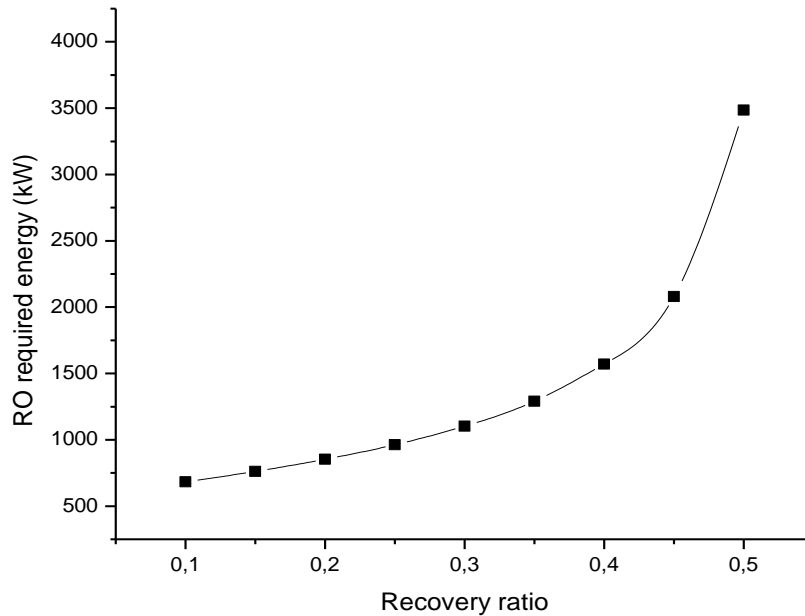
Diagram 4: Effect of recovery ratio on high pressure pump required energy

Which is reasonable considering that the more distillate product produced, the more pressure applied and the more energy required.

Diagram 5 illustrates the effect of RR on specific power consumption SPC:
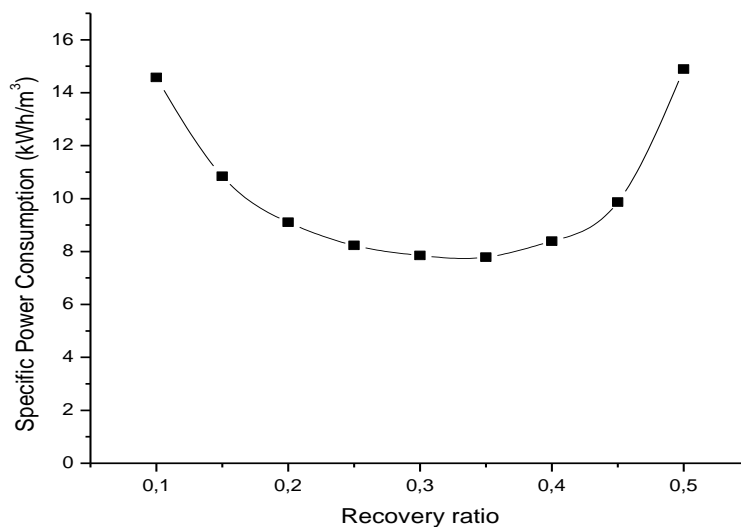
Diagram 5: Specific power consumption on varying recovery ratio

From the diagram above, it is obvious that the least energy consumed by the membrane can be achieved for *RR* around 0.3-0.35. On the other hand, total exergy destruction, I_{total}, increases with the growth of *RR*:
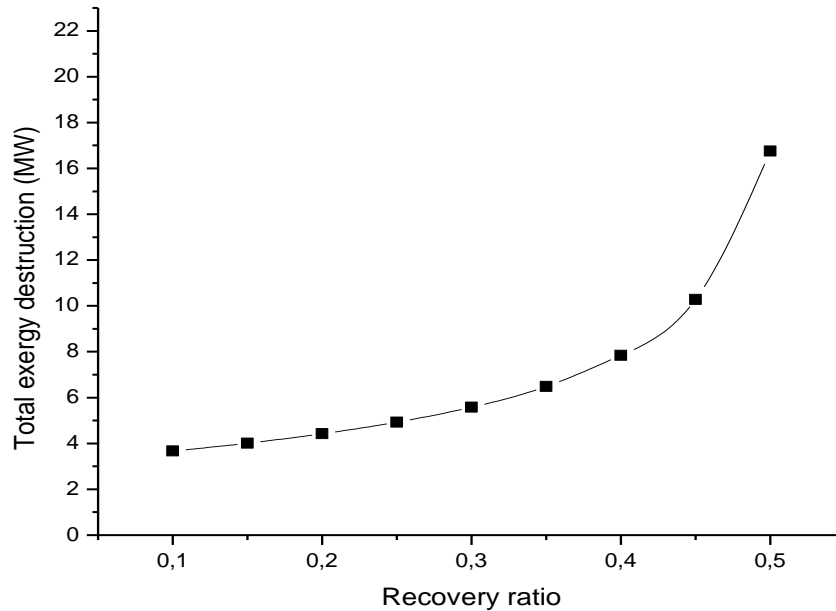
Diagram 6: Raise of irreversibility with the raise of recovery ratio

Finally, the specific total cost, C_t:
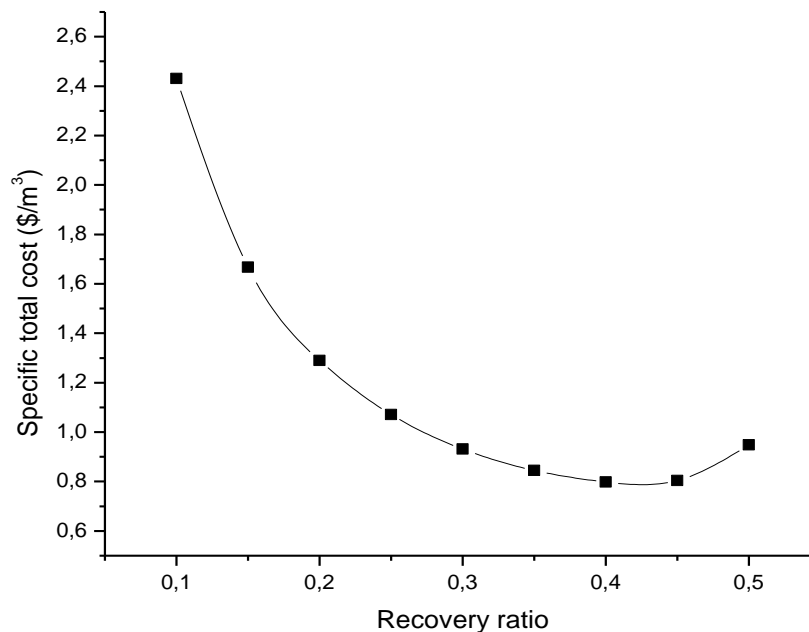
Diagram 7: Relation of recovery ratio and specific total cost

From Diagram 6, it can be assumed that *SPC* minimizes for *RR* around 0.4-0.45.

Ioannis Kylindris   Page 64

4.3.2 Operating temperature

Operating temperature T_1 varies between 170 and 300 ^{0}C. [52] Diagrams 8-11 show that with the raise of T_1, ORC flow rate m_{orc}, total irreversibility I_{total}, specific total cost C_t and net pressure difference across the membrane ΔP_n slightly decrease:
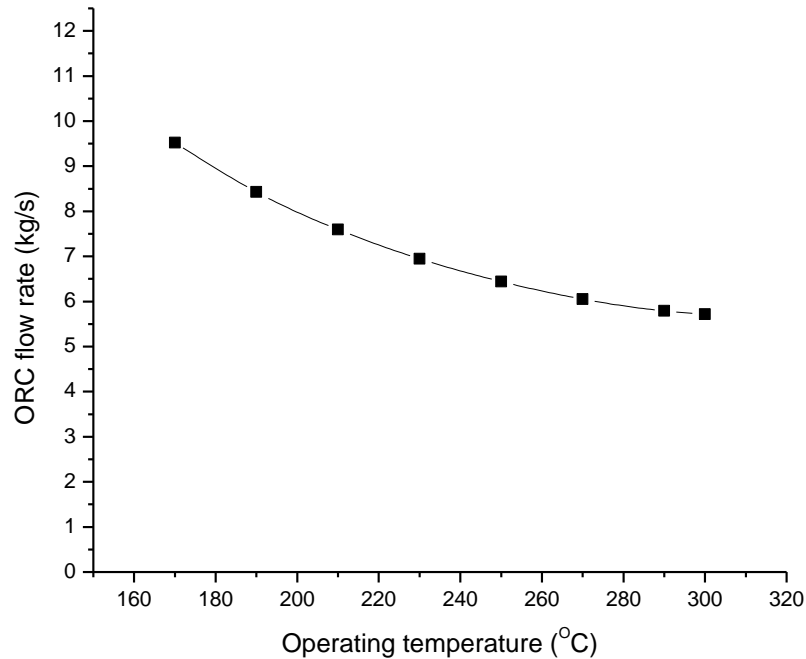
Diagram 8: Effect of operating temperature on ORC flow rate
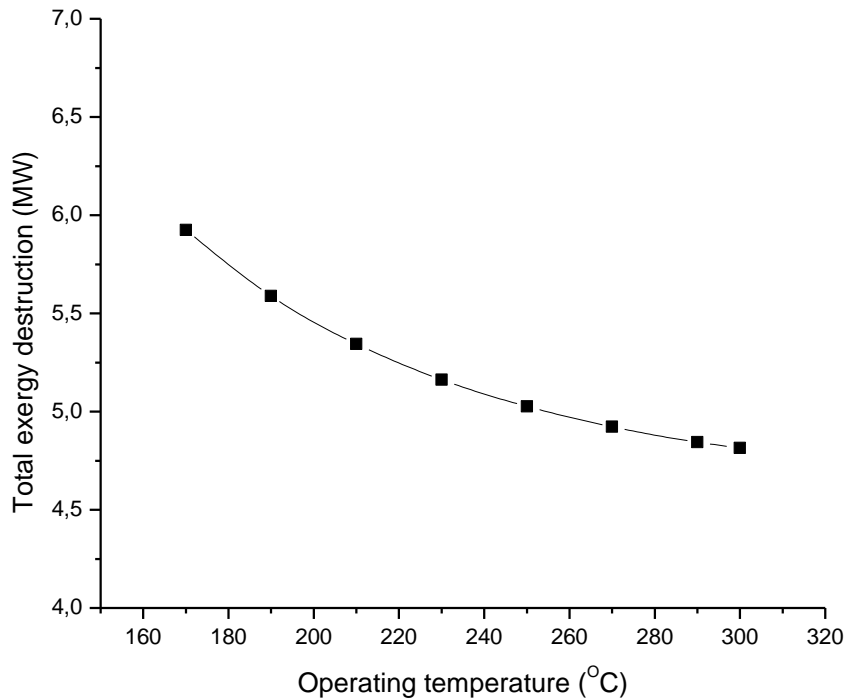
Diagram 9: Relation between operating temperature and total exergy destruction
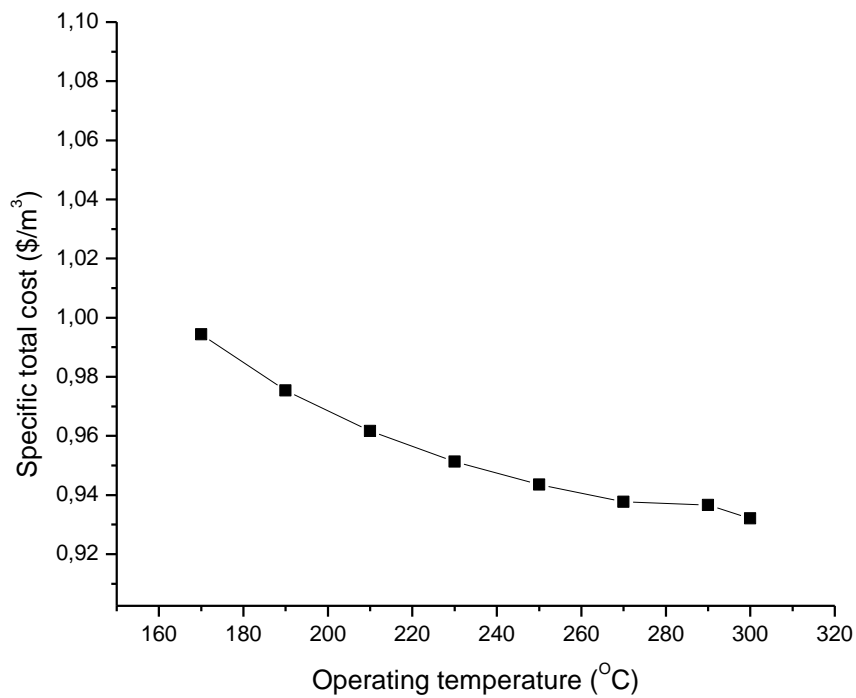
Diagram 10: Specific total cost on varying operating temperature
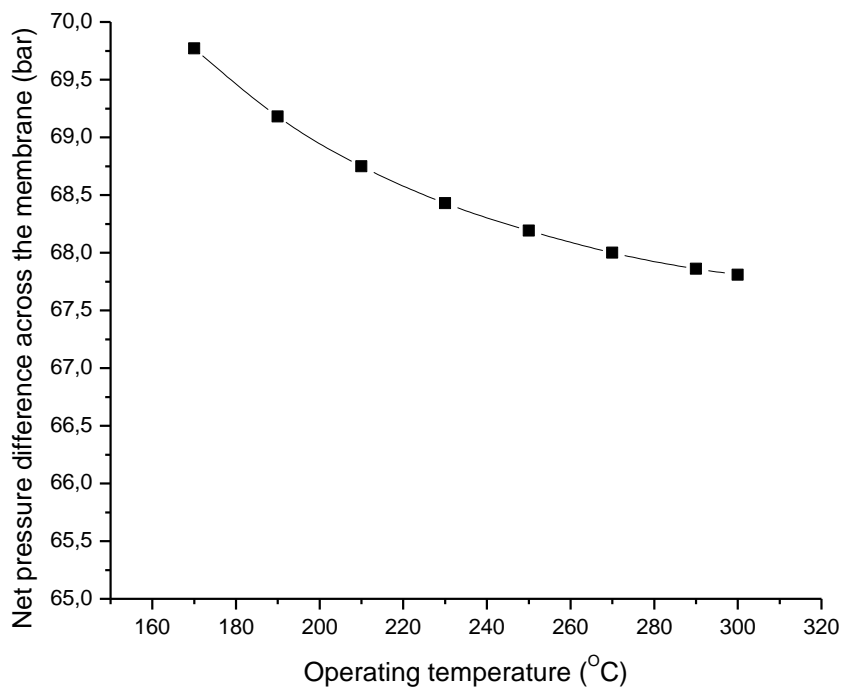
Diagram 11: Relation of operating temperature on net pressure difference across the membrane

Diagrams 12 and 13 show that RO required energy W_5 and specific total consumption *SPC* remain steady with the raise of T_1:
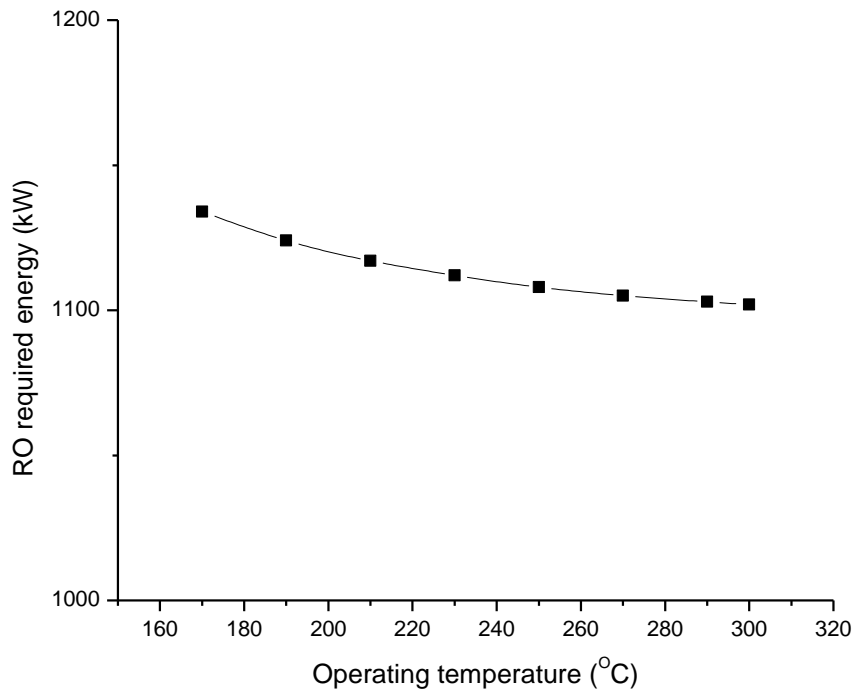
Diagram 12: RO required energy on varying operating temperature
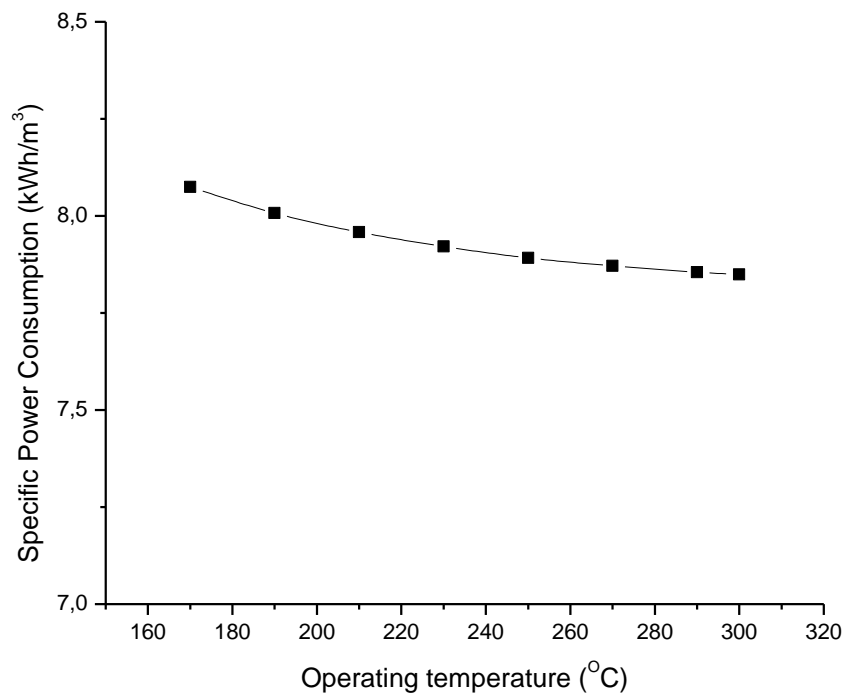
Diagram 13: Effect of operating temperature on specific power consumption

Finally, the ORC efficiency η_R increases on higher temperatures as expected:
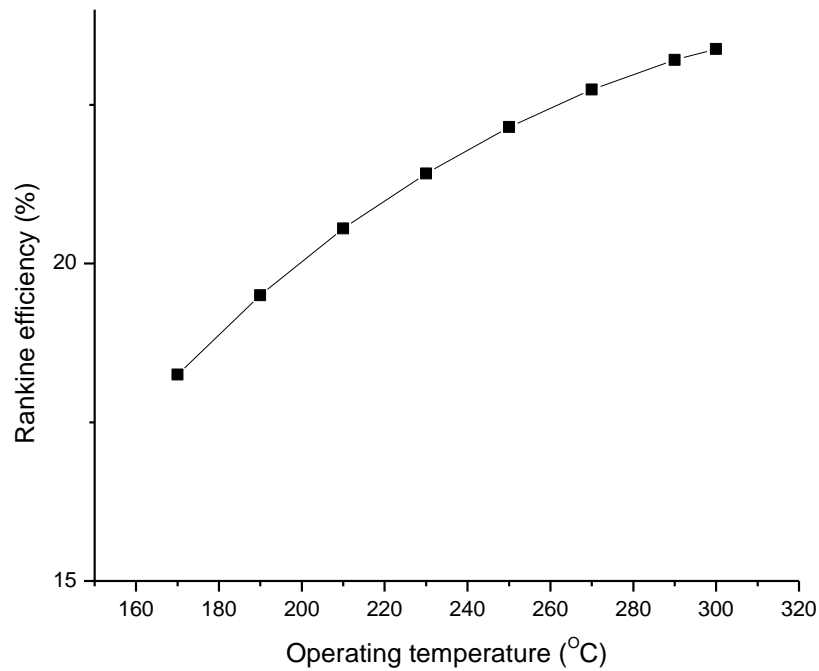
Diagram 14: Increase of ORC efficiency with the raise of operating temperature

4.3.3 Condensation temperature

Condensation temperature T_3 varies between 15 and 40 ^{0}C. [25] With the increase of T_3, W_5, W_2, membrane feed temperature T_6, SPC, I_{total} and C_t slightly increase:
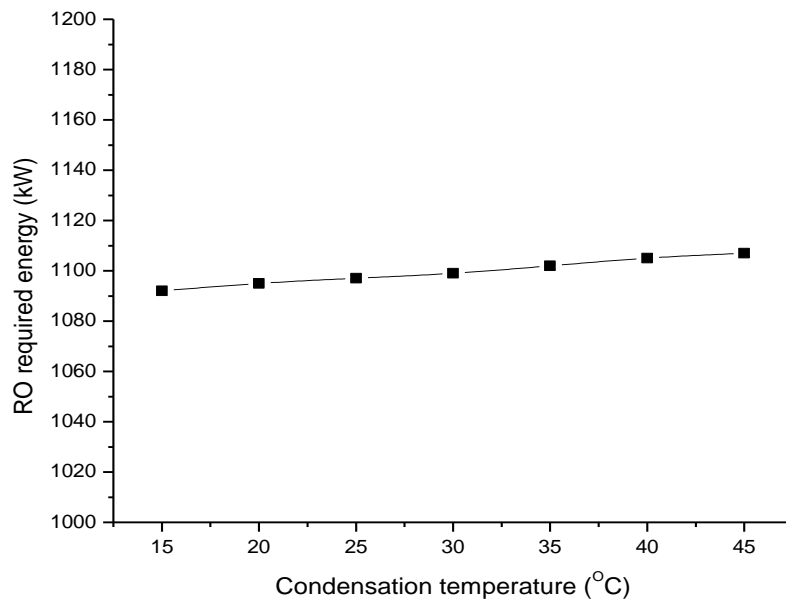
Diagram 15: High pressure pump required work with altering condensation temperature
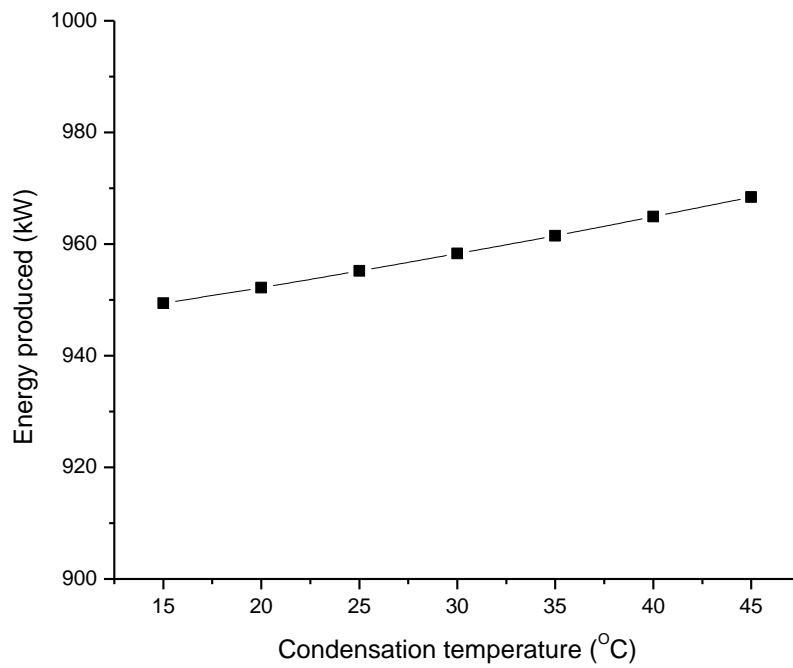
Diagram 16: Effect of condensation temperature on turbine work produced
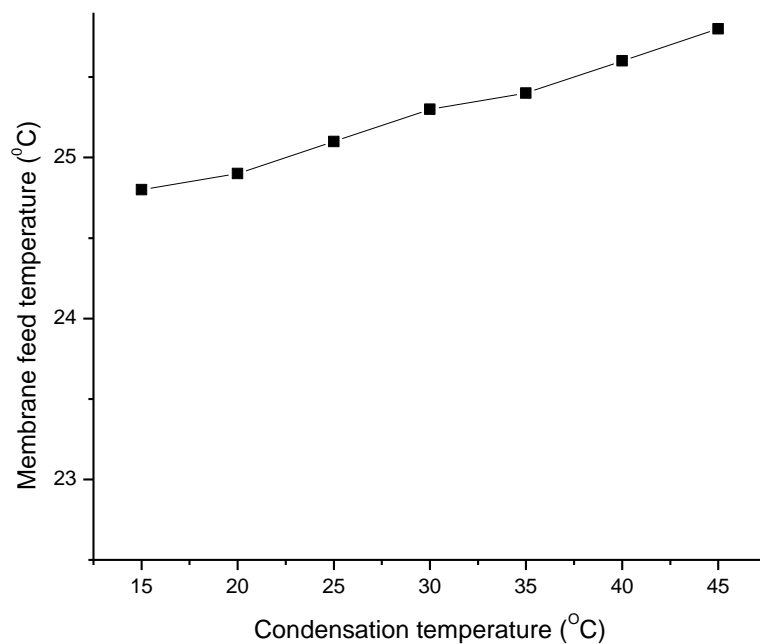
Diagram 17: Relation of condensation temperature with membrane feed temperature
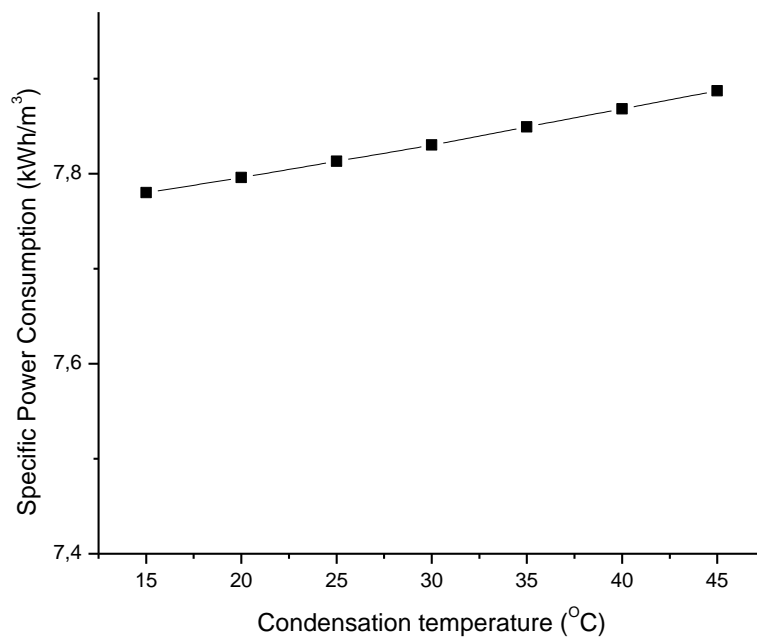
Diagram 18: Condensation temperature effect on specific power consumption
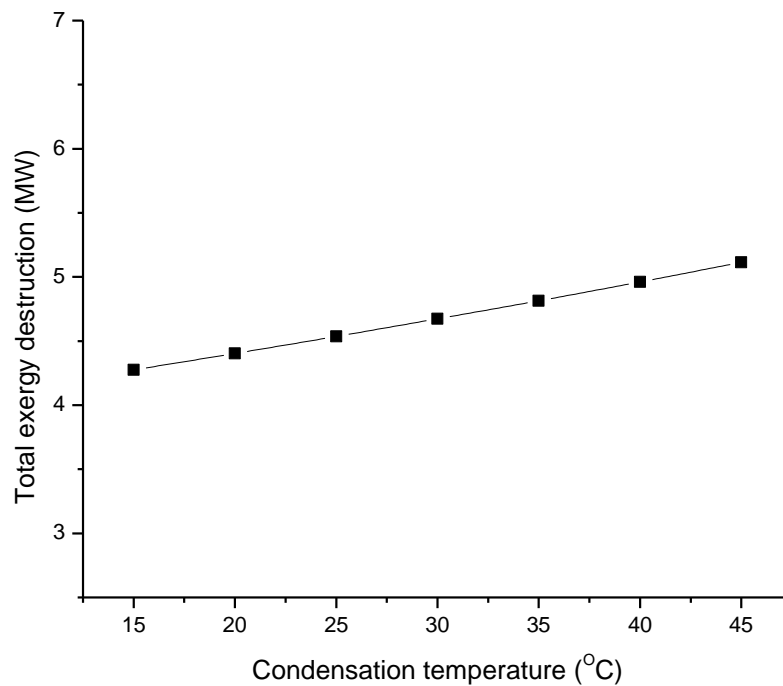
Diagram 19: Slight raise of irreversibility with the raise of condensation temperature
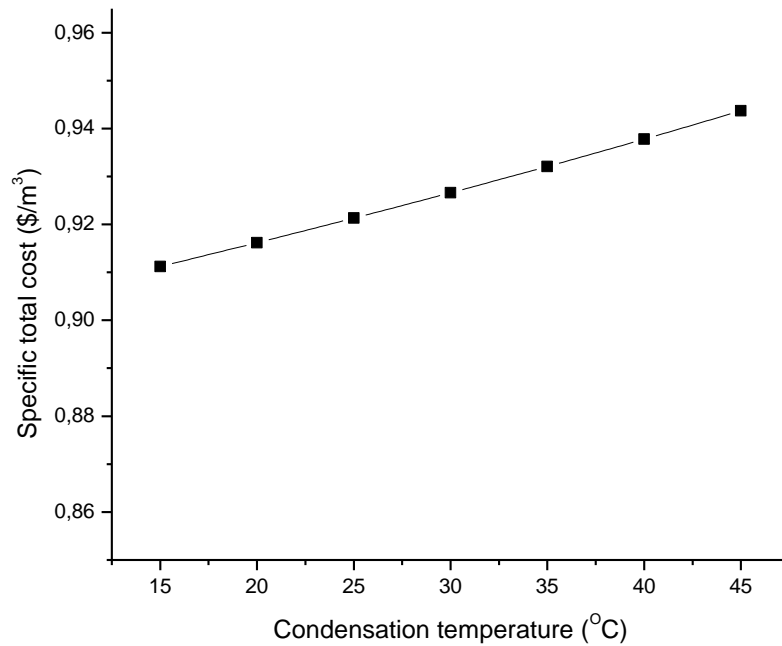
Diagram 20: Slight raise of specific total cost with the increase of condensation temperature

4.3.4 Seawater feed

Seawater temperature T_5 is very important in a desalination plant. In the Mediterranean Sea it varies between 15 and 30 ^{0}C. [70] In the following diagrams RO required energy W_5, turbine work W_2, ORC flow rate m_{orc}, membrane feed temperature T_6, specific power consumption *SPC*, total exergy destroyed I_{total} and specific total cost C_t increase with the raise of T_5:
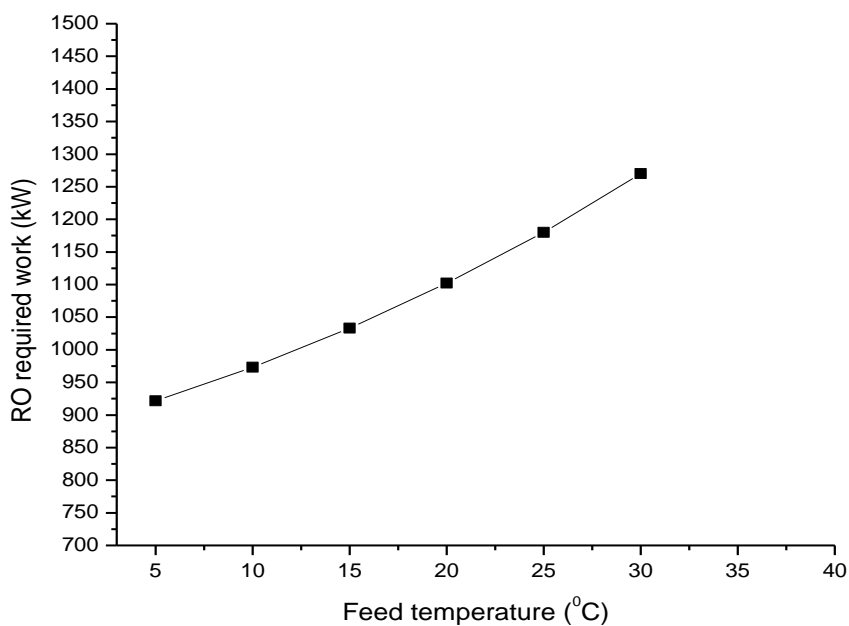
Diagram 21: Relation of feed temperature to high pressure pump required work

Ioannis Kylindris   Page 71
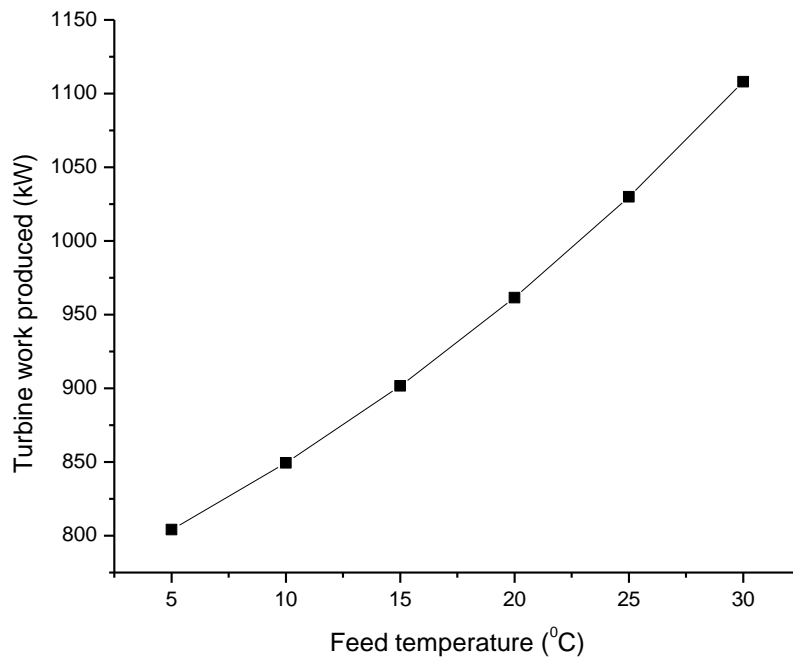
Diagram 22: Raise of turbine work with the increase of feed temperature
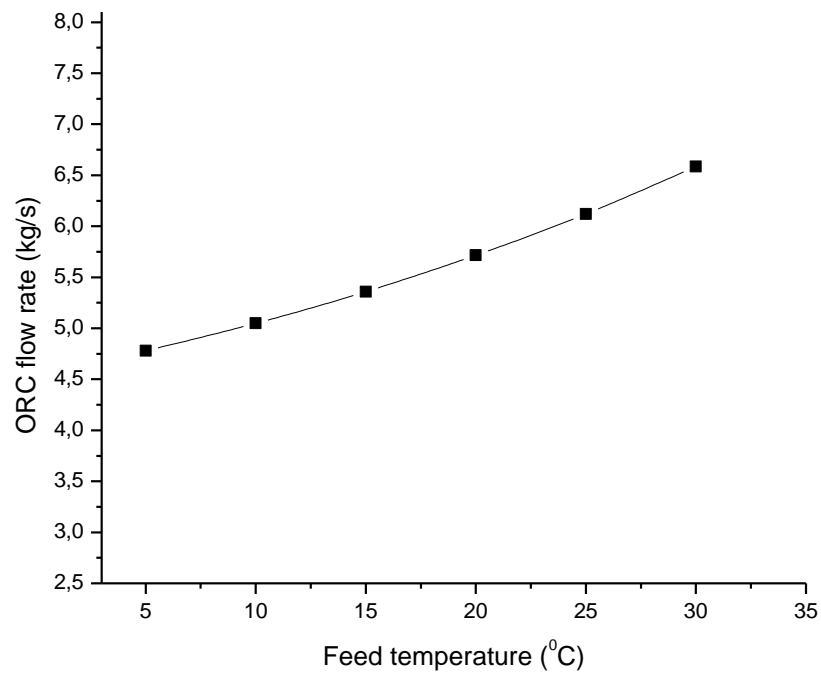
Diagram 23: Feed temperature relation with ORC flow rate
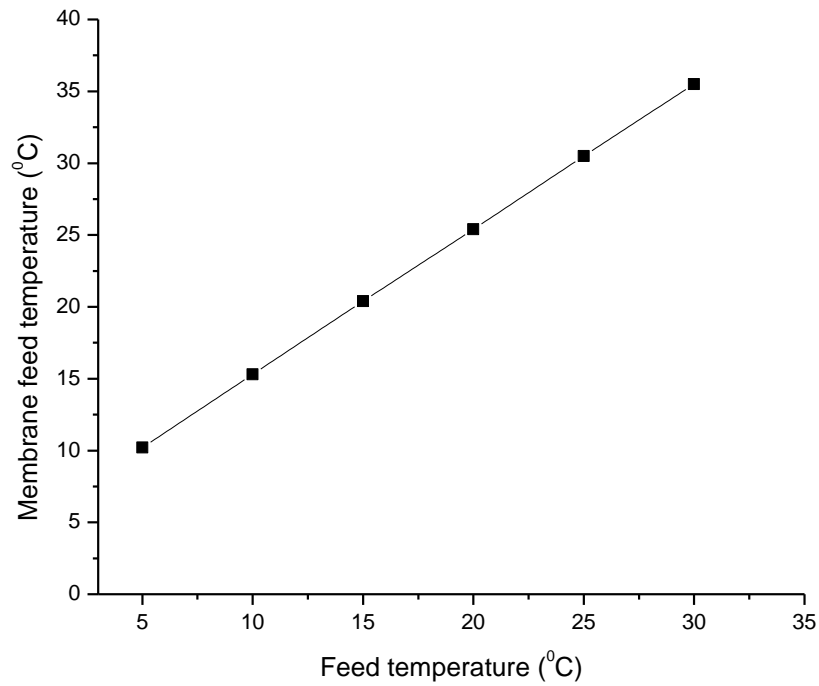
Diagram 24: Feed temperature effect on membrane feed temperature
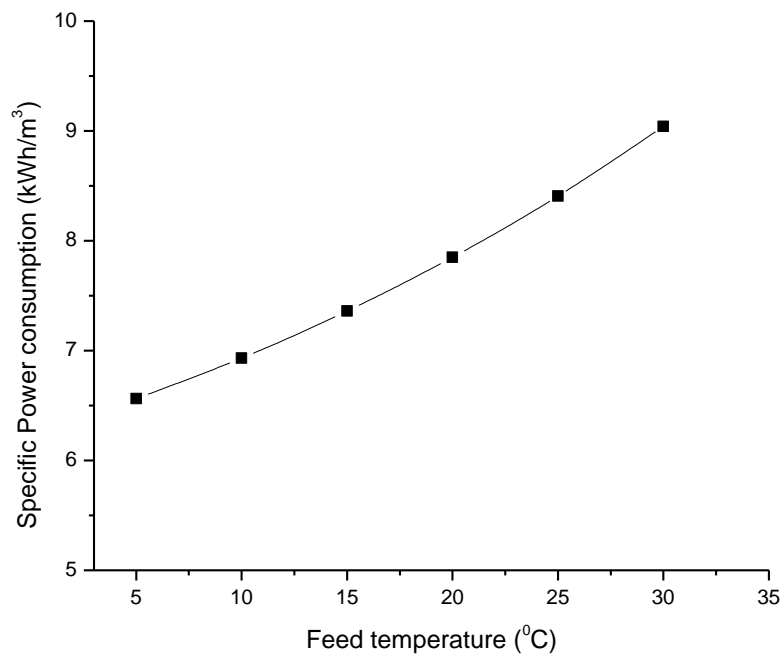
Diagram 25: Raise of specific power consumption with the increase of feed temperature
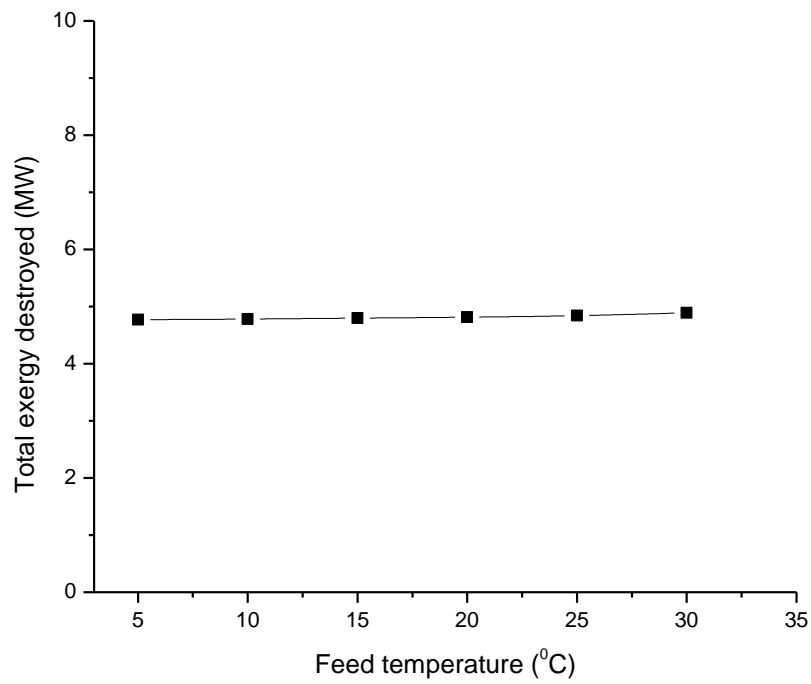
Diagram 26: Effect of feed temperature on irreversibility
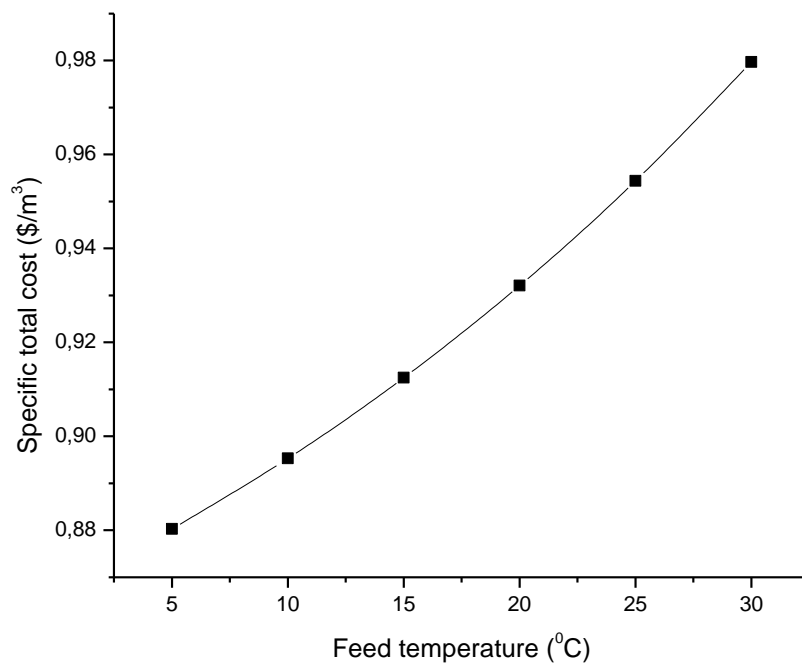
Diagram 27: Slight raise of specific total cost with the increase of feed temperature

Finally, RO required energy W_5, turbine work W_2, specific power consumption *SPC*, total exergy destroyed I_{total} and specific total cost C_t slightly increase with the increase of seawater salinity X_f:
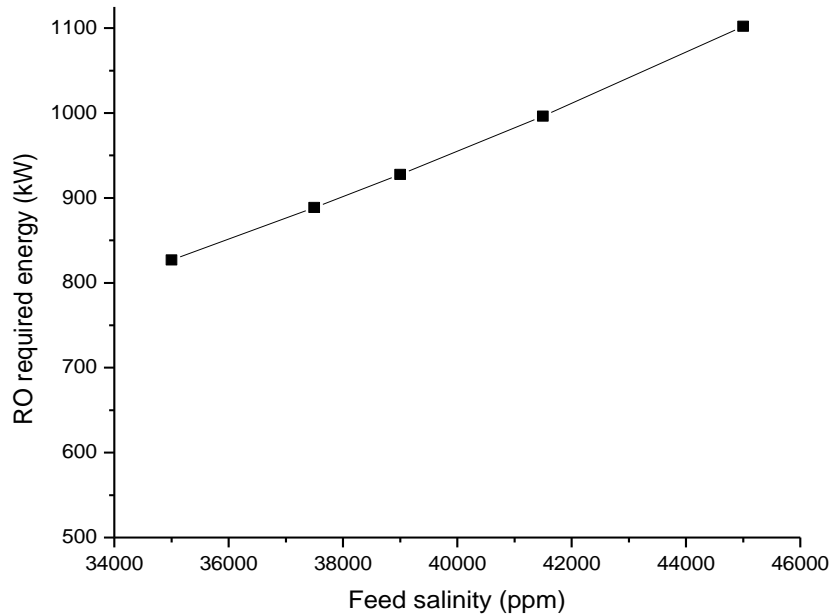
Diagram 28: Raise of high pressure pump required work with the increase of seawater salinity
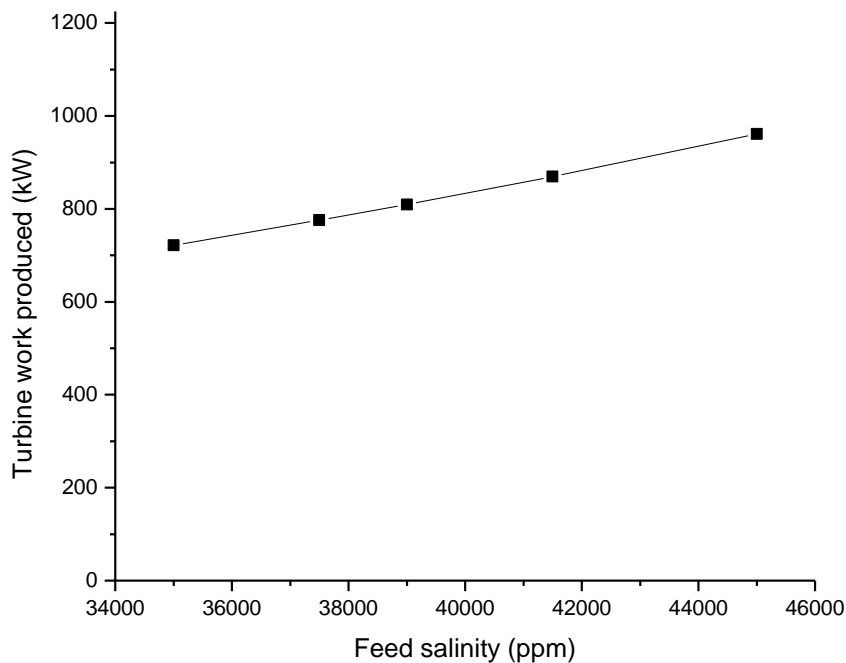
Diagram 29: Feed seawater salinity effect on turbine work
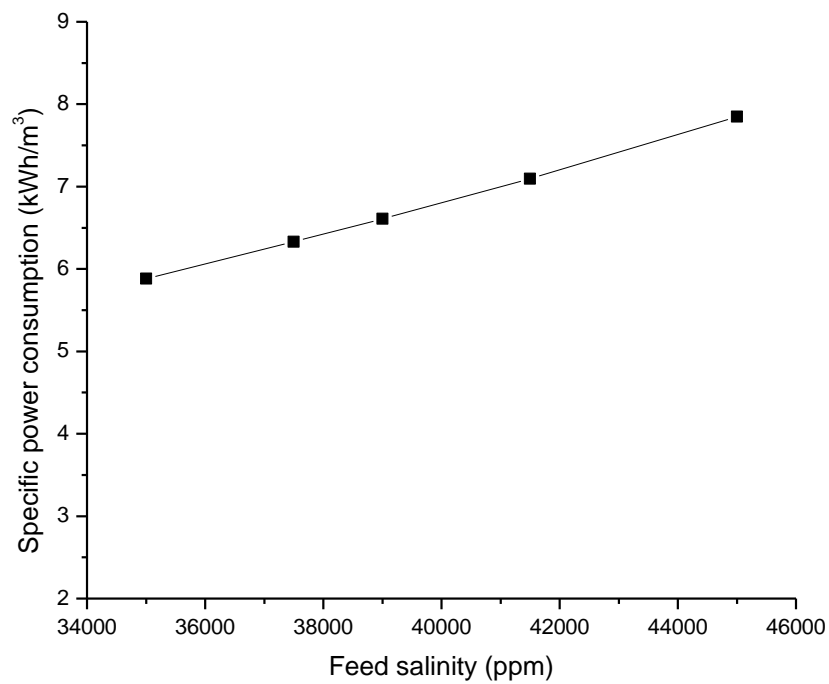
Diagram 30: Relation of seawater salinity to specific power consumption
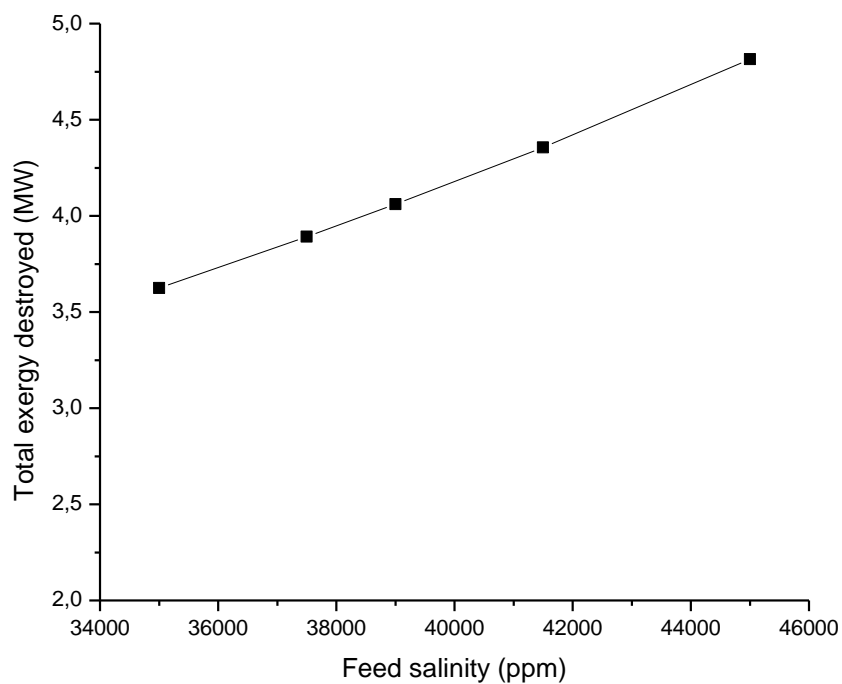
Diagram 31: Effect of seawater salinity on total exergy destruction

Ioannis Kylindris   Page 76
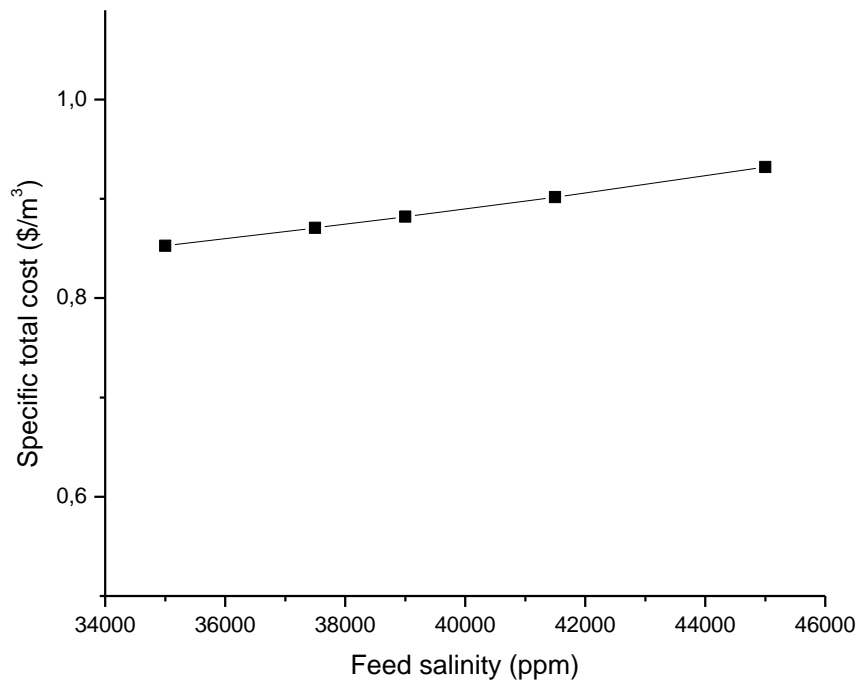
Diagram 32: Raise of specific total cost with the increase of feed seawater salinity

4.3.5 Product quality

Potable water salinity is up to 1500 ppm, according to bibliography. [4] In this present work, it is proved that product quality X_d does not affect RO required energy W_5, turbine work produced W_2, specific power consumption SPC, total irreversibility I_{total} and specific total cost C_t:
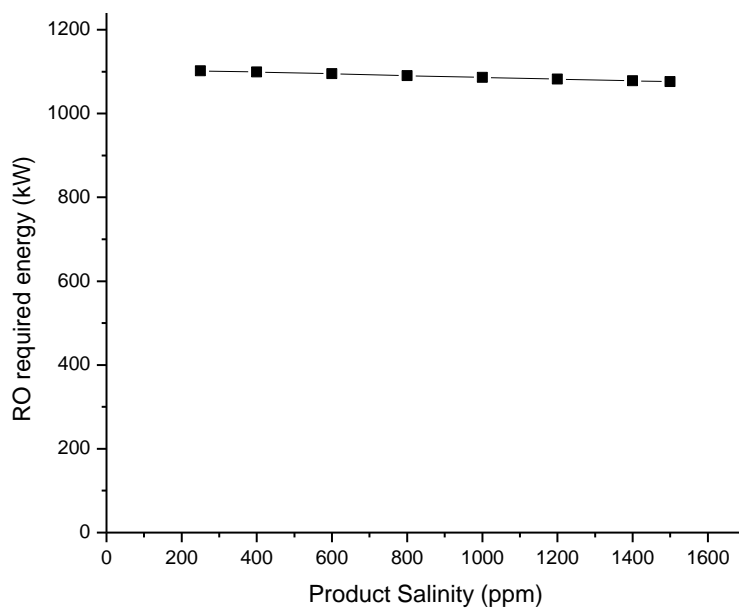
Diagram 33: Effect of product quality on high pressure required work
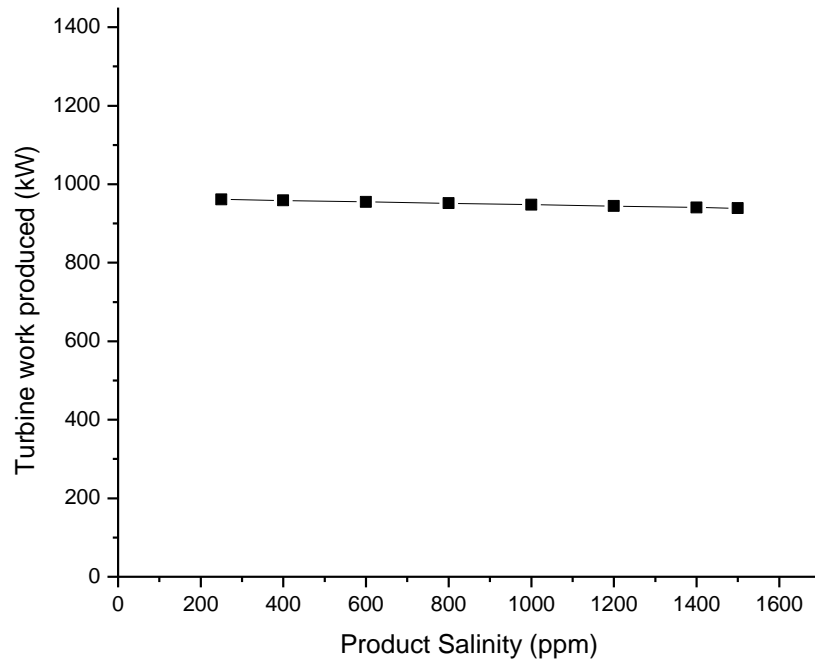
Diagram 34: Relation of product quality to turbine work
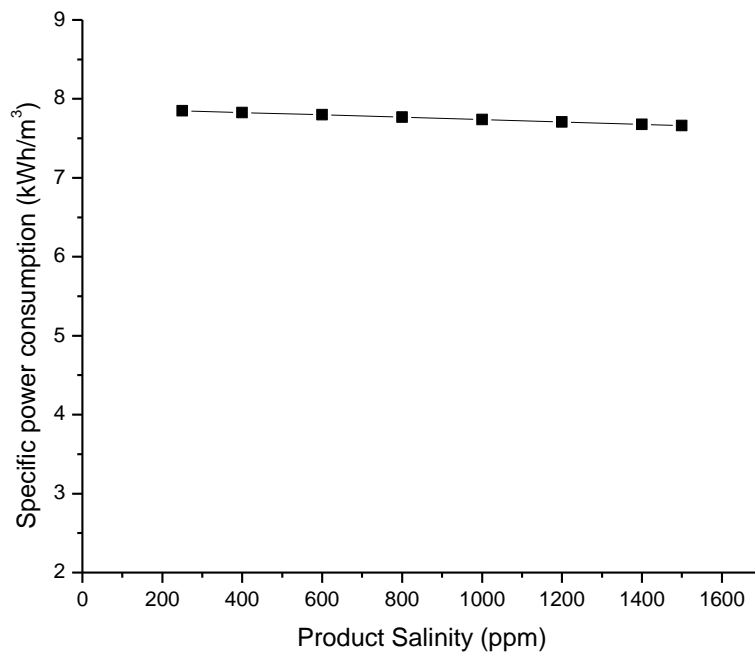
Diagram 35: Slight decrease of specific power consumption with the increase of product quality
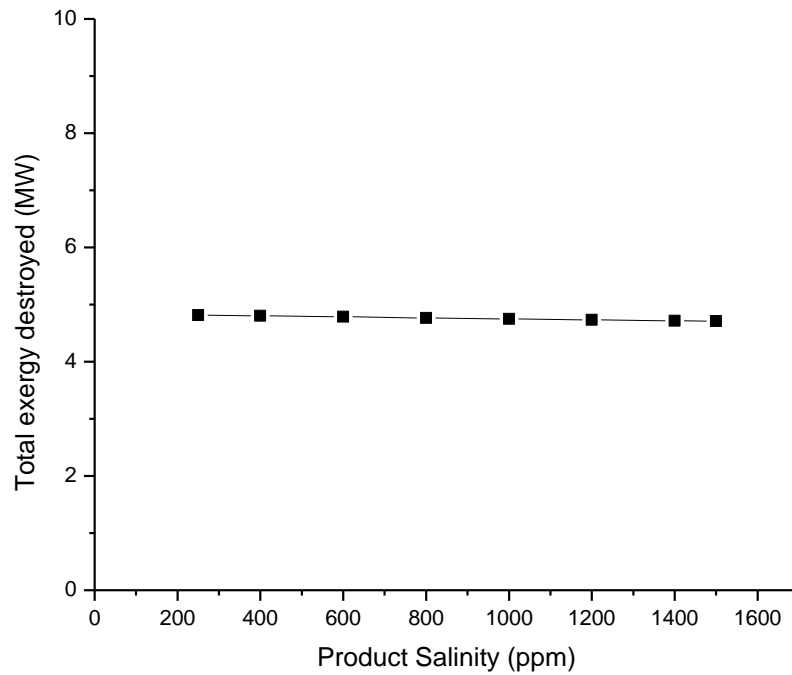
Diagram 36: Slight decrease of irreversibility with the increase of product salinity
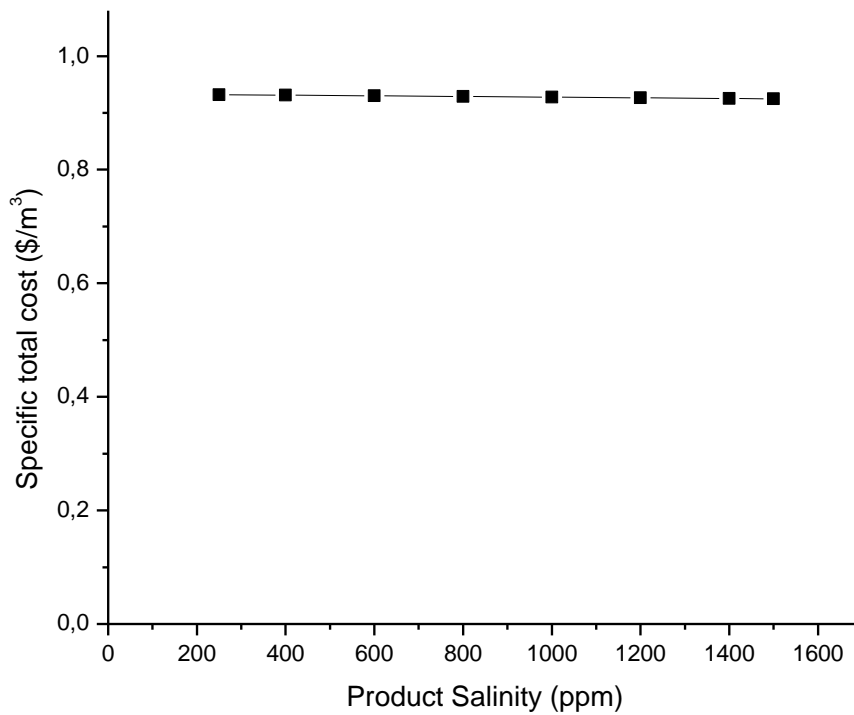
Diagram 37: Relation of product salinity on specific total cost

5. OPTIMIZATION

5.1 Plant design

Due to membrane fouling, osmotic pressure will grow and thus more energy to drive the RO-unit is required while keeping the plant capacity steady. This means that every year more useful collector area should be used on the ORC-unit, which is impossible as the solar collector can be bought once.

Table 23: **Change of RO-unit results with time**

Year of operation	0	1	2	3	4
φ	1.043	1.043	1.044	1.044	1.045
A_t, m^2	35.4	35.03	34.67	34.3	33.93
ΔP_n, bar	69.61	69.93	70.26	70.59	70.94
W_5, kW	1128	1133	1138	1144	1149
A_{col}, m^2	6876	6908	6940	6974	7007

That fact is detected in all energy recovery systems configurations and it is presented in the following figure:
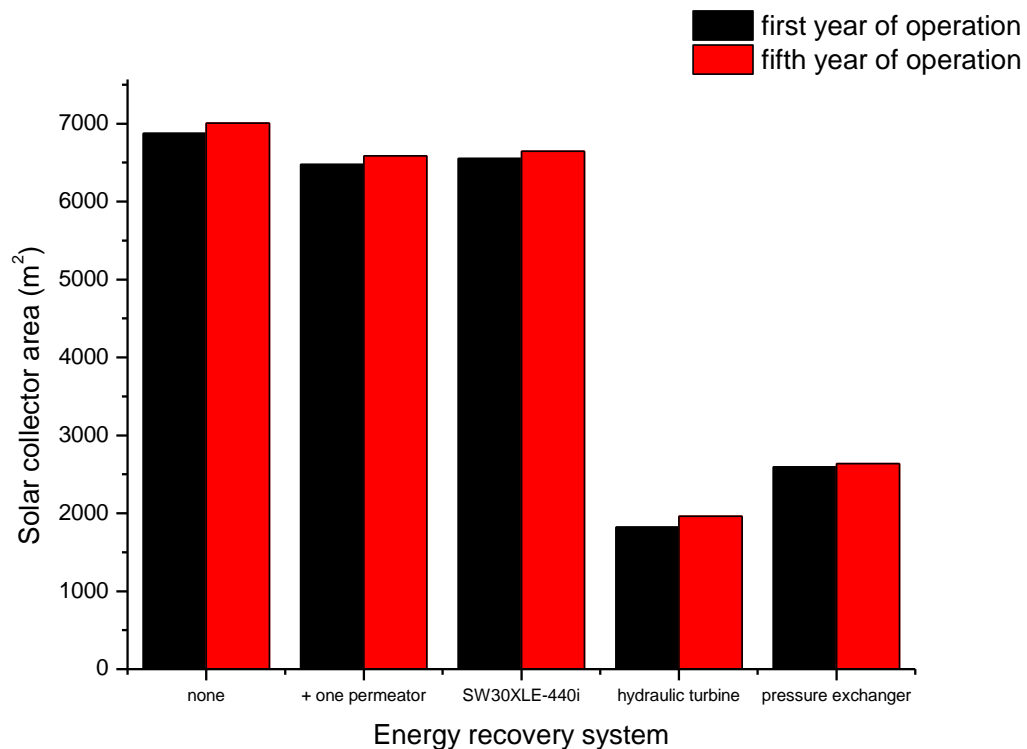
Diagram 38: Solar collector area required on the first and fifth year per energy recovery system used

The plant was designed with the 5th year's solar collector area needed. The excess electric energy produced is going to be sold to the local electricity company. The

following tables present results with no energy recovery system used at the first year of operation:

Table 24: Present results using 7007 m^2 solar collector area for the first year

Cycle flow rate, m_{orc}, kg/s	Feed flow rate Q_f, m^3/h	ORC-pump required energy W_4, kW	High pressure pump required energy W_5, kW
5.963	466.7	32.12	1130
Specific Power Consumption *SPC*, kWh/m^3	**Total Exergy Destroyed I_{total}, MW**	**Specific Cost C_t, $/m^3**	
8.069	5.026	0.9214	

Table 25: Arrays table using 7007 m^2 solar collector area for the first year

	Temperature, ^{0}C	Pressure, bar	Enthalpy, kJ/kg	Entropy, kJ/kg K
1	300	32,8	599,4	1,195
2	148.8	0.06531	423.6	1.341
3	35	0.06204	-141.3	-0.4088
4	35	34.52	-135.9	-0.4131
5	20	2	81,56	0.294
6	25.69	69	107.6	
7	25.69	-0.7133	114.5	
8	25.74	65.55	104.7	
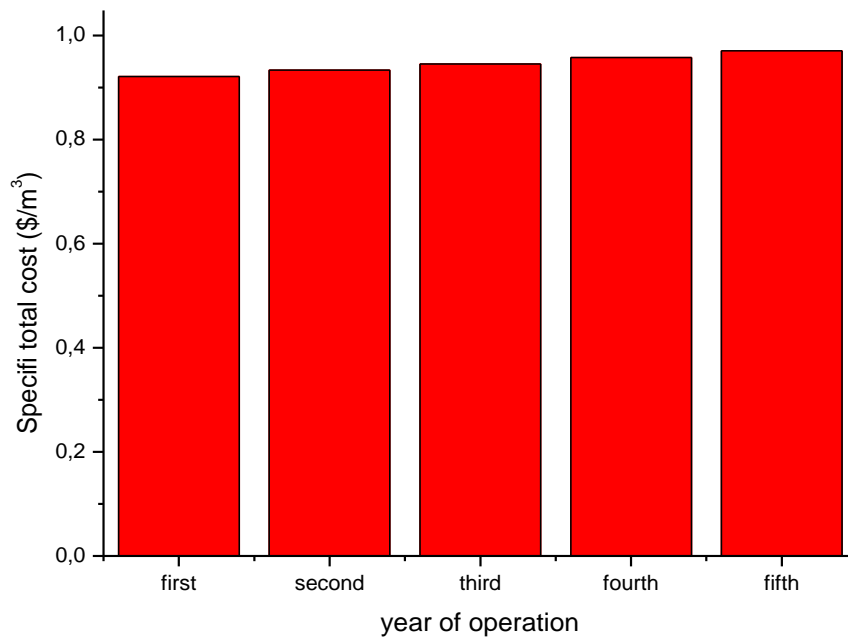
Diagram 39: Variation of specific total cost with time

Ioannis Kylindris   Page 82

Using a hydraulic turbine as energy recovery unit, the results are:

Table 26: Present results using a hydraulic turbine as energy recovery unit and energy generation for the first year of operation

Cycle flow rate, m_{orc}, kg/s	Solar collector area A_{col}, m^2	Feed flow rate Q_f, m^3/h	ORC-pump required energy W_4, kW
1.668	1960	466.7	8.985
High pressure pump required energy W_5, kW	**Specific Power Consumption *SPC*, kWh/m^3**	**Total Exergy Destroyed I_{total}, MW**	**Specific Cost C_t, \$/m^3**
1074	7.671	3.023	0.7587

Table 27: Arrays table using a hydraulic turbine as energy recovery unit and energy generation

	Temperature, ^{0}C	Pressure, bar	Enthalpy, kJ/kg	Entropy, kJ/kg K
1	300	32,8	599,4	1,195
2	148.8	0.06531	423.6	1.341
3	35	0.06204	-141.3	-0.4088
4	35	34.52	-135.9	-0.4131
5	20	2	81,56	0.294
6	21.6	69	88.84	0.3157
7	21.3	2.763	94.76	0.3172
8	21.7	65.55	86.31	0.3166
9	23.7	1	95.36	0.3468

Finally, with a pressure exchanger:

Table 28: Present results using pressure exchanger as energy recovery system and energy generation for the first year of operation

Cycle flow rate, m_{orc}, kg/s	Solar collector area A_{col}, m^2	Feed flow rate Q_f, m^3/h	ORC-pump required energy W_4, kW
1.89	2221	466.7	10.18
High pressure pump required energy W_5, kW	**Specific Power Consumption *SPC*, kWh/m^3**	**Total Exergy Destroyed I_{total}, MW**	**Specific Cost C_t, \$/m^3**
355.3	2.538	1.288	0.7467

Table 29: Arrays table using pressure exchanger as energy recovery system and energy generation

	Temperature, ^{0}C	Pressure, bar	Enthalpy, kJ/kg	Entropy, kJ/kg K
1	300	32,8	599,4	1,195
2	148.8	0.06531	423.6	1.341
3	35	0.06204	-141.3	-0.4088
4	35	34.52	-135.9	-0.4131
5	20	2	81,56	0.294
6	21.85	69	89.81	0.3187
7	21.85	2.55	95.78	0.3203
8	21.9	1.8	87.86	0.3211

5.2 Plant optimization

From the analysis before, it becomes clear that only operating temperature T_1 and condensation temperature T_3 have major effect on plant's behavior.

Table 30: Independent variables and their bounds used in optimization

Independent variable	Symbol	Guess	Lower bound	Upper bound
Recovery Ratio	*RR*	0.3	0.1	0.5
Operating temperature, ^{0}C	T_1	300	170	300
Condensation temperature, ^{0}C	T_3	20	15	40

EES is able to calculate minimums or maximums, performing optimization by this way. The first step is to choose the independent variables and set the variable bounds. The next step is to choose the variable to optimize (Fig.51):
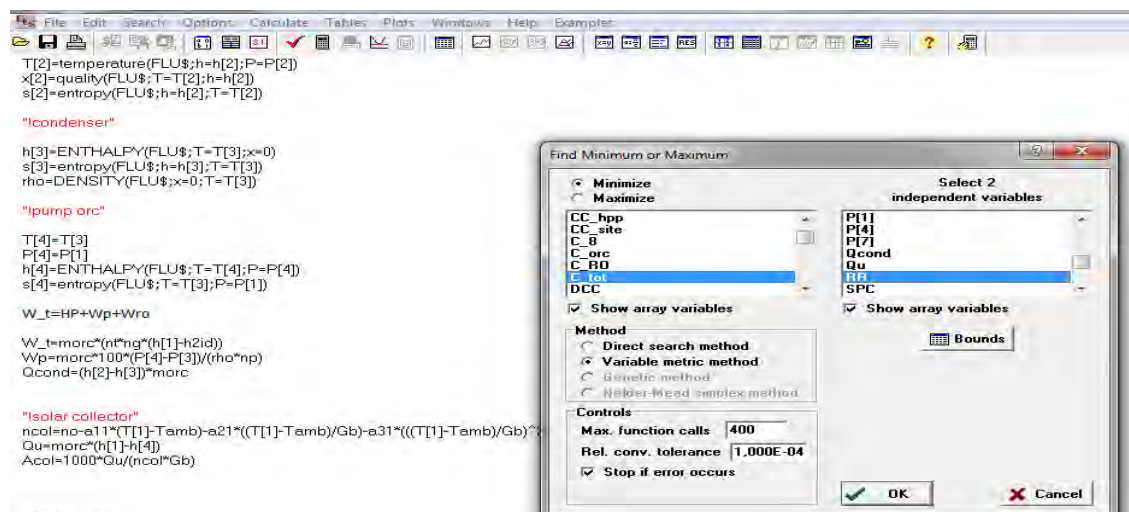
Figure 51: Optimization window

Ioannis Kylindris   Page 84

The variable to be optimized is the specific total cost C_t, which is calculated by the equation:

$$C_t = \frac{C_{ORC} + C_{RO}}{Q_d}$$

By minimizing C_t, plant optimum conditions of operation can be found in minimum cost available. The results with no energy recovery unit are presented in the following tables:

Table 31: Optimized results with no energy recovery system

Cycle flow rate, m_{orc}, kg/s	ORC-pump required energy W_4, kW	Recovery ratio, RR	Feed flow rate Q_f, m^3/h
5.698	30.08	0.28	500
High pressure pump required energy W_5, kW	**Specific Power Consumption SPC, kWh/m^3**	**Total Exergy Destroyed I_{total}, MW**	**Specific Cost C_t, \$/m^3**
1171	8.366	4.935	0.7435

Table 32: Optimized arrays table with no energy recovery system

	Temperature, ^{0}C	Pressure, bar	Enthalpy, kJ/kg	Entropy, kJ/kg K
1	300	32,8	599,4	1,195
2	132	0.2306	397.5	1,371
3	15	0,02191	-175,3	-0,5229
4	15	34.52	-170	-0.5271
5	20	2	81,56	0.294
6	25.17	69	105.1	0.3653
7	25.17	1.537	111.9	0.3671
8	25.21	65.55	102.5	0.366

The optimized results with a hydraulic turbine are:

Table 33: Optimized results using a hydraulic turbine as energy recovery system

Cycle flow rate, m_{orc}, kg/s	Feed flow rate Q_f, m^3/h	ORC-pump required energy W_4, kW	High pressure pump required energy W_5, kW
1.594	466.7	8.413	1073
Specific Power Consumption SPC, kWh/m^3	**Total Exergy Destroyed I_{total}, MW**	**Specific Cost C_t, \$/m^3**	
7.666	2.981	0.6785	

Table 34: Optimized arrays table using a hydraulic turbine as energy recovery system and energy generation

	Temperature, ^{0}C	Pressure, bar	Enthalpy, kJ/kg	Entropy, kJ/kg K
1	300	32,8	599,4	1,195
2	132	0.02306	397.5	1.371
3	15	0.2191	-175.3	-0.5229
4	15	34.52	-170	-0.5271
5	20	2	81,56	0.294
6	21.58	69	88.62	0.315
7	21.58	2.763	94.52	0.3165
8	21.64	65.55	86.09	0.3159
9	23.67	1	95.17	0.3461

Finally, using a pressure exchanger:

Table 35: Optimized results using a pressure exchanger as energy recovery unit and energy generation

Cycle flow rate, m_{orc}, kg/s	ORC-pump required energy W_4, kW	Recovery ratio, RR	Feed flow rate Q_f, m^3/h
1.806	9.533	0.31	451.6
High pressure pump required energy W_5, kW	**Specific Power Consumption SPC, kWh/m^3**	**Total Exergy Destroyed I_{total}, MW**	**Specific Cost C_t, \$/m^3**
348.5	2.49	1.234	0.6412

Table 36: Optimized arrays table using a pressure exchanger as energy recovery unit

	Temperature, ^{0}C	Pressure, bar	Enthalpy, kJ/kg	Entropy, kJ/kg K
1	300	32,8	599,4	1,195
2	132	0.02306	397.5	1.371
3	15	0.02191	-175.3	-0.5229
4	15	34.52	-170	-0.5271
5	20	2	81,56	0.294
6	21.85	69	89.83	0.3188
7	21.85	1.645	95.79	0.3203
8	21.91	1.8	87.15	0.3212

6. RESULTS CONVERSATION

In this work, an analysis of a combined solar Rankine engine for RO desalination process is presented with two different energy recovery systems. The ORC is consisted of a solar field, a turbine unit for energy generation, a condenser unit and a pump.

Table 37: A comparison between the present work and ref. [52] for the ORC-unit without energy recovery system

Parameter	Present results	Ref. [52]
P_1, bar	32.8	32.75
P_3, bar	0.06204	0.06215
A_{col}, m^2	6971	6747
η_R, %	22.36	22.82
m_{orc}, kg/s	5.932	5.75

The RO desalination unit is consisted of a pump, a seawater preheating unit (seawater is used as a coolant in the ORC condenser unit) and RO module.

Table 38: A comparison between the present work and ref. [52] for the RO-unit without energy recovery system

Parameter	Present results	Ref. [52]
W_5, kW	1133	1131
I_{total}, MW	5.007	4.951
SPC, kWh/m^3	8.073	7.677
C_t, \$/m^3	0.9413	0.903

In ref. [52], the turbine unit produced work to drive only the RO module unit, while in this work the turbine unit not only drives the RO module unit, but the ORC pump unit as well. So, it is clear that more power W_2 must be produced, which is presented in the table above. Due to the fact that W_2 and working fluid cycle flow rate m_{orc} are analog, m_{orc} is increased and thus more collector area is needed.

All RO-unit results have a slight increase as expected except specific total cost C_t. RO-unit required work is not expected to change with this different energy balance. C_t increases due to solar collector area A_{col} increase; bigger solar field requires greater solar collector total capital cost TCC_{col} and thus greater total investment and operating and maintenance cost for the ORC-unit C_{orc}.

The next step was to determine potable water flow rate Q_d. It is more rational to design a plant by using the consumer needs on the product. A comparison of product flow rate determined results with feed flow rate determined results are presented in the following table. No dramatic changes were made since, with the recovery ratio determined, feed flow rate does not alter significantly.

Table 39: A comparison between the feed flow rate determined present results and the product flow rate determined results

Parameter	Feed flow rate determined	Product flow rate determined
A_{col}, m^2	6971	6943
m_{orc}, kg/s	5.932	5.908
W_5, kW	1133	1129
I_{total}, MW	5.007	4.986
SPC, kWh/m^3	8.073	8.063
C_t, $/m^3	0.9413	0.9429
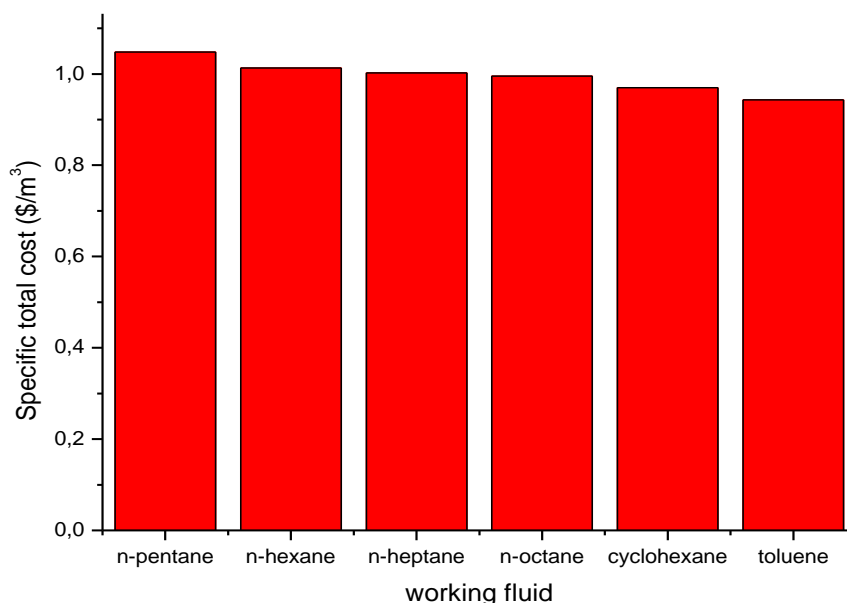
Diagram 40: Desalination specific total cost for various ORC working fluids

The fourth step was to place a fouling model in *EES* code, which it is consisted of two parts: a complete pore blocking model and a concentration polarization model.

Table 40: Effect of membrane fouling on plant configuration: a brief comparison between the present work results and ref. [52] with feed flow rate determined

Parameter	With fouling model	Ref. [52]
A_{col}, m^2	6971	6747
m_{orc}, kg/s	5.932	5.75
W_5, kW	1133	1131
I_{total}, MW	5.007	4.951
SPC, kWh/m^3	8.073	7.677
C_t, $/m^3	0.9413	0.903

Due to fouling each year more pressure is needed to be applied on the membrane and thus more energy is required. This fact is presented on the following diagram using various working fluids:

Ioannis Kylindris
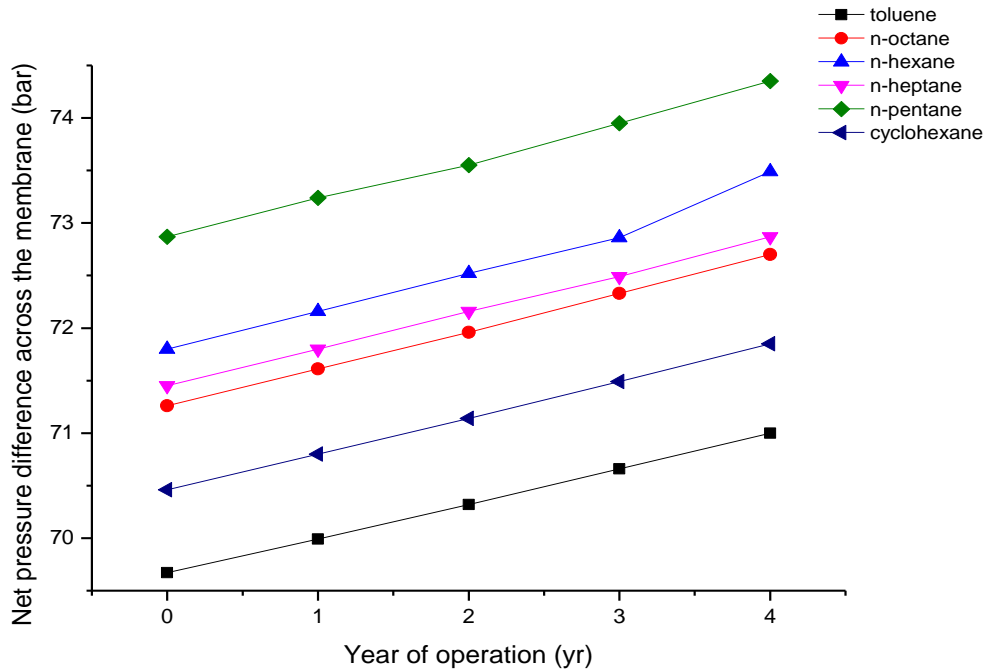
Diagram 41: Raise of net pressure difference across the membrane per year of operation for various ORC working fluids.

By the analysis been made, it was extracted that concentration polarization does not play major role on membrane fouling and performance with polarization factor Γ around 0.044. If Γ is below 0.1, it can be ignored as concentration polarization is not important to the overall plant performance. [8] This fact confirms the theory in which spiral-wound modules are used in seawater desalination due to the fact that concentration polarization is negligible. [10]

Table 41: Values of concentration polarization factor per year of desalination plant operation and energy recovery unit.

Year of operation	No energy recovery system	Hydraulic turbine	Pressure exchanger
0	1.042	1.043	1.043
1	1.043	1.044	1.044
2	1.044	1.044	1.044
3	1.044	1.045	1.045
4	1.045	1.045	1.045

Another step was to use an energy recovery unit as brine stream comes out from the membrane on high pressure. The first energy recovery system was a hydraulic turbine. The next table presents a comparison between the results with no energy recovery system and hydraulic turbine:

Ioannis Kylindris

Table 42: A comparison between the results with no energy recovery system and hydraulic turbine

Parameter	No energy recovery system	Hydraulic turbine
A_{col}, m^2	6943	1821
m_{orc}, kg/s	5.908	1.549
W_5, kW	1129	1072
I_{total}, MW	4.986	2.908
SPC, kWh/m^3	8.063	7.66
C_t, \$/m^3	0.9429	0.8041

Even though the same amount of energy is required to drive the RO-unit, all results dramatically decrease. That happens because energy is produced not only by ORC-unit but also by a hydraulic turbine. This means less collector area and lower cost even if one more unit was added. Toluene is the best choice for ORC working fluid (Diagram 42):
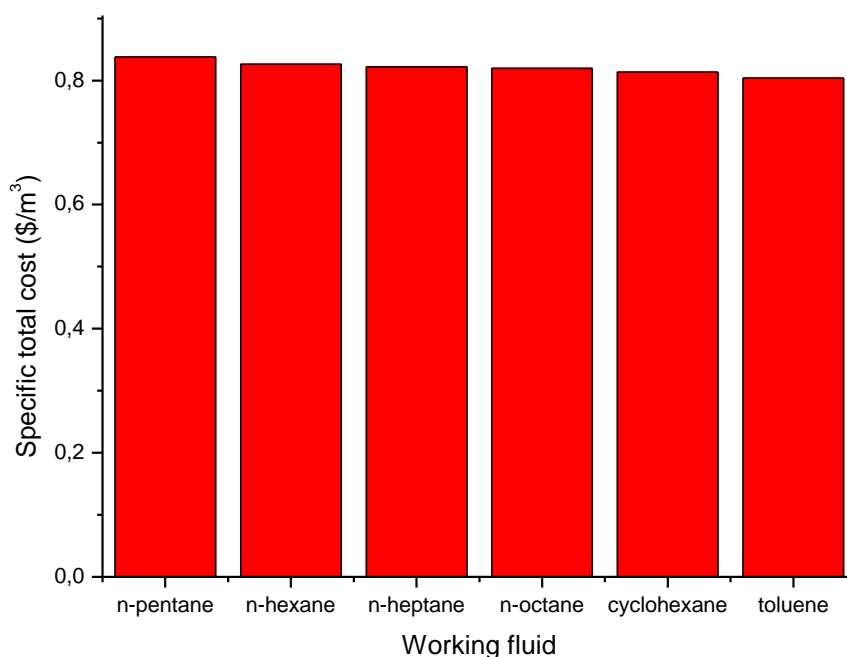
Diagram 42: Desalination specific total cost for various ORC working fluids using a hydraulic turbine as energy recovery unit.

The second energy recovery system to try was the pressure exchanger. Brief results and comparison are shown on the next table:

Table 43: A comparison between desalination plant with no energy recovery system, hydraulic turbine and pressure exchanger.

Parameter	No energy recovery system	Hydraulic turbine	Pressure exchanger
A_{col}, m^2	6943	1821	2184
m_{orc}, kg/s	5.908	1.549	1.859
W_5, kW	1129	1072	355.2
I_{total}, MW	4.986	2.908	1.265
SPC, kWh/m^3	8.063	7.66	2.537
C_t, \$/m^3	0.9429	0.8041	0.7595

The above table presents that an ORC solar desalination plant with pressure exchanger is the best solution. The high pressure pump required work W_5 is much less than the two other systems. Toluene provides the best choice for the role of ORC working fluid which is described by the following diagram:
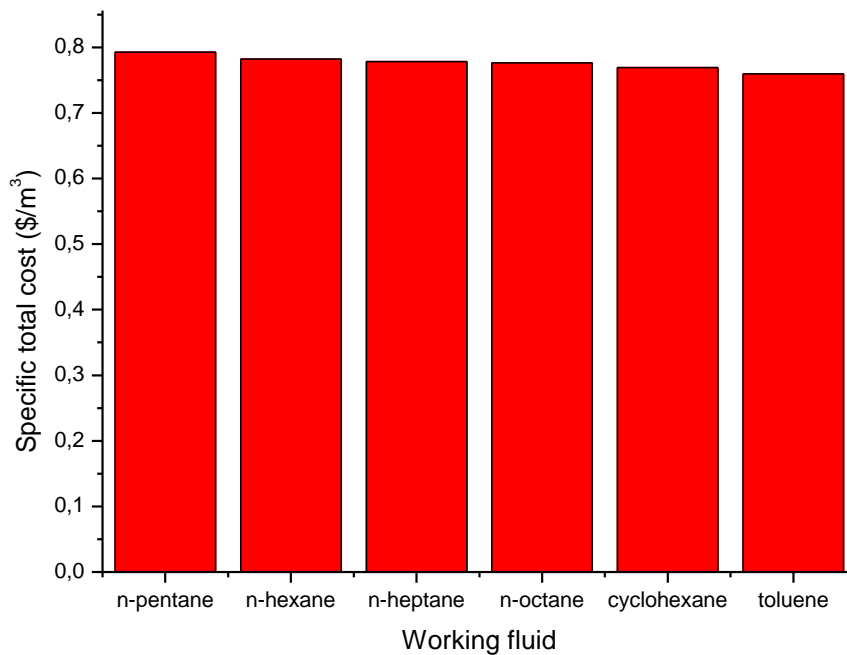
Diagram 43: Desalination specific total cost for various ORC working fluids using a pressure exchanger as energy recovery unit.

The final step was to use constant solar collector area A_{col}. As it was presented in chapter before, more energy is required with the pass of time. This means that the more energy required the bigger solar collector must be obtained. The excess power produced is going to be sold to the local electricity network. Once again, toluene is the best choice for ORC working fluid.
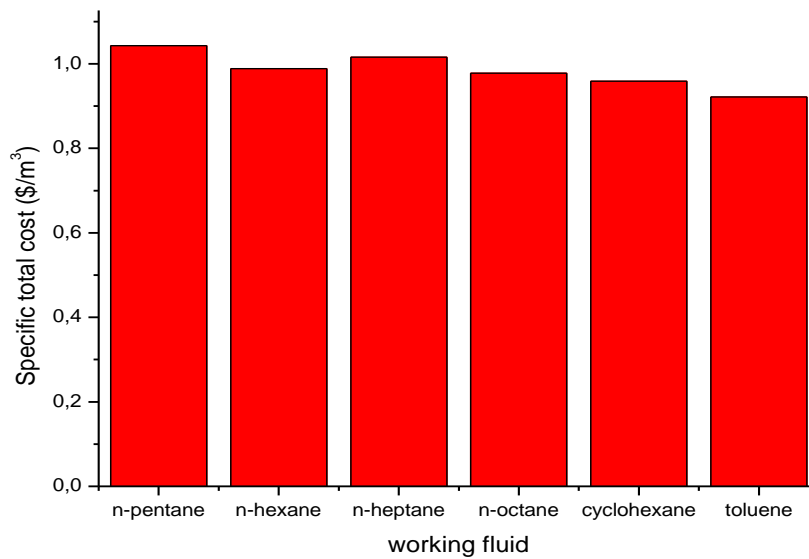
Diagram 44: Desalination specific total cost with no energy recovery system and energy generation for various working fluids

The case was also studied using one more permeator and a different membrane. The new membrane used was SW30XLE-440i and has the same dimensions with the basic used (SW30HR-380), but membrane element area 41 m^2 and salt rejection factor 99.7%. A brief results comparison is presented on the table which follows:

Table 44: A comparison between present results, results with another membrane and results with one more permeator

Parameter	Present program with SW30HR-380	Present program with one more permeator	Present program with SW30XLE-440i
A_{col}, m^2	6943	6477	6551
m_{orc}, kg/s	5.908	5.51	5.574
X_d, ppm	270	270	135
X_b, ppm	54350	54350	64230
W_5, kW	1129	1062	1074
I_{total}, MW	4.986	4.63	4.674
SPC, kWh/m^3	8.063	7.588	7.67
C_t, \$/m^3	0.9429	1.016	1.025

No dramatic changes are observed but the specific total cost C_t. This happens because with that way the membrane surface is raised. The larger membrane element surface used, the greater specific total cost should be paid to produce the desirable potable water quantity. Once again toluene is the best choice for ORC working fluid:
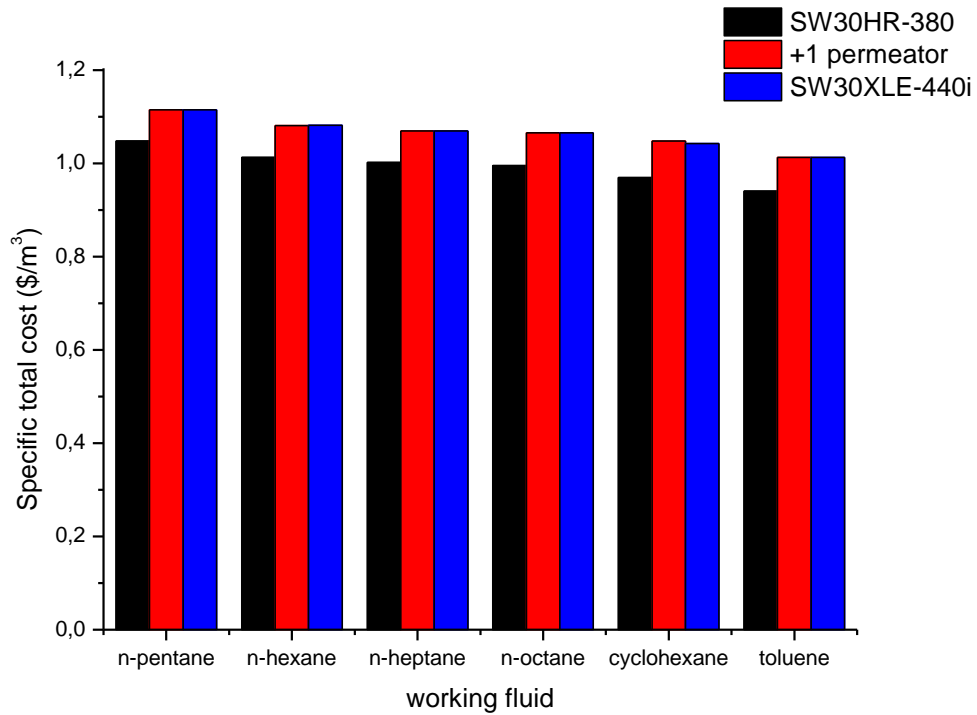
Diagram 45: Specific total cost variation with different membrane systems and ORC working fluids.

The same scenario was studied at the basic program for the both energy recovery systems used. For the hydraulic turbine:
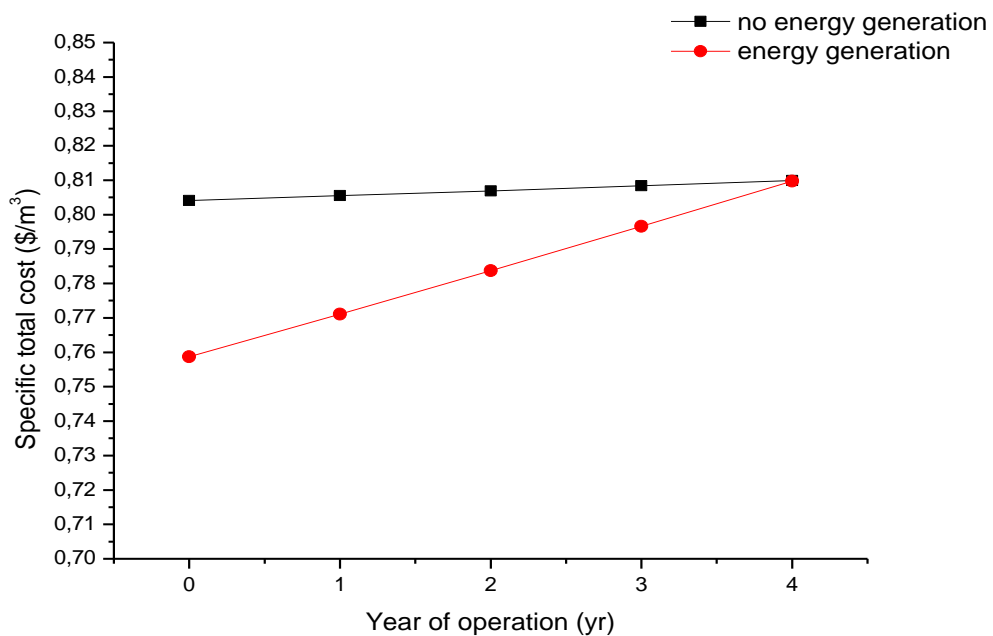
Diagram 46: A comparison between the specific total cost per year of operation for a hydraulic turbine with and without energy generation

Toluene and cyclohexane are the best working fluids for this job:
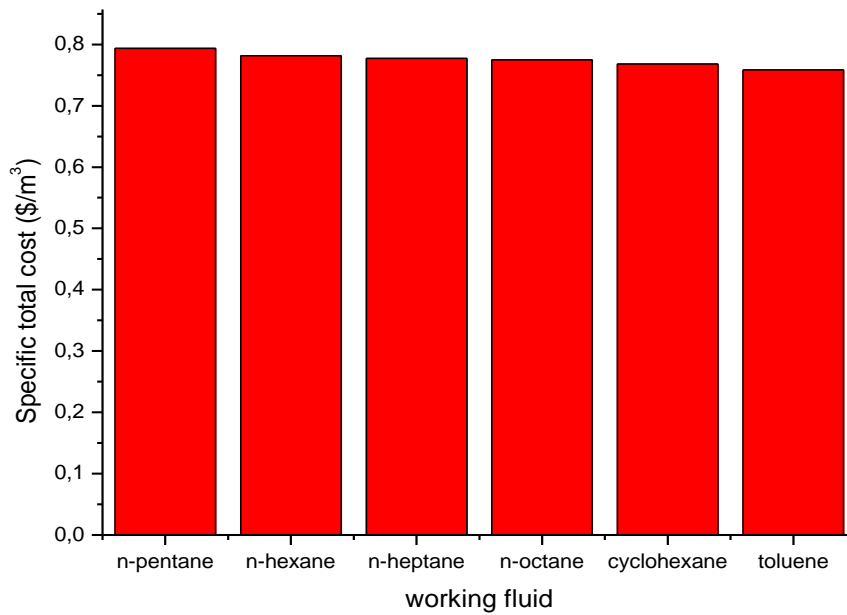
Diagram 47: Desalination specific total cost with hydraulic turbine and energy generation for various working fluids

For the pressure exchanger:
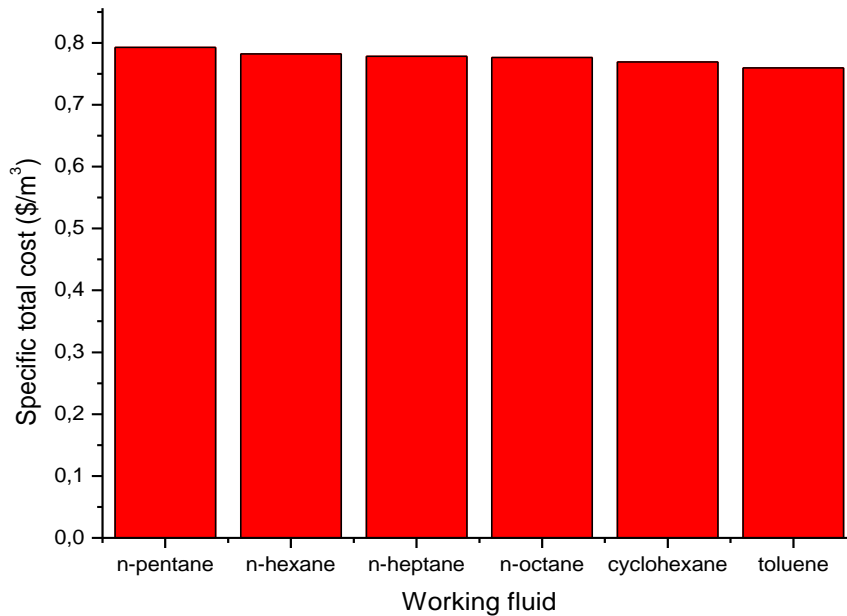
Diagram 48: Desalination specific total cost with pressure exchanger and energy generation for various working fluids

From the analysis above, it has become clear that the pressure exchanger is the best economic choice:
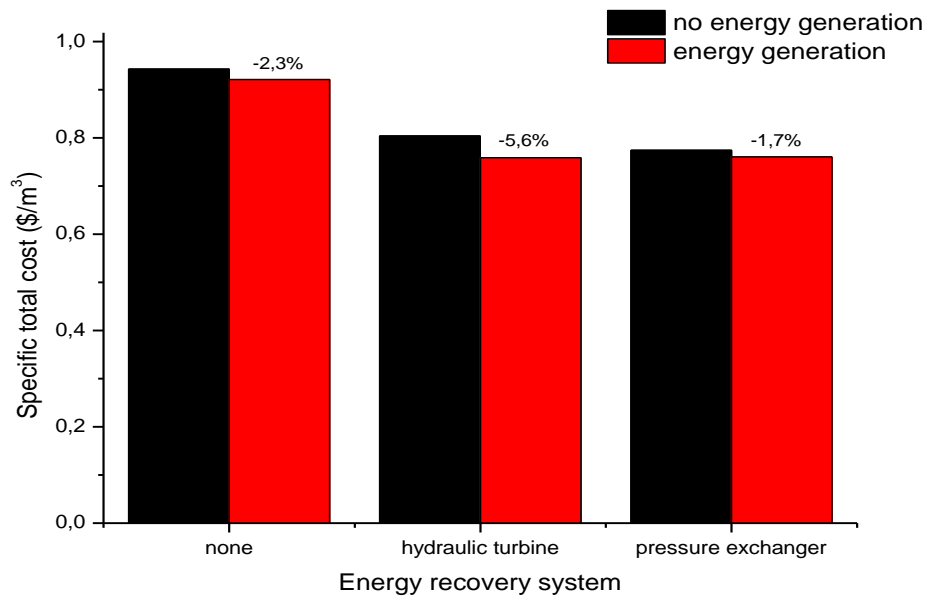
Diagram 49: A comparison between specific total costs on various energy recovery systems

And it has the less irreversibility:
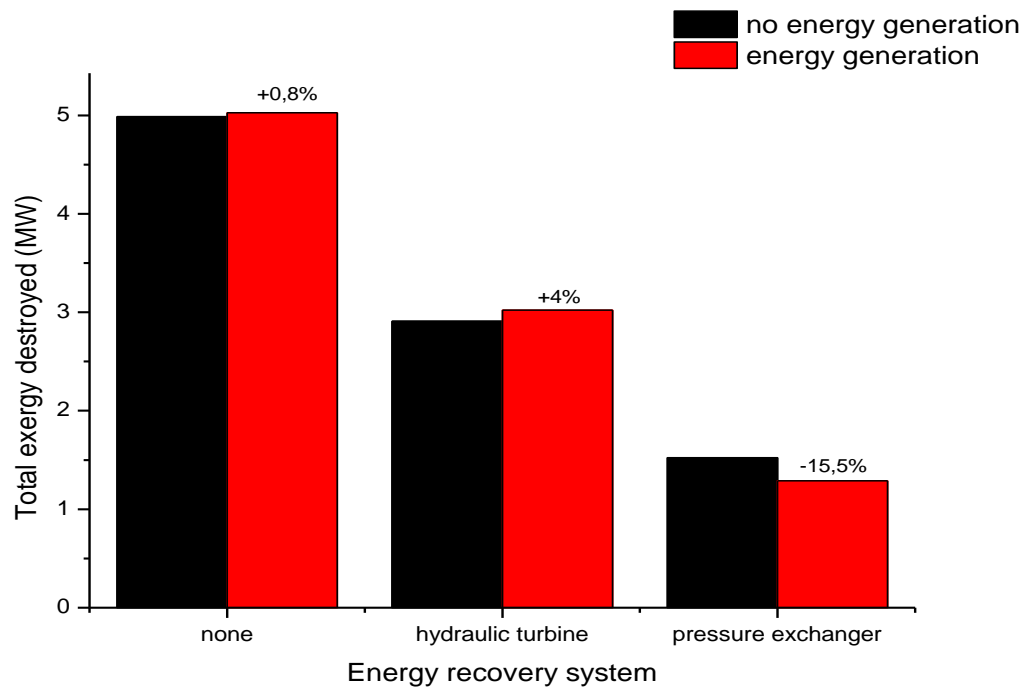
Diagram 50: Irreversibility on various energy recovery systems

In parameter analysis, many useful conclusions were extracted. With the raise of recovery ratio RR, more pressure must be applied and thus more energy is needed to drive the RO-unit. In all cases RR minimized around 0.25-0.35.

Operating temperature T_1 is vital on ORC performance. Parameter analysis did not show major changes regarding the energy production rate W_2, the high pressure pump required energy W_5, specific power consumption *SPC* and product specific total cost C_t. On the other hand, it is obvious that with the raise of T_1, ORC flow rate m_{orc} and total exergy destruction I_{total} were decreased and eventually minimized at 300 ^{0}C.

The same happened with condensation temperature T_3. All parameters affecting the ORC-unit and the RO-unit were decreased with the decrease of T_3 and minimized at 15 ^{0}C.

In northern countries such as UK or the Netherlands, where sea temperature varies between 5 and 20 ^{0}C, seawater feed T_5 temperature could play a significant role in desalination plant design. That does not occur in Mediterranean Sea countries, which have potential water scarcity problems, thus with the raise of T_5, a slight increase is observed of turbine work produced W_2, high pressure pump required work W_5, specific power consumption *SPC*, total exergy destruction I_{total} and product specific total cost C_t.

Feed salinity can affect RO desalination performance. Highly concentrated seawater needs more energy to be desalinated and thus more energy should be produced. On the other hand, seawater salinity varies according to the location of the desalination plant and thus it cannot be used as a design parameter.

Potable water quality does not affect the performance of a desalination plant. Parameter analysis showed slight decrease of high pressure pump required work W_5 (confirming the theory [10]) and specific power consumption *SPC* with the increase of potable water salinity X_d. Turbine work W_2, total exergy destruction I_{total} and specific total cost C_t remained untouched with the variation of X_d. It must be referred that potable water quality depends only to the membrane used. Each membrane element has different salt rejection factor *SR* which leads to the outcome that it cannot be used as optimization parameter by itself.

The following table presents a comparison between optimized results for the three different cases that have been studied:

Table 45: Comparison between optimized results for the three cases studied.

Parameter	No energy recovery system	Hydraulic turbine	Pressure exchanger
A_{col}, m^2	7007	1960	2221
RR	0.28	0.3	0.31
T_1, ^{0}C	300	300	300
T_3, ^{0}C	15	15	15
m_{orc}, kg/s	5.698	1.594	1.806
SPC, kWh/m^3	8.366	7.666	2.49
I_{total}, MW	4.935	2.981	1.234
C_t, \$/m^3	0.7435	0.6785	0.6412

Cyclohexane, toluene and n-octane are the best choices for economic reasons with no energy recovery system:
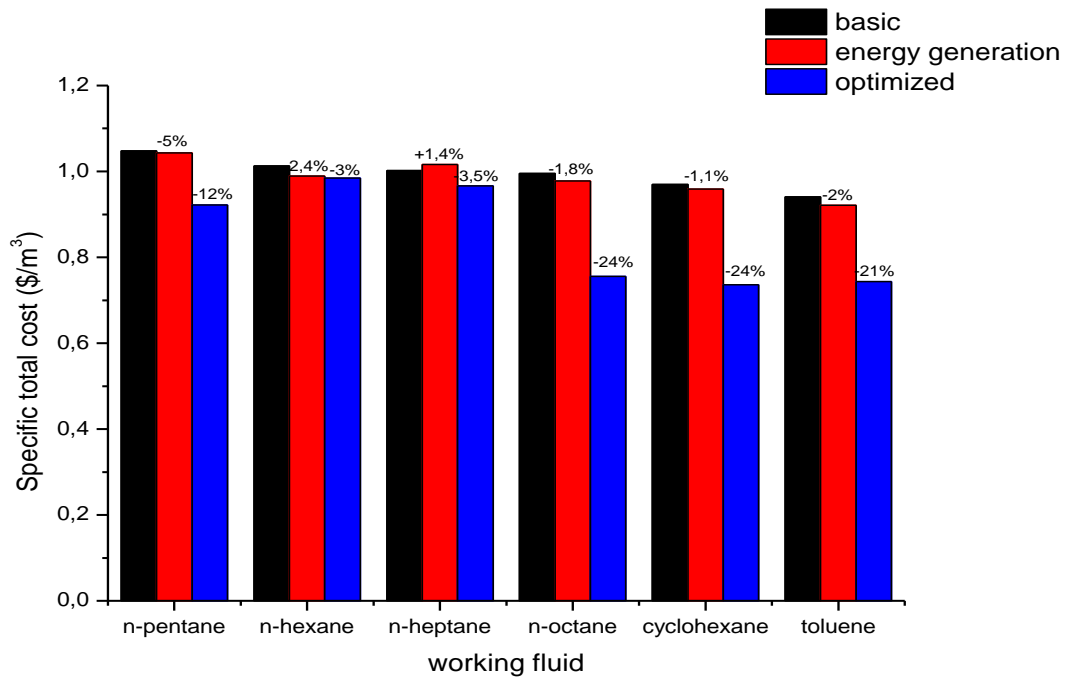
Diagram 51: Comparison between the basic program, with energy generation and optimized specific total cost for various ORC working fluids.

While toluene and cyclohexane are more befitting to drive the ORC-unit:
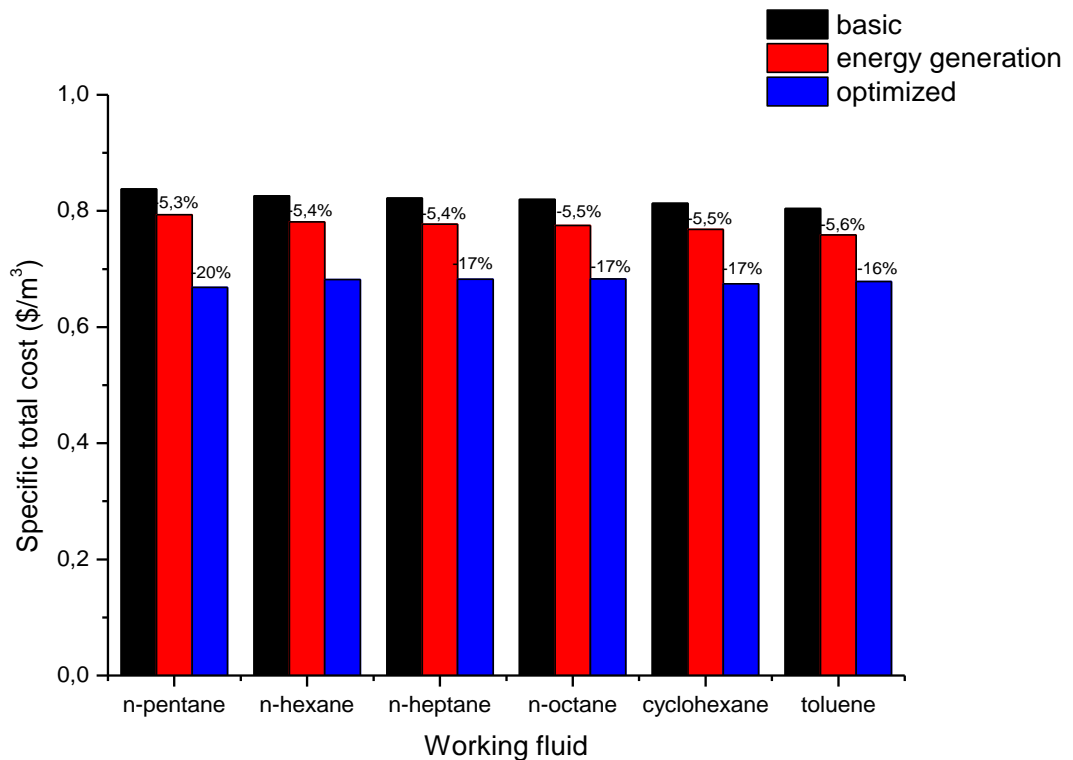
Diagram 52: Comparison between the specific total costs of the main program with a hydraulic turbine, energy generation and optimized results for various working fluids.

Finally, with a pressure exchanger, all ORC working fluids provided similar results based on product specific total cost C_t:
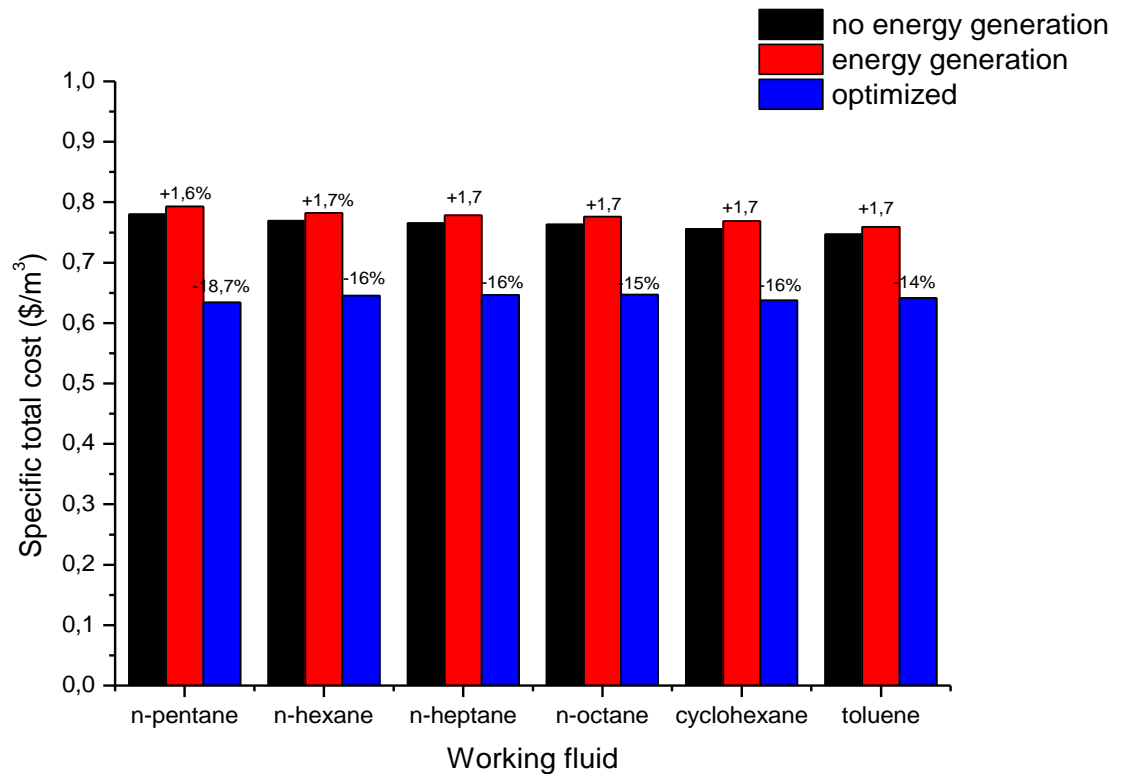
Diagram 53: Comparison between the specific total costs of the main program with a pressure exchanger, energy generation and optimized results for various working fluids.

Also toluene is the most suitable working fluid with less irreversibility, I_{total}, using pressure exchanger:
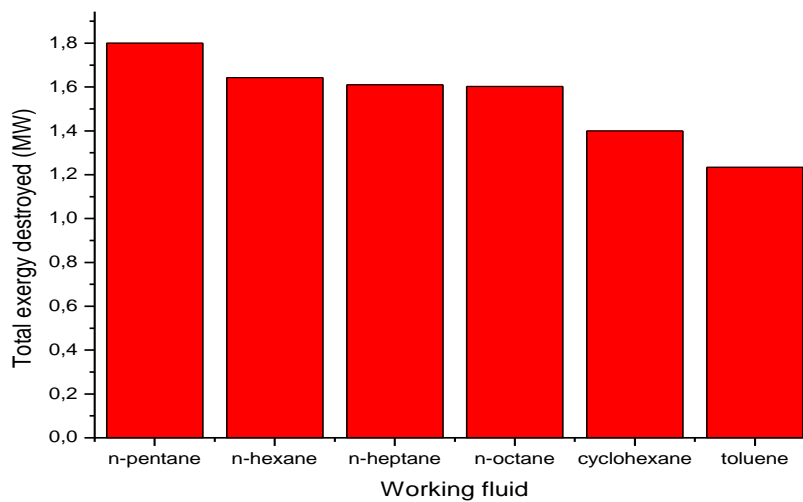
Diagram 54: Variation of irrevirsibility for different working fluids

Nafey in his work presented a solar driven ORC RO desalination plant based on an actual plant in Sharm El-Shiekh, Egypt. [52], [53] Having specified design parameters the recovery ratio *RR* and the total productivity Q_d, the case study was not optimized. In this present work, a proposal has been made to produce the same amount of potable water using different energy recovery systems with energy production sold to the local electricity company.
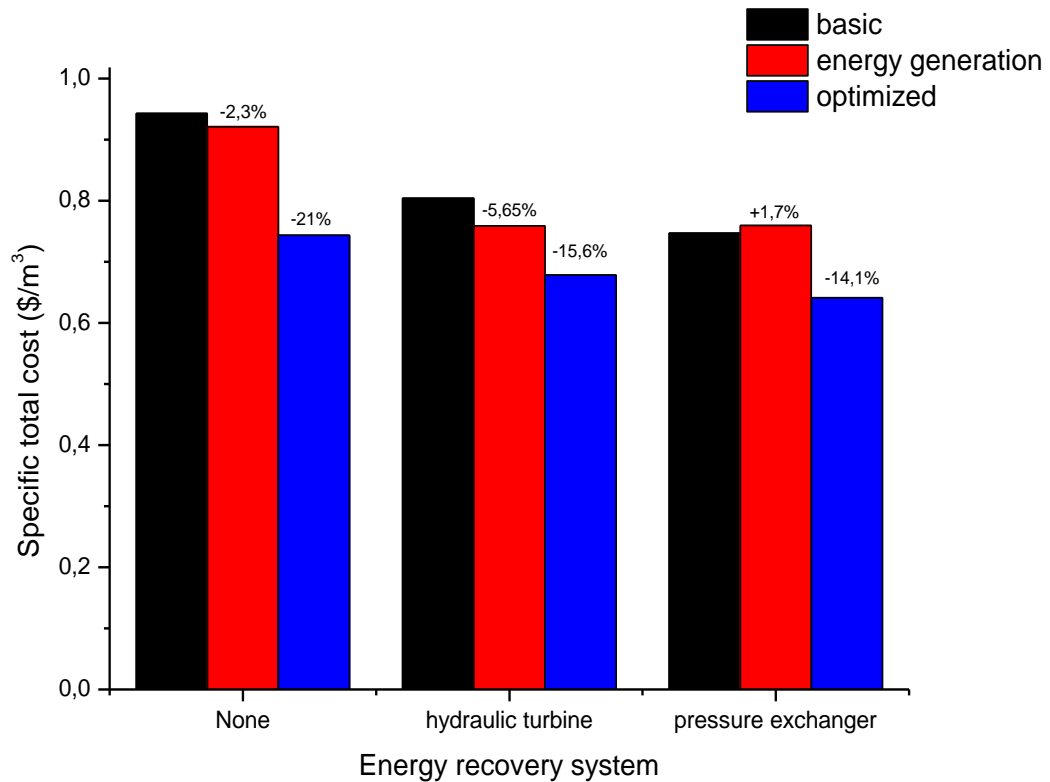
Diagram 55: Comparison between this work's results

The best method of desalting water is ORC driven RO plant using a pressure exchanger which is presented in the diagram above. It must be referred that the Greek Electricity Company (Δ.Ε.Η.) buys electricity at €0.16/kWh. [80] In other countries, local electricity companies buy electricity much more expensive. In this work, calculations were made using the prices of the Greek Electricity Company. Nevertheless, toluene is proven to be the best ORC working fluid for all three configurations, providing the lowest desalting costs C_t and having the least irreversibility I_{total} and specific power consumption *SPC*.

7. CONCLUSION

In this present work, a desalination plant was studied with various energy recovery systems. The case study is consisted of two parts: organic Rankine cycle unit which provides the necessary power to drive the RO desalination unit. Different configurations were taken for various ORC working fluids with and without energy recovery systems. It was calculated that with the use of a hydraulic turbine as energy recovery system total exergy destruction I_{total}, specific power consumption *SPC* and specific total cost C_t decrease by 42%, 10% and 15%, respectively. By using a pressure exchanger, total exergy destruction I_{total}, specific power consumption *SPC* and specific total cost C_t decrease by 75%, 68% and 20%, respectively. The plant was optimized and it was proven that a RO desalination plant driven by an ORC-unit using toluene as working fluid coupled with a pressure exchanger is the best choice for both economic and exergy reasons.

It was taken into serious account membrane fouling. In the basic program two different mechanisms of membrane fouling were added: concentration polarization and membrane complete pore blocking. There was a serious effort made to couple these models to the basic program with time and this lead to the outcome that all plant parameters change with time. However, there are not the only two existing membrane fouling mechanisms. There are also many other mechanisms concerning suspended particles, such as intermediate pore blocking or cake layer formation. There was not also taken into account membrane biofouling for which there is not a general mathematical model existing. It must also be referred that all fouling models happen simultaneously and affect each other. *EES* failed to fulfill this task by just calculating the membrane fouling mechanisms simultaneously but separately from each other. With a different mathematical tool, more reliable results could have been provided. In every way, membrane fouling affects the overall plant performance: while RO-unit required energy W_5 and total exergy destruction I_{total} remain constant, due to concentration polarization the solar collector area A_{col} is raised by 3%, specific power consumption by 5% and the specific total cost C_t by 4% for the plant first year of operation.

With the pass of time, more pressure is required across the membrane. The more pressure needed, the more energy should be produced by the ORC-unit. Since solar collector is the part that produces energy, a bigger solar collector should be used. By using the 5th year's solar collector area, the energy produced is more than enough to drive the RO-unit and the excess is sold to the local electricity network company. Among the optimization parameters, there was not product flow rate, Q_d. *EES* again did not provide satisfying results for that case. In this method, all ORC working fluids provided comparable results in terms of specific power consumption C_t with toluene having the least total exergy destroyed. In every way, for toluene both specific total cost C_t and irreversibility I_{total} are 30% and 75% respectively less than ref. [52].

Finally, only parallel module array was studied in this present work. It was not studied a RO plant with modules on series array nor tapered array. By studying all three module arrays and couple them with an ORC-unit for various fluids, one can say which method gives the best results.

8. REFERRENCES

Books and Articles in Encyclopedias:

1. Baker, R. W. (2000). Membrane Separation. In *Encyclopedia of Seperation Science* (pp. 189-210). Academic Press.

2. Baker, R. W., Cussler, E. L., Eykamp, W., & Strathmann, H. (1991). *MEMBRANE SEPERATION SYSTEMS-Recent developments and future direction.* Park Ridge, New Jersey, USA: Noyes Data Corp.

3. Cheremisinoff, P. N. (1995). *PROCESS ENGINEERING HANDBOOK SERIES-Solids/Liquids Separation.* Lancaster, USA: Technomic Publishing Co., Inc.

4. Cipollina, A., Micale, G., & Rizzuti, L. (2009). *Seawater Desalination: Conventional and Renewable Energy Processes.* Palermo,Italy: Springer Heidelberg Dordrecht London New York.

5. Cussler, E. L. (1997). *Diffusion-Mass Transfer in Fluid Systems* (2nd Edition). Cambridge, UK: Cambridge University Press.

6. Hisham El-Dessuky, T., & Hisham Ettouney, M. (2002). *Fundamental of salt desalination.* Kuwait University: Elsevier Science.

7. Kreith, F. (1998). *The CRC Handbook of Mechanical Engineering.* Washington, DC, USA: CRC Press Inc.

8. McCabe, W. L., Smith, J. C., & Harriott, P. (2001). *UNIT OPERATIONS OF CHEMICAL ENGINEERS* (6th edition). New York, USA: McGraw-Hill.

9. Meloan, C. E. (1999). *Chemical Seperators: Principles, Techniques and Experiments.* Chicago, USA: John Wiley and Sons.

10. Perry, R. H., & Green, D. W. (1997). *Perry's Chemical Engineers' Handbook* (7th Edition). New York: McGraw-Hill Companies, Inc.

11. Pinnau, I. (2000). Membrane Preparation. In *Encyclopedia of Seperation Science* (pp. 1755-1764). Academic Press.

12. Rousseau, R. W. (1987). *Handbook of Separation Process Technology.* Atlanta, USA: John Wiley & Sons, Inc.

13. Sourirajan, S. (1970). *Reverse Osmosis.* New York, USA: Acapemic Press.

14. Thain, J. F. (1967). *Principles of Osmotic Phenomena-Monographs for teachers No.13.* London: Royal Institute of Chemistry.

15. Αναγνωστόπουλος, A. K. (1998). *Σύγχρονη Ανόργανη Χημεία-Ειδικά Κεφάλαια* (Τόμος Δεύτερος). Θεσσαλονίκη: University Studio Press.

16. Καστρινάκης, Ε. Γ. (1999). *Μηχανικές Φυσικές Διεργασίες.* Θεσσαλονίκη: Εκδόσεις Τζίολα.

17. Μαρκόπουλος, Ι. Ν. (2002). *ΔΙΕΡΓΑΣΙΕΣ ΔΙΑΧΩΡΙΣΜΟΥ ΜΕ ΜΕΜΒΡΑΝΕΣ-Εισαγωγή στις βασικές αρχές τους και τις εφαρμογές τους.* Θεσσαλονίκη: University Studio Press.

Journal Articles:

18. Al-Bastaki, N. M., & Abbas, A. (1999). Modeling an industrial reverse osmosis unit. *Desalination* (126), pp. 33-39.

19. Al-Shayji, K. A., & Liu, Y. A. (2002). Predictive modeling of large scale commercial water desalination plants: Data-based neural network and model-based process simulation. *Ind. Eng. Chem. Res* (41), pp. 6460-6474.

20. Avlonitis, S. A. (2002). Operational water cost and productivity improvements for small size RO desalination plants. *Desalination* (142), pp. 295-304.

21. Avlonitis, S. A., Kouroumbas, K., & Vlachakis, N. (2003). Energy consumption and membrane replacement cost for seawater RO desalination plants. *Desalination* (157), pp. 151-158.

22. Avlonitis, S. A., Poulios, I., Vlachakis, N., Tsitmidelis, S., Kouroumbas, K., Avlonitis, D., et al. (2002). Water resources management for the prefecture of Dodekanisa of Greece. *Desalination* (152), pp. 41-50.

23. Baker, J. S., & Dudley, L. Y. (1998). Biofouling in membrane systems-A review. *Desalination* (118), pp. 81-90.

24. Bouzayani, N., Galanis, N., & Orfi, J. (2009). Thermodynamic analysis of combined electric power generation and water desalination plants. *Applied Thermal Engineering* (29), pp. 624-633.

25. Bruno, J. C., Lopez-Villada, J., Letelier, E., Romera, S., & Coronas, A. (2008). Modelling and optimisation of solar organic rankine cycle engines for reverse osmosis desalination. *Applied Thermal Engineering* (28), pp. 2212-2226.

26. Chen, K. L., Song, L., Ong, S. L., & Ng, J. W. (2004). The development of membrane fouling in full-scale RO processes. *Journal of Membrane Science* (232), pp. 63-72.

27. Choi, J.-S., Lee, S., Kim, J.-M., & Choi, S. (2009). Small-scale desalination plants in Korea: Technical challenges. *Desalination* (249), pp. 222-232.

28. Delyannis, E. E., & Belesiotis, V. (1995). Solar application in desalination: the Greek Islands experiment. *Desalination* (100), pp. 27-34.

29. Deng, R., Xie, L., Lin, H., Liu, J., & Han, W. (2010). Integration of thermal energy and seawater desalination. *Energy* (35), pp. 4368-4374.

30. Flemming, H.-C. (1997). Reverse Osmosis Membrane Biofouling. *Experimental Thermal and Fluid Science* (14), pp. 382-391.

31. Fritzmann, C., Lowenberg, J., Wintgens, T., & Melin, T. (2007). State-of-the-art of reverse osmosis desalination. *Desalination* (216), pp. 1-76.

32. Hamed, O. A., Zamamiri, A. M., Aly, S., & Lior, N. (1996). Thermal performane and exergy analysis of thermal vapor compression desalination system. *Energy Conversion and Management* (37), pp. 379-384.

33. Helal, A. M., Al-Malek, S. A., & Al-Katheeri, E. (2008). Economic feasibility of alternative designs of a PV-RO desalination unit for remote areas in the United Arab Emirates. *Desalination* (221), pp. 1-16.

34. Hoek, E. M., Allred, J., Knoell, T., & Jeong, B.-H. (2008). Modeling the effects of fouling on full-scale reverse osmosis processes. *Journal of Membrane Science* (314), pp. 33-49.

35. Huang, H., Young, T. A., & Jacangelo, J. G. (2008). Unified membrane fouling index for low pressure membrane filtration of natural waters: Principles and methology. *Evironmental Science and Technology* (42), pp. 714-720.

36. Jonnson, G., Pradanos, P., & Hernandez, A. (1996). Fouling phenomena in microporous membranes. Flux decline, kinetics and structural modifications. *Journal of Membrane Science* (112), pp. 171-183.

37. Kaldellis, J. K., & Kondili, E. M. (2007). The water shortage problem in the Aegean archipelago islands: cost-effective desalination prospects. *Desalination* (216), pp. 123-138.

38. Kaldellis, J. K., Kavadias, K. A., & Kondili, E. (2004). Renewable energy desalination plants for the Greek islands-technical and economic considerations. *Desalination* (170), pp. 187-203.

39. Kalogirou, S. A. (2005). Seawater desalination using renewable energy sources. *Progress in Energy and Combustion Science* (31), pp. 242-281.

40. Kahraman, N., & Cengel, Y. A. (2005). Exergy analysis of a MSF distilation plant. *Energy Conversion and management* (46), pp. 2625-2636

41. Kapooria, R. K., Kumar, S., & Kasana, K. S. (2008). An analysis of a thermal power plant working on a Rankine cycle: A theoretical investigation. *Journal of Energy in Southern Africa* (19), pp. 77-83.

42. Karagiannis, I. C., & Soldatos, P. G. (2007). Current status of water desalination in the Aegean islands. *Desalination* (203), pp. 56-61.

43. Kurihara, M., Yamamura, H., & Nakanishi, T. (1999). High recovery / high pressure membranes for brine conversion SWRO process development and its performance data. *Desalination* (125), pp. 9-15.

44. Kwak, S.-Y., Kim, S. H., & Kim, S. S. (2001). Hybrid organic/inorganic Reverse Osmosis (RO) membrane for bactericidal anti-fouling. 1. Preparation and characterizaion of TiO2 nanoparticle self-assembled aromatic polyamide Thin-Film-Composite (TFC) membrane. *Environmental Science and Technology* (35), pp. 2388-2394.

45. Lu, Y.-Y., Hu, Y.-D., Zhang, X.-L., Wu, L.-Y., & Liu, Q.-Z. (2007). Optimum design of reverse osmosis system under different feed concentration and product specification. *Journal of Membrane Science* (287), pp. 219–229.

46. Mairal, A. P., Greenberg, A. R., Krantz, W. B., & Bond, L. J. (1999). Real-time measurement of inorganic fouling of RO desalination membranes using ultrasonic time-domain reflectometry. *Journal of Membrane Science* (159), pp. 185-196.

47. Malek, A., Hawlader, M., & Ho, J. (1996). Design and economics of RO seawater desalination. *Desalination* (105), pp. 245-261

48. Manolakos, D., Papadakis, G., Kyritsis, S., & Bouzianas, K. (2007). Experimental evaluation of an autonomous low-temperature solar Rankine cycle system for reverse osmosis desalination. *Desalination* (203), pp. 366-374

49. Marcovecchio, M. G., Aguirre, P. A., & Scenna, N. J. (2005). Global optimal design of reverse osmosis network for seawater desalination: modelling and algorithm. *Desalination* (184), pp. 259-271.

50. Marriott, J. I., Sorensen, E., & Bogle, I. L. (2001). Detailed mathematical modeling of membrane modules. *Computers and Chemical Engineering* (25), pp. 693-700.

51. Mathioulakis, E., Belessiotis, V., & Delyannis, E. (2007). Desalination by using alternative energy: Review and state-of-the-art. *Desalination* (203), pp. 346-365.

52. Nafey, A. S., & Sharaf, M. (2010). Combined solar organic Rankine cycle with reverse osmosis desaliantion process: Energy, exergy and cost evaluations. *Renewable Energy* (35), pp. 2571-2580.

53. Nafey, A. S., Sharaf, M. A., & Garcia-Rodriguez, L. (2010). Thermo-economic analysis of a combined solar organic Rankine cycle-reverse osmosis desaliantion process with different energy recovery configurations. *Desalination* (261), pp. 138-147.

54. Potts, D. E., Ahlert, R. C., & Wang, S. S. (1981). A critical rewiew of fouling of reverse osmosis membranes. *Desalination* (36), pp. 235-264.

55. Sayyaadi, H., & Saffari, A. (2010). Thermoeconomic optimization of multi effect distillation desalination systems. *Applied Energy* (87), pp. 1122-1133.

56. Stover, R. L. (2008). SWRO process simulator. *Desalination* (221), pp. 126–135.

57. Villafafila, A., & Mujtaba, I. M. (2003). Fresh water by reverse osmosis based desalination: simulation and optimisation. *Desalination* (155), pp. l-13.

58. Voivontas, D., Misirlis, K., Manoli, E., Arampatzis, G., Assimakopoulos, D., & Zervos, A. (2001). A tool for the design of desalination plants powered by renewable energies. *Desalination* (133), pp. 175-198.

59. Wang, Y., & Lior, N. (2006). Performance analysis of combined humidified gas turbine power generation and multi-effect thermal vapor compression desalination systems-Part 1: The desalination unit and its combination with a steam ejected gas turbine power system. *Desalination* (196), pp. 84-104.

60. Wolf, P. H., Siverns, S., & Monti, S. (2005). UF membranes for RO desalination pretreatment. *Desalination* (182), pp. 293-300.

Conferences:

61. Djebedjian, B., Gad, H., Khaled, I., & Abou Rayan, M. (2008). Optimization of Reverse Osmosis desalination system using genetic algorithms technique. *Twelfth International water Technology Conference*, (pp. 1047-1067). Alexandria, Egypt.

62. Manolakos, D., Kyritsis, S., Karagiannis, J., & Soldatos, P. (November 2005). Cost analysis of an autonomous low-temperature solar Rankine cycle system for reverse osmosis desalination. *Int. Conf. on ENVIRONMENT, ECOSYSTEMS and DEVELOPMENT* (pp. 266-271). Venice, Italy: WSEAS.

63. Perysinaki, A., & Gekas, V. (July, 22-24, 2008). Combined Management of Eolian and Water Management through Coupling of RO Desalination and Wind Energy. *WSEAS International Conference on ENGINEERING MECHANICS, STRUCTURES, ENGINEERING GEOLOGY (EMESEG '08)*, (pp. 376-384). Heraklion, Greece.

64. Sinai, J., & Fisher, U. (2007). 1 MW SOLAR POWER PLANT Using ORMAT® ENERGY CONVERTER. *Proceedings of the 14th Sede Boqer Symposium on Solar Electricity Production*, (pp. 53-56). Negev, Israel.

Sites in the internet:

65. *About Salt-Physical properties*. Retrieved 2011, from Salt Institute: www.saltinstitute.org/About-Salt/Physical-properties

66. *American Membrane Technology Association.* Retrieved 2011 from AMTA: www.amtaorg.com

67. *Desalination*. Retrieved 2010 from Wikipedia: http://en.wikipedia.org/wiki/Desalination

68. *Desalination*. Retrieved 2010 from Suiki desalination systems: www.f-suiki.or.jp

69. *Drink Seawater*. Retrieved 2011 from G.A. Water: http://ga.water.usgs.gov/edu/drinkseawater.html

70. *EEA* . Retrieved 2011 from European Environmet Agency: http://www.eea.europa.eu/themes/coast_sea/todays-sea-surface-temperature/todays-sea-surface-temperature

71. *F-Chart Software*. Retrieved 2011 from F-Chart Software : Engineering Software: http://www.fchart.com/ees/

72. *Filmtech SW30HR-380*. Retrieved 2011 from Lenntech-Water Treatment Solutions: http://www.lenntech.com/replacement/filmtech_sw30hr_380.htm

73. *Goverment Programms-Desalination History*. Retrieved 2011 from Victorian Department of Sustainability and Environment: http://www.water.vic.gov.au/programs/desalination/desalination/desalination-history

74. *Osmosis*. Retrieved 2011 from Science Aid: http://scienceaid.co.uk/biology/cell/osmosis.html

75. *PermSelect Membrane Modules.*. Retrieved 2011 from MedArray: www.permselect.com/membranes

76. *Reverse Osmosis Filtration*. Retrieved 2011 from Innovative Water: http://innovative-water.com/Reverse_Osmosis_Filters.html

77. *Spiral wound membranes*. Retrieved 2011 from Tecna: http://www.tecna-italy.com/html/mbn_spiral_eng.html.mht

78. *What is desalination?* . Retrieved 2012 from Desal Solution in Australia - a division of IBC Water Group Pty Ltd: http://www.desalsolutions.com.au/what-is-desalination.html

79. *Αφαλάτωση*. Retrieved 2010 from Wikipedia: http://el.wikipedia.org/wiki/Αφαλάτωση

80. *ΔΗΜΟΣΙΑ ΕΠΙΧΕΙΡΗΣΗ ΗΛΕΚΤΡΙΣΜΟΥ Α.Ε.* (2012). Retrieved from ΔΕΗ: www.dei.gr

Appendix A
Results

Table 46: Basic program results table

Variable	Calculated price	Units	Variable	Calculated price	Units	Variable	Calculated price	Units
ACC_{ro}	380252	$/y	I_3	74.25	kW	TCC_{pump}	1785	$
A_{col}	6943	m^2	I_4	7.731	kW	$TCC_{turbine}$	83872	$
A_f	0.08024	y^{-1}	I_5	596.5	kW	TCF	0.9807	
C_{orc}	39.88	$/h	I_{total}	4.986	MW	W_1	4344	kW
C_{ro}	92.13	$/h	K_s	1.816E-08		W_2	1161	kW
C_t	0.9429	$/m^3	k_w	1.678E-09		W_3	3337	kW
CC_e	2124000	$	m_{orc}	5.908	kg/s	W_4	31.83	kW
CC_{eqp}	3392000	$	OC_{chm}	5.04	$	W_5	1129	kW
CC_{hhp}	1132000	$	OC_{ins}	1901	$	X_{av}	52890	ppm
CC_{site}	339211	$	OC_{lb}	1.26	$	X_b	64170	ppm
CC_{swip}	135977	$	OC_{mmb}	424800	$	Γ	0,04297	
DCC	3731000	$	OC_{pwr}	60.96	$	ΔP	69.67	bar
h_{2id}	365	kJ/kg	OC_{ro}	426769	$	$\Delta \Pi$	4.296	bar
ICC	1007000	$	P_p	354000	$	η_{col}	0.7361	
ICC_{cond}	4283	$	PV_p	3.387	$	η_{orc}	0.2317	
ICC_{col}	2853000	$	Q_b	326.7	m^3/h	Π_b	4.867	bar
ICC_{pump}	17799	$	SPC	8.063	kWh/m^3	Π_d	0.2048	bar
$ICC_{turbine}$	836182	$	TCC	4739000	$	ρ	853	kg/m^3
I_1	4163	kW	TCC_{col}	263267	$	ρ_w	998	kg/m^3
I_2	308.5	kW	TCC_{cond}	429.6	$	φ	1,043	

Table 47: Basic program with hydraulic turbine results table

Variable	Calculated price	Units	Variable	Calculated price	Units	Variable	Calculated price	Units
ACC_{ro}	380251	$/y	I_4	2.027	kW	$TCC_{turbine}$	30735	$
A_{col}	1821	m^2	I_5	615.5	kW	TCF	1.113	
A_f	0.08024	y^{-1}	I_6	817.1	kW	W_1	1139	kW
C_{orc}	12.09	$/h	I_{total}	2.908	MW	W_2	258.7	kW
C_{ro}	100.5	$/h	K_s	2.071E-08		W_3	857.2	kW
C_t	0.8041	$/m^3$	k_w	1.702E-09		W_4	8.349	kW
CC_e	2124000	$	m_{orc}	1.549	kg/s	W_5	1072	kW
CC_{eqp}	3392000	$	OC_{chm}	5.04	$	W_6	822.1	kW
CC_{hhp}	1132000	$	OC_{ins}	1901	$	X_{av}	52890	ppm
CC_{site}	339211	$	OC_{lb}	1.26	$	X_b	64170	ppm
CC_{swip}	135977	$	OC_{mmb}	424800	$	Γ	0,04344	
DCC	3731000	$	OC_{pwr}	87.91	$	ΔP	66.19	bar
h_{2id}	365	kJ/kg	OC_{ro}	426765	$	ΔP_{hydro}	64.55	bar
ICC	1007000	$	P_p	354000	$	$\Delta \Pi$	4.298	Bar
ICC_{cond}	4283	$	PV_p	3.217	$	η_{col}	0.7361	
ICC_{col}	799916	$	Q_b	326.7	m^3/h	η_{orc}	0.2317	
ICC_{pump}	9448	$	SPC	7.66	kWh/m^3	Π_b	4.867	bar
$ICC_{turbine}$	306418	$	TCC	4739000	$	Π_d	0.2048	bar
I_1	1431	kW	TCC_{col}	73817	$	ρ	853	kg/m^3
I_2	80.9	kW	TCC_{cond}	429.6	$	ρ_w	998	kg/m^3
I_3	34.37	kW	TCC_{pump}	951.7	$	φ	1,043	

Ioannis Kylindris

Table 48: Basic program with pressure exchanger results table

Variable	Calculated price	Units	Variable	Calculated price	Units	Variable	Calculated price	Units
ACC_{ro}	380241	$/y	I_3	32.45	kW	TCC_{pump}	1037	$
A_{col}	2184	m^2	I_4	2.433	kW	$TCC_{turbine}$	35235	$
A_f	0.08024	y^{-1}	I_5	107.3	kW	TCF	1.013	
C_{orc}	14.21	$/h	I_{total}	1.265	MW	W_1	1367	kW
C_{ro}	92.12	$/h	K_s	2.051E-08		W_2	366.2	kW
C_t	0.7595	$/m^3	k_w	1.700E-09		W_3	1050	kW
CC_e	2124000	$	m_{orc}	1.859	kg/s	W_4	10.01	kW
CC_{eqp}	3392000	$	OC_{chm}	5.04	$	W_5	355.2	kW
CC_{hhp}	1132000	$	OC_{ins}	1901	$	X_{av}	52890	ppm
CC_{site}	339201	$	OC_{lb}	1.26	$	X_b	64170	ppm
CC_{swip}	135977	$	OC_{mmb}	424800	$	Γ	0,0434	
DCC	3731000	$	OC_{pwr}	19.18	$	ΔP	66.43	bar
h_{2id}	365	kJ/kg	OC_{ro}	426727	$	$\Delta\Pi$	4.298	bar
ICC	1007000	$	P_p	354000	$	η_{col}	0.7361	
ICC_{cond}	4283	$	PV_p	3.066	$	η_{orc}	0.2317	
ICC_{col}	951081	$	Q_b	326.7	m^3/h	Π_b	4.867	bar
ICC_{pump}	10336	$	SPC	2.537	kWh/m^3	Π_d	0.2048	bar
$ICC_{turbine}$	351286	$	TCC	4739000	$	ρ	853	kg/m^3
I_1	1310	kW	TCC_{col}	87765	$	ρ_w	998	kg/m^3
I_2	97.06	kW	TCC_{cond}	429.6	$	φ	1,043	

Table 49: Basic program with energy generation results table

Variable	Calculated price	Units	Variable	Calculated price	Units	Variable	Calculated price	Units
ACC_{ro}	380252	\$/y	I_4	7.803	kW	$TCC_{turbine}$	84453	\$
A_f	0.08024	y^{-1}	I_5	596.3	kW	TCF	0.9792	
C_{orc}	40.21	\$/h	I_{total}	5.026	MW	W_1	4384	kW
C_{ro}	88.78	\$/h	K_s	1.831E-08		W_2	1162	kW
C_t	0.9214	\$/m^3	k_w	1.678E-09		W_3	3368	kW
CC_e	2124000	\$	m_{orc}	5.963	kg/s	W_4	32.12	kW
CC_{eqp}	3392000	\$	OC_{chm}	5.04	\$	W_5	1130	kW
CC_{hhp}	1132000	\$	OC_{ins}	1901	\$	W_a	987.5	kW
CC_{site}	339211	\$	OC_{lb}	1.26	\$	W_b	8.262	kW
CC_{swip}	135977	\$	OC_{mmb}	424800	\$	X_{av}	52890	ppm
DCC	3731000	\$	OC_{pwr}	61	\$	X_b	64170	ppm
h_{2id}	365	kJ/kg	OC_{ro}	426769	\$	ΔP	69.71	bar
ICC	1007000	\$	P_p	354000	\$	$\Delta\Pi$	4.296	bar
ICC_{cond}	4283	\$	PV_p	3.389	\$	η_{col}	0.7361	
ICC_{col}	2878000	\$	Q_b	326.7	m^3/h	η_{orc}	0.2317	
ICC_{pump}	17876	\$	SPC	8.069	kWh/m^3	Π_b	4.867	bar
$ICC_{turbine}$	841981	\$	TCC	4739000	\$	Π_d	0.2048	bar
I_1	4201	kW	TCC_{col}	265582	\$	ρ	853	kg/m^3
I_2	311.4	kW	TCC_{cond}	429.6	\$	ρ_w	998	kg/m^3
I_3	75.66	kW	TCC_{pump}	1793	\$	φ	1,043	

Table 50: Basic program with hydraulic turbine and energy generation results table

Variable	Calculated price	Units	Variable	Calculated price	Units	Variable	Calculated price	Units
ACC_{ro}	380251	\$/y	I_5	614.8	kW	TCF	1.109	
A_f	0.08024	y^{-1}	I_6	815.9	kW	W_1	1226	kW
C_{orc}	12.91	\$/h	I_{total}	3.023	MW	W_2	278.5	kW
C_{ro}	93.81	\$/h	K_s	2.063E-08		W_3	942.2	kW
C_t	0.7587	\$/m^3	k_w	1.701E-09		W_4	8.985	kW
CC_e	2124000	\$	m_{orc}	1.668	kg/s	W_5	1074	kW
CC_{eqp}	3392000	\$	OC_{chm}	5.04	\$	W_6	822.1	kW
CC_{hhp}	1132000	\$	OC_{ins}	1901	\$	W_a	260.8	kW
CC_{site}	339210	\$	OC_{lb}	1.26	\$	W_b	17.68	kW
CC_{swip}	135977	\$	OC_{mmb}	424800	\$	X_{av}	52890	ppm
DCC	3731000	\$	OC_{pwr}	57.99	\$	X_b	64170	ppm
h_{2id}	365	kJ/kg	OC_{ro}	426766	\$	ΔP	66.28	bar
ICC	1010000	\$	P_p	354000	\$	ΔP_{hydro}	64.55	bar
ICC_{cond}	4283	\$	PV_p	3.222	\$	$\Delta \Pi$	4.298	Bar
ICC_{col}	857993	\$	Q_b	326.7	m^3/h	η_{col}	0.7361	
ICC_{pump}	9823	\$	SPC	7.671	kWh/m^3	η_{orc}	0.2317	
$ICC_{turbine}$	323851	\$	TCC	4739000	\$	Π_b	4.867	bar
I_1	1541	kW	TCC_{col}	79175	\$	Π_d	0.2048	bar
I_2	87.09	kW	TCC_{cond}	429.6	\$	ρ	853	kg/m^3
I_3	33.55	kW	TCC_{pump}	985.2	\$	ρ_w	998	kg/m^3
I_4	2.183	kW	$TCC_{turbine}$	32483	\$	φ	1,043	

Ioannis Kylindris

Table 51: Basic program with pressure exchanger and energy generation results table

Variable	Calculated price	Units	Variable	Calculated price	Units	Variable	Calculated price	Units
ACC_{ro}	380241	\$/y	I_4	2.473	kW	$TCC_{turbine}$	35676	\$
A_f	0.08024	y^{-1}	I_5	107.7	kW	TCF	1.102	
C_{orc}	14.42	\$/h	I_{total}	1.288	MW	W_1	1390	kW
C_{ro}	90.12	\$/h	K_s	2.049E-08		W_2	370	kW
C_t	0.7467	\$/m^3	k_w	1.700E-09		W_3	1068	kW
CC_e	2124000	\$	m_{orc}	1.89	kg/s	W_4	10.18	kW
CC_{eqp}	3392000	\$	OC_{chm}	5.04	\$	W_5	355.3	kW
CC_{hhp}	1132000	\$	OC_{ins}	1901	\$	W_a	365.5	kW
CC_{site}	339201	\$	OC_{lb}	1.26	\$	W_b	4.94	kW
CC_{swip}	135977	\$	OC_{mmb}	424800	\$	X_{av}	52890	ppm
DCC	3731000	\$	OC_{pwr}	19.19	\$	X_b	64170	ppm
h_{2id}	365	kJ/kg	OC_{ro}	426727	\$	ΔP	66.45	bar
ICC	1007000	\$	P_p	354000	\$	$\Delta \Pi$	4.298	bar
ICC_{cond}	4283	\$	PV_p	1.066	\$	η_{col}	0.7361	
ICC_{col}	966188	\$	Q_b	326.7	m^3/h	η_{orc}	0.2317	
ICC_{pump}	10417	\$	SPC	2.538	kWh/m^3	Π_b	4.867	bar
$ICC_{turbine}$	355684	\$	TCC	4739000	\$	Π_d	0.2048	bar
I_1	1332	kW	TCC_{col}	89159	\$	ρ	853	kg/m^3
I_2	98.69	kW	TCC_{cond}	429.6	\$	ρ_w	998	kg/m^3
I_3	32.3	kW	TCC_{pump}	1045	\$	φ	1,043	

Table 52: Basic program with energy generation optimized results table

Variable	Calculated price	Units	Variable	Calculated price	Units	Variable	Calculated price	Units
ACC_{ro}	381117	\$/y	I_5	647.5	kW	$TCC_{turbine}$	90556	\$
A_f	0.08024	y^{-1}	I_{total}	4.935	MW	TCF	0.995	
C_{orc}	40.9	\$/h	K_s	1.843E-08		W_1	4384	kW
C_{ro}	63.18	\$/h	k_w	1.753E-09		W_2	1209.4	kW
C_t	0.7435	\$/m^3	m_{orc}	5.698	kg/s	W_3	3264	kW
CC_e	2124000	\$	OC_{chm}	5.04	\$	W_4	30.08	kW
CC_{eqp}	3400000	\$	OC_{ins}	1906	\$	W_5	1171	kW
CC_{hhp}	1132000	\$	OC_{lb}	1.26	\$	W_a	1201.1	kW
CC_{site}	339983	\$	OC_{mmb}	424800	\$	W_b	8.262	kW
CC_{swip}	143693	\$	OC_{pwr}	63.25	\$	X_{av}	52890	ppm
DCC	3740000	\$	OC_{ro}	426775	\$	X_b	64170	ppm
h_{2id}	330.2	kJ/kg	P_p	354000	\$	Γ	0.04303	
ICC	1009000	\$	PV_p	3.514	\$	ΔP	67.46	bar
ICC_{cond}	4283	\$	Q_b	360	m^3/h	$\Delta\Pi$	4.226	bar
ICC_{col}	2878000	\$	Q_f	500	m^3/h	η_{col}	0.7361	
ICC_{pump}	17331	\$	RR	0.28		η_{orc}	0.2555	
$ICC_{turbine}$	902826	\$	SPC	8.366	kWh/m^3	Π_b	4.732	bar
I_1	4208	kW	TCC	4750000	\$	Π_d	0.2048	bar
I_2	357.2	kW	TCC_{col}	265582	\$	ρ	871.6	kg/m^3
I_3	271.1	kW	TCC_{cond}	429.6	\$	ρ_w	998	kg/m^3
I_4	7.089	kW	TCC_{pump}	1738	\$	φ	1,043	

Table 53: Basic program with hydraulic turbine and energy generation optimized results table

Variable	Calculated price	Units	Variable	Calculated price	Units	Variable	Calculated price	Units
ACC_{ro}	380251	$/y	I_6	816.5	kW	TCF	1.111	
A_f	0.08024	y^{-1}	I_{total}	2.981	MW	W_1	1226	kW
C_{orc}	13.17	$/h	K_s	2.067E-08		W_2	305.7	kW
C_{ro}	81.82	$/h	k_w	1.702E-09		W_3	913	kW
C_t	0.6785	$/m^3	m_{orc}	1.594	kg/s	W_4	8.413	kW
CC_e	2124000	$	OC_{chm}	5.04	$	W_5	1073	kW
CC_{eqp}	3392000	$	OC_{ins}	1901	$	W_6	822.1	kW
CC_{hhp}	1132000	$	OC_{lb}	1.26	$	W_a	46.06	kW
CC_{site}	339210	$	OC_{mmb}	424800	$	W_b	52.89	kW
CC_{swip}	135977	$	OC_{pwr}	57.96	$	X_{av}	52890	ppm
DCC	3731000	$	OC_{ro}	426766	$	X_b	64170	ppm
h_{2id}	330.2	kJ/kg	P_p	354000	$	Γ	0.4343	
ICC	1007000	$	PV_p	3.22	$	ΔP	66.24	bar
ICC_{cond}	4283	$	Q_b	326.7	m^3/h	ΔP_{hydro}	64.55	bar
ICC_{col}	857993	$	Q_f	466.7	m^3/h	$\Delta \Pi$	4.298	bar
ICC_{pump}	9523	$	RR	0.3		η_{col}	0.7361	
$ICC_{turbine}$	347254	$	SPC	7.666	kWh/m^3	η_{orc}	0.2555	
I_1	1542	kW	TCC	4739000	$	Π_b	4.867	bar
I_2	99.91	kW	TCC_{col}	79175	$	Π_d	0.2048	bar
I_3	91.12	kW	TCC_{cond}	429.6	$	ρ	871.6	kg/m^3
I_4	1.983	kW	TCC_{pump}	955.2	$	ρ_w	998	kg/m^3
I_5	615.1	kW	$TCC_{turbine}$	34831	$	φ	1,043	

Table 54: Basic program with pressure exchanger and energy generation optimized results table

Variable	Calculated price	Units	Variable	Calculated price	Units	Variable	Calculated price	Units
ACC_{ro}	379846	\$/y	I_5	114.6	kW	$TCC_{turbine}$	38254	\$
A_f	0.08024	y^{-1}	I_{total}	1.234	MW	TCF	1.102	
C_{orc}	14.71	\$/h	K_s	2.049E-08		W_1	1390	kW
C_{ro}	75.05	\$/h	k_w	1.662E-09		W_2	400.2	kW
C_t	0.6412	\$/m^3	m_{orc}	1.806	kg/s	W_3	1035	kW
CC_e	2124000	\$	OC_{chm}	5.04	\$	W_4	9.533	kW
CC_{eqp}	3388000	\$	OC_{ins}	1889	\$	W_5	348.5	kW
CC_{hhp}	1132000	\$	OC_{lb}	1.26	\$	W_a	358	kW
CC_{site}	338849	\$	OC_{mmb}	424800	\$	W_b	42.2	kW
CC_{swip}	132456	\$	OC_{pwr}	18.82	\$	X_{av}	52890	ppm
DCC	3727000	\$	OC_{ro}	426724	\$	X_b	64170	ppm
h_{2id}	330.2	kJ/kg	P_p	354000	\$	Γ	0.0434	
ICC	1006000	\$	PV_p	1.046	\$	ΔP	67.36	bar
ICC_{cond}	4283	\$	Q_b	311.6	m^3/h	$\Delta \Pi$	4.335	bar
ICC_{col}	966188	\$	Q_f	451.6	m^3/h	η_{col}	0.7361	
ICC_{pump}	10100	\$	RR	0.31		η_{orc}	0.2555	
$ICC_{turbine}$	381387	\$	SPC	2.49	kWh/m^3	Π_b	4.937	bar
I_1	1334	kW	TCC	4734000	\$	Π_d	0.2048	bar
I_2	113.2	kW	TCC_{col}	89159	\$	ρ	871.6	kg/m^3
I_3	96.09	kW	TCC_{cond}	429.6	\$	ρ_w	998	kg/m^3
I_4	2.247	kW	TCC_{pump}	1013	\$	φ	1,043	

Ioannis Kylindris

Appendix B
Seawater thermophysical properties

Seawater enthalpy was calculated by the relation: [52]

$$h = h_0 + A \times (T - 273) + \frac{B}{2} \times (T - 273)^2 + \frac{C}{3}(T - 273)^3 + \frac{D}{4}(T - 273)^4$$

where:

$$A = 4206.8 - 6.6197 \times \frac{X}{1000} + 1.2288 \times 10^{-2} \times \left(\frac{X}{1000}\right)^2$$

$$B = -1.1262 + 5.4178 \times 10^{-2} \times \frac{X}{1000} - 2.2719 \times 10^{-4} \times \left(\frac{X}{1000}\right)^2$$

$$C = 1.2026 - 5.3566 \times 10^{-4} \times \frac{X}{1000} + 1.8906 \times 10^{-6} \times \left(\frac{X}{1000}\right)^2$$

$$D = 6.8774 \times 10^{-7} + 1.517 \times 10^{-6} \times \frac{X}{1000} - 4.4268 \times 10^{-9} \times \left(\frac{X}{1000}\right)^2$$

and

$$h_0 = 9.6296 \times \frac{X}{1000} - 0.4312402 \times \left(\frac{X}{1000}\right)^2$$

For seawater, D, μ and ρ can be expressed as: [61]

$$D = 6.725 \times 10^{-6} \exp\left(0.1546 \times 10^{-3} C_f - \frac{2513}{273.15 + T}\right)$$

$$\mu = 1.234 \times 10^{-6} \exp\left(0.00212 C_f + \frac{1965}{273.15 + T}\right)$$

And

$$\rho = 498.4b + \sqrt{248400 b^2 + 752.4 b C_f}$$

With:

$$b = 1.0069 - 2.757 \times 10^{-4} T$$

Appendix C

Glossary of terms

Anion	Negatively charged ion
Brine/Retentate	The wastewater steam from the reverse osmosis unit, which contains most of the dissolved solids of the feed in a concentrated form
Cation	Positively charged ion
Concentration	Amount of mass per unit of solution volume
Desalination	Potable water production technique using seawater
Desalination Pretreatment	Disposal of suspended particles and microorganisms
Feed	The water to be treated in desalination plant
Flux	The measurement of rated permeate expressed in m^3/h under a given feed-water temperature, salinity and operating pressure
Ion	Electrically charged atom, radical or molecule
Membrane	Thin film used to separate two phases or two different volumes of the same phase and allowing mass transfer between them
Membrane fouling	Deposition of materials on the membrane
Membrane module	Mechanical membrane types used in membrane separation techniques
Membrane preparation	Techniques for membrane production
Osmosis	The movement of solvent molecules through a semi-permeable membrane from a less concentrated solution to a dense solution
Osmotic Equilibrium	The state on which the free energy of both the solvent and the solution are equal
Osmotic pressure	The required pressure difference to produce zero solvent flow through the semi-permeable membrane
Permeate/Distillate	The purified product passing through the membrane
Plant capacity	The daily amount of product expressed in m^3/d
Recovery Ratio	The feed water percentage converted into product
Reverse Osmosis	The process where the solvent is forced through a semi-permeable membrane by an applied pressure from a more concentrated solution to a more dilute solution
Salinity	Amount of salts in water
Salt Rejection	The Total Dissolved Solids' percentage held back by the membrane
Salt Scaling	The deposition of salts
Semi-permeable Membrane	The membrane which impedes solute passage, but allows solvent flow
Solute	Materials dissolved by solvent
Total Dissolved Solids	Organic and inorganic materials present in the RO-unit streams
Working Fluid	The fluid to produce energy in the ORC